Norwegian University
of Life Sciences

Master's Thesis 2016 30 ECTS
Norwegian University of Life Sciences
Faculty of Environmental Science and Technology
Department of Mathematical Sciences and Technology

Monitoring of Building Attached Photovoltaics in Norway

Anne Marte Minge Engh
Environmental Physics and Renewable Energy

Preface and Acknowledgments

This study is a master thesis in solar energy at the Norwegian University of Life Sciences (NMBU), as part of an engineering degree in Energy and Environmental Physics. The thesis originates from an initiative from Dr. Erik Stensrud Marstein, Center Manager at the Norwegian Centre for Solar Cell Technology at the Institute for Energy Technology (IFE).

The study was conducted to investigate and analyze some of the challenges of monitoring BAPV systems in Norway. The main focus is on irradiation, different measurement equipment and comparison of irradiation from different locations. Monitoring of PV systems can give valuable information about the performance of the systems under different conditions. The documentation of PV system monitoring in Norway is limited. The study was carried out during the fall semester of 2016.

First of all, I want to thank my supervisor at IFE, Dr. Erik Stensrud Marstein for enthusiastic, optimistic and dedicated guidance through this thesis. Your knowledge, commitment and positive attitude towards everything is clearly an inspiration. Further I want to thank my supervisor at NMBU, Arne Auen Grimenes for valuable advices and for thoroughly review of my writing.

Furthermore, I would like to thank Josefine Helene Selj and Lenny Enström for access to inverter data from the PV systems at IFE. I also want to thank Flemming Idsøe at Omsorgsbygg KF and Marius Brenden at ITAS for access to the meteorological data at the Økern nursing home, and Signe Kroken and Hildegunn Nygård for providing meteorological data and information about the stations at Ås and Blindern respectively.

Finally, I would like to thank my family and friends for motivation and support during the work with this thesis. A special thanks to Mikke, my mom and dad, Veslemøy, Alex, Siri, Ellen and Mari.

Ås, December 12, 2016

Anne Marte Minge Engh

Abstract

In this thesis, several challenges associated with monitoring of BAPV systems in Norway are investigated. Monitoring of PV systems can give valuable information of the performance of the system and notify when failures occur in the PV system. The main challenge with monitoring of BAPV is the lack of meteorological data measured at the PV site. This thesis focuses on irradiation data and investigates the possibility of using irradiation data measured at other locations for use in analytical monitoring of PV systems.

A selection of the available sources for irradiation data near Oslo are examined. The selected sources are the PV system with meteorological equipment at the Økern nursing home, the meteorological measurement station at Blindern and the meteorological measurement station at Ås. Data from two different databases are examined and compared with the measured values for the irradiation. The databases used in this thesis are PVGIS and NASA SSE. The databases are derived from satellite data over a given period.

The different sources for irradiation data is compared for the reference year August 2015 to August 2016. The purpose of the comparison is to investigate the opportunity of using irradiation data from other sources when irradiation data is missing at the PV site. The challenges of comparing irradiation data was discovered along the way. Especially the different methods for measuring irradiation, the use of a pyranometer or a reference cell, is discussed. Irradiation measured horizontally with a pyranometer is easier to compare than irradiation measured in the module plane. Irradiation measured in the module plane with a reference cell can differ both in the slope, the orientation and the material of the reference cell, which make the data hard to compare.

A PV system located at Kjeller that does not have equipment for measuring meteorological factors at the PV site, is investigated. This system consists of modules of two different technologies, CIS and silicon. Here, a comparative approach has been adopted, wherein the relative performance of the two system parts have been compared. The research done for the two systems in this thesis has shown that the CIS modules have a higher specific yield than the silicon modules, even though the silicon modules are specified with a higher module efficiency than the CIS modules.

This thesis is concluding that meteorological measurements parallel with the inverter data are necessary for analytic monitoring. The irradiation from other sources can be difficult to use as a replacement, due to the distance between the sources and different methods for measuring irradiation. When choosing between using a pyranometer or a reference cell, it is important to consider the intended use of the resulting irradiation data. If the yield of the PV system is to be compared with other systems, a pyranometer is the best option. If the use of the irradiation data only is for monitoring of the PV system, then a reference cell is a good choice.

Sammendrag

Hovedtemaet for denne masteroppgaven er overvåkning av bygningsmonterte solcellesystemer i Norge. Overvåkning av solcellesystemer kan gi verdifull informasjon om ytelsen til et system og varsle om det oppstår feil på systemet. Hovedutfordringen med overvåkning av solcelleanlegg er at mange anlegg mangler målinger av meteorologiske data. Denne oppgaven fokuserer på innstrålingsdata og undersøker muligheten for å bruke innstrålingsdata fra andre nærliggende datakilder til bruk i analytisk overvåkning av solcellesystemer.

Et utvalg av tilgjengelige kilder for innstrålingsdata i Osloområdet er undersøkt. De utvalgte kildene er et solcellesystem instrumentert for metrologiske målinger på Økern sykehjem, en meteorologisk målestasjon på Blindern og en meteorologisk målestasjon på Ås. Data fra to forskjellige databaser er undersøkt og sammenlignet med de målte verdiene for innstråling. Databasene undersøkt i denne oppgaven er PVGIS og NASA SSE. Databasene er basert på satellittdata midlet over en gitt periode.

De forskjellige kildene for innstrålingsdata er sammenligner for referanseåret august 2015 til august 2016. Formålet med sammenligningen er å undersøke muligheten for å bruke innstrålingsdata fra andre kilder når innstrålingsdata mangler for solcellesystemet. Utfordringene med å sammenligne innstrålingsdata viste seg underveis i oppgaven. Spesielt de forskjellige metodene for å måle innstråling er diskutert. I denne oppgaven er innstråling fra pyranometer og referansecelle vurdert. Horisontal innstråling målt med et pyranometer gir et bedre sammenlikningsgrunnlag enn innstråling målt i modulplanet. Innstråling målt i modulplanet med en referansecelle kan variere med viklingen på referansecellen, hvilken himmelretning referansecellen har og hva slags materiale den er laget av.

Oppgaven undersøker et anlegg på Kjeller, som ikke er instrumentert for måling av meteorologiske data. Dette systemet består av moduler av to forskjellige solcelleteknologier, CIS og silisium. Undersøkelsene gjort i denne oppgaven viser at CIS-modulene har en høyere spesifikk ytelse enn silisiummodulene, selv om silisiummodulene er spesifisert med høyere virkningsgrad enn CIS-modulene.

Denne oppgaven konkluderer med at måling av meteorologiske faktorer er nødvendig for analytisk overvåkning. Innstråling fra andre kilder kan være vanskelig å bruke grunnet avstand mellom kildene og ulike måter å måle innstråling på. Ved valg av metode for å måle innstråling er det viktig a vurdere hensikten med målingene. Skal solcellesystemets ytelse sammenlignes med andre systemer er pyranometer det beste alternativet. Om innstrålingsdataene kun skal brukes til overvåkning, er referansecelle et godt alternativ.

Nomenclature

Abbreviations	**Exploration**
AC	Alternating current
AM	Air mas
BAPV	Building attached photovoltaics
BOS	Balance of system
CIS	Copper indium selenide
CIGS	Copper indium gallium selenide
CSV	Comma-separated values
DC	Direct current
IR	Infrared
LID	Light Induced Degradation
MPP	Maximum power point
MPPT	Maximum power point tracker
NOCT	Nominal operating cell temperature
PR	Performance ratio
PV	Photovoltaic
STC	Standard test conditions
UV	Ultraviolet
c-Si	Crystalline silicon
OC	Open circuit
SC	Short circuit

A	Cross section, m^2
E_c	The conduction band
E_g	The band gap energy, eV
E_{light}	Energy of the light reaching the module, eV
E_v	The valence band
G_{diff}	Diffuse irradiation, W/m^2
G_{dir}	Direct irradiation, W/m^2
G_{global}	Global irradiation, W/m^2
G_{mp}	Irradiation in the module plane
G_{ref}	Reflected irradiation, W/m^2
G_{sc}	The solar constant, W/m^2
G_{STC}	Irradiation corresponding to STC, W/m^2
I	The total current for the equivalent circuit, A
I_d	The current through the diode, A
I_{light}	The light induced current, A
l	Length, m
R_{cable}	Resistance, Ω
r	Radius, m
V	Voltage, V
P	Power, W

α_s	The solar altitude angle
β	The module slope
ρ	Specific resistivity, $\Omega \cdot m$
θ_z	The zenith angle
σ	Specific conductance, $(\Omega \cdot m)^{-1}$
γ	The surface azimuth angle
γ_s	The solar azimuth angle

Contents

1. Introduction

1.1 Motivation

The PV industry is a part of "The Green Shift", the transition from fossil fuels to sustainable, renewable energy sources. The PV industry continuous to grow worldwide. The installed power is increasing and the prices continuous to decline. 53 GW of PV energy was installed globally in 2015. Analysis estimates that between 61 GW and 74 GW will be installed globally in 2016. The module pricing has been reported to be between $0.40/W and $0.50/W in the second half of 2016, and still decreasing. [1]

The entry of the PV technology into the commercial energy marked requires knowledge about the performance and reliability of the different technologies. This knowledge is valuable when considering the financial factors, business models and the impact of PV systems connected to the grid. Silicon based PV systems are the ones dominating todays marked, but numbers of other technologies have made their entry. The PV technologies are specified under standard test conditions (STC). The testing under STC gives a basis for comparison of the different technologies. The real conditions will off course differ from the STC and the different technologies will behave differently under these varying conditions.

To be able to say something about the performance and sustainability of the PV systems under real conditions, analytical monitoring over a longer period is necessary. Analytical data demands parallel measurements of meteorological data at the PV site and production data from PV systems inverters. Analytical monitoring gives valuable information about the performance and sustainability of the system, but can also alert if failures of the system occurs. When failure occurs in a PV system is it important with knowledge of the degree of error. A PV system with a failure of important character can highly reduce the total yield if not mended in short time.
A study of failures for residential grid-connected PV systems of 1-5 kW_p installed in Germany in the 1990's [2] showed that statistic failure happened every 4.5 years per plant. For the total failures were 63% caused by the inverters, 15% by the PV modules and 22% by other components of the system. The performance ratio (PR) of PV systems has increased from 0.50-0.70 in the 1980's, to a typical value over 0,80 nowadays [3]. Monitoring of PV systems has contributed to this increase in PR.

The PV industry in Norway follow the global trends. 2,45 MW of building attached photovoltaics (BAPV) was installed in 2015. This is an increase of 10% compared to 2014, when 2.2 MW was installed. The average price for a PV system in Norway in 2015 was 18 NOK/W for systems under 10 kW and 15 NOK/W for systems between 10 kW and 100 kW. The prices are exclusive the value-added tax. [4] The monitoring of PV systems in Norway is almost non-existent, or at least not well documented. Since the climate in Norway tends to differ from the typical PV site (especially with available irradiation in mind) is monitoring of PV system under these conditions highly interesting and relevant. This thesis will study the

challenges of real time monitoring of BAPV in Norway. This is a comprehensive issue, so the thesis is limited by the attempt to answer the problem statements listed below.

1.2 Thesis outline

The original idea for this thesis was to do analytical monitoring of a PV system located on the roof of Økern nursing home in Oslo. The PV system is well equipped for measuring local meteorological factors and has 25 string inverters connected to the PV system on the roof. This gives a lot of good parameters for monitoring. The meteorological data has good resolution and is easily available on a web user interface. This thesis started with analyzing meteorological data from Økern and to get a good overview of the design of the PV system. Unfortunately, it was difficult to get access to the inverter data and this process took over two months. These data were not easily available at a web user interface as the meteorological data, but were available in a CSV-format with three files of approximately 500 kB each representing one day. Unfortunately, no one could give information about the numbers in the CSV-files either. To sort this data and get some useful information were demanding the use of programming scripts. This was considered not possible considering the time left of the semester.

The meteorological data at Økern were used as basis for the study of meteorological data. To prevent more delays from collection of data, a PV system at Økern were used as a source of inverter data.

This thesis is divided into

- Chapter 1 introduces the thesis, the motivation for the work done in this thesis and gives an overview of the problem statements.
- Chapter 2 provides the reader with all the necessary theoretical prerequisites required for reading this thesis along with some recommended literature.
- Chapter 3 gives the methodology used in this thesis. This chapter explains the methods and sources for collecting data for the analysis of the thesis.
- Chapter 4 provides the results of the analysis. The discussion of the results is presented together with the results for a more orderly overview for the reader.
- Chapter 5 gives the conclusion drawn to the problem statements of the thesis.
- Chapter 6 presents further works to be conducted for the field of the thesis.
- Chapter 7 is listing the stated references sited.

1.3 Problem statements

- What are the available sources of irradiation data for a PV system in Oslo, Norway?
- How much does this irradiation data differ from each other?
- How is irradiation measured and how do the different methods differ from each other?
- Is it possible to use irradiation data from other sources, when local data are not available at the PV site?
- What is the error of replacing missing data points with existing data points from other sources?
- What is possible to say about a PV systems performance without local meteorological data, but only with access to inverter data?
- What is the result of using meteorological data from other locations for a PV site without local meteorological data?

1.4 Recommended literature

The listed literature below will give valuable prerequisite knowledge related to the topic of this thesis.

- Smets, A., Jäger, K, Isabelle. O., Van Swaaij, R. & Zeman, M. (2016). Solar Energy.The Physics and Engineering of Photovoltaic Conversion Technologies and Systems. England, UIT Cambridge Ltd.
- Duffie, John A., Beckman, William A. (1980) Solar Engineering of Thermal Processes. Canada, John Wiley & Sons, Inc.
- International Energy Agency. (2014). Analytical Monitoring of Grid-connected Photovoltaic Systems. Good Practices for Monitoring and Performance Analysis. Report, IEA-PVPS T13-03:2014. 75 s.
- Honsberg, C & Bowden, S. The Photovoltaic Education Network. http://pveducation.org

2. Theoretical Prerequisites

2.1 The Sun and properties of light

The Sun, as an energy source, is the most important basis for life on earth. The total power from the Sun is $3.8 \cdot 10^{26}$ W [5]. The world's total energy consumption was in 2014 estimated by the International Energy Agency to be $18 \cdot 10^{12}$ W, for comparison [6]. The Sun consists mainly of hydrogen and helium, and in its core the high temperature and pressure causes nuclear fusion. From the nuclear fusion, we get electromagnetic radiation [5]. The Sun radiates in the spectrum from short wave radiation as gamma rays with wavelength shorter than 10^{-11} m, to long wave radiation as radio waves with wavelength longer 10^{-1} m.

A typical photovoltaic cell only absorbs and utilizes the energy from near UV, through the visible light into the near IR parts of the spectrum [7]. The energy from the solar spectrum is utilized in solar cells to produce electrical power.

2.2 The Sun-earth relationship

If one looks at the energy from the Sun as a moving circular plane heading towards the Earth, the energy is distributed on a circle with the area of πr^2. When reaching Earth, the same amount of energy must be distributed around Earth with an area of $4\pi r^2$, as illustrated in Figure 1.

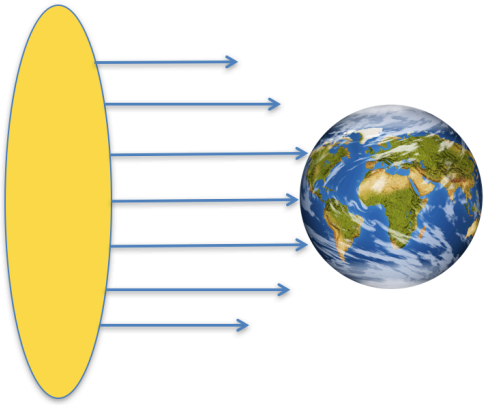

Figure 1: The distribution of the solar energy on Earth.

The irradiation outside the Earth's atmosphere is called the solar constant, G_{SC}, and its value is 1367 W/m^2 [8]. The solar constant is the irradiation value for the mean distance between the Earth's atmosphere and the Sun, on a plane perpendicular to the direction of the Sun [5] and is illustrated in Figure 2.

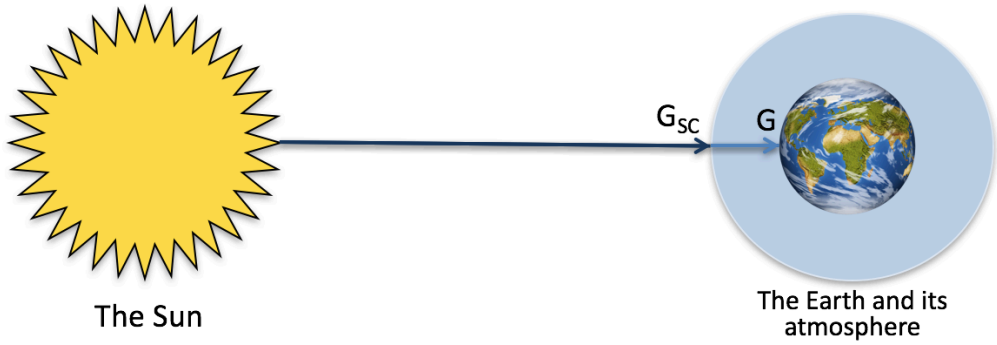

Figure 2: An illustration of the solar constant.

On its way through the atmosphere the light from the Sun is attenuated and the result is that the irradiation on Earth varies in power and spectral distribution. The reason for this attenuation is that the light is scattered, absorbed and reflected by gasses, dust, and aerosols. The gases H_2O, O_2, CO_2 and O_3 all absorb different parts of the solar spectrum. Because of this attenuation the total irradiation on a location on earth consists of direct irradiation, G_{dir}, diffuse irradiation, G_{dif}, and reflected light from the surroundings, G_{ref}. The global irradiation G_{global} is the sum of G_{dir} and G_{diff}. Figure 3 illustrates the total irradiation on a PV module.

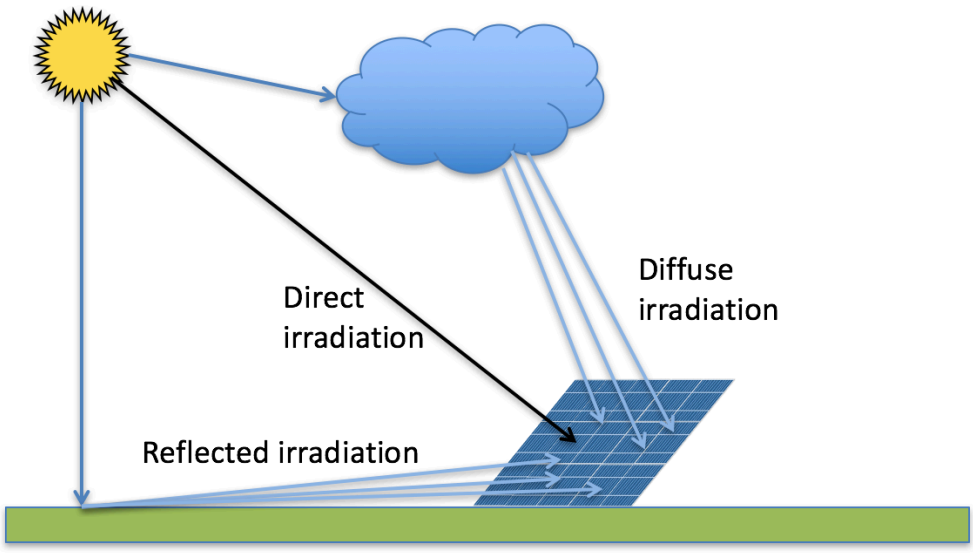

Figure 3: A solar panel receives direct, diffuse and reflected irradiation.

On Earth the irradiation value is not constant, but varies due to several reasons. The Earth's orbit around the Sun has an elliptic path, and is illustrated in Figure 4. The elliptic path together with the fact that the Earth is revolving around itself is the reason for the daily and seasonal variation in the solar irradiation on Earth. Yearly radiation also varies because the Earth doesn't follow the exact same orbit every year. The Earth is tilted 23.45° relative to the perpendicular plane on the Earths orbital plane [7]. The tilt and Earths spherical form is also a reason that the irradiation on the earth's surface is varying with the latitude. The Earth's tilt and its path around the Sun are illustrated in Figure 4.

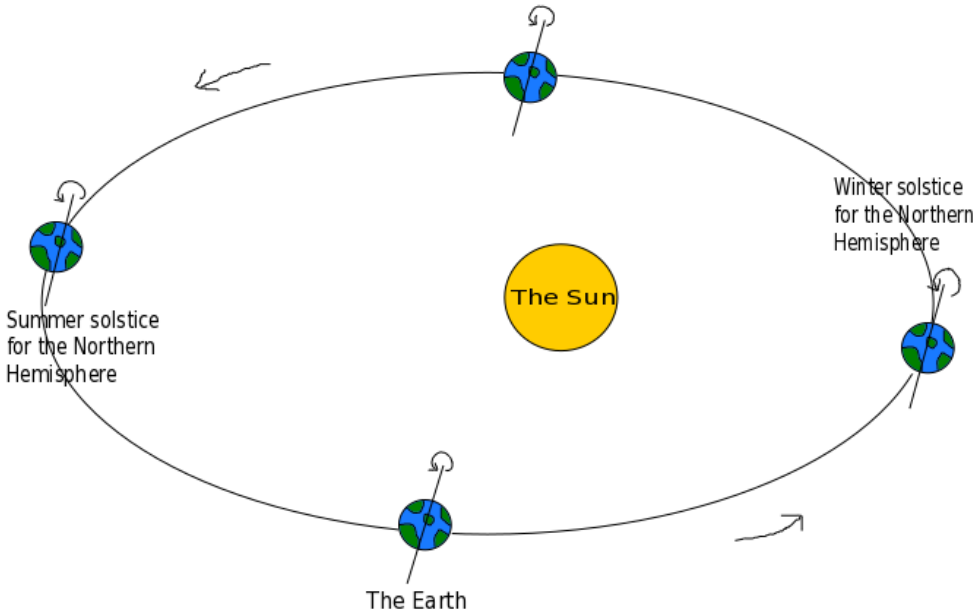

Figure 4: The Earth's orbit and tilt.

Air Mass (AM) is a term used to express the path that the light travels through the atmosphere. AM is relative to the shortest possible path, where the Sun is in Zenith [7] and is illustrated in Figure 5. The Sun is in Zenith when the Sun is in the position normal to the horizontal plane. The amount of atmosphere that the light has to traverse increases when the Sun moves away from Zenith. The value for AM can be calculated by the following formula

$$AM = \frac{1}{\cos(\theta)} \tag{1}$$

where θ is the Zenith angle.

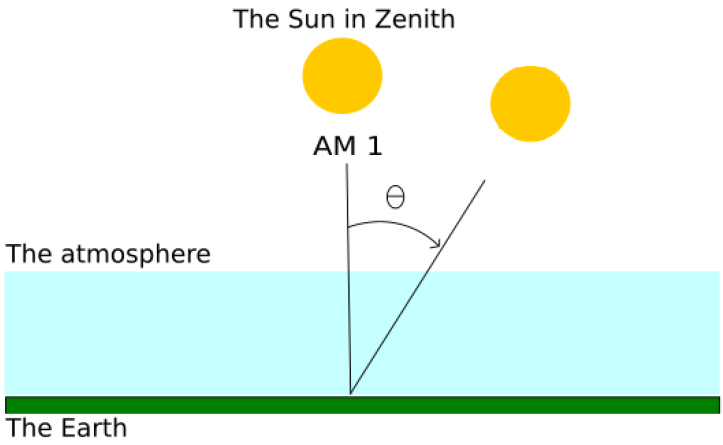

Figure 5: The Sun in Zenith and the position of the Sun relative to the zenith angle with a displacement θ. Figure inspired by [3].

The value for AM is therefore varying with the position of the Sun during the day. When the Sun is in Zenith, AM is 1 [7]. The Sun's position during the day is described in the following section and is illustrated in Figure 6. The relevant angles for a solar panel are also illustrated in the same figure. Figure and definitions are inspired by [8].

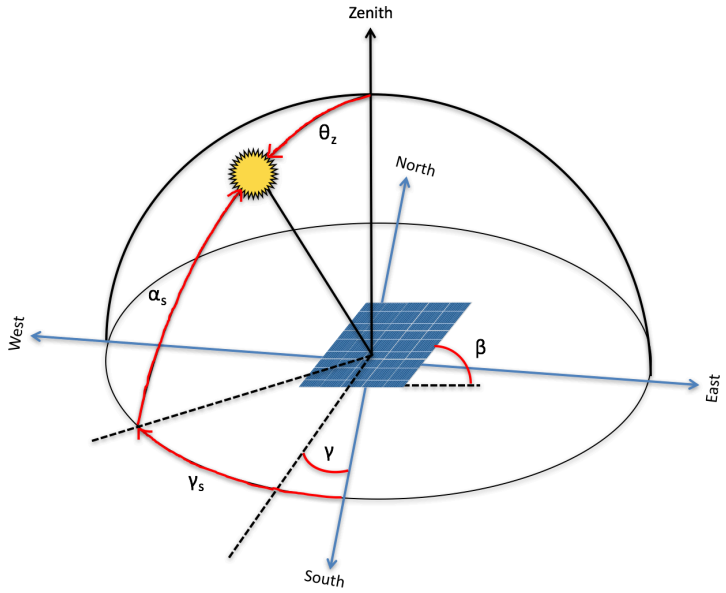

Figure 6: The angles that describe the Sun's position during the day. The relevant angles for the mounting of the solar panel are also illustrated.

In the northern hemisphere, the Sun rises in the east and sets in the west. The solar azimuth angle γ_s, describes the angular displacement from the south of the projection of beam radiation on the horizontal plane. Displacements east of south are negative and west of south

are positive. The solar altitude angle α_s, describes the angle between the horizontal plane and the line to the Sun. The Zenith angle is illustrated as θ_z. The surface azimuth angle γ, describes the deviation of the projection on a horizontal plane of the normal to the surface, with zero due south, east negative, west positive and $-180° \leq \gamma \leq 180°$. The slope β, describes the angle between the module and horizontal plane.

The radiation on a module varies with the angle of the module relative to the horizontal plane. For a city like Oslo in Norway, which is located approximately 59° north of the equator, a module with the slope of approximately 37° will achieve maximum radiation during the year [7].

2.3 Working principle of the solar cell

The following section gives a brief overview of the working principle for a solar cell. The working principle of a solar cell is based on the photovoltaic effect. The contents of Chapter 2.3 and the figures are inspired by [5].

2.3.1 Properties of Silicon

A solar cell consists of semiconducting materials. The most common material used in solar cells today is crystalline silicon (c-Si) [7]. The c-Si can be either mono- or polycrystalline silicon. Monocrystalline silicon has the best efficiency, but the polycrystalline silicon is cheaper to produce. Silicon has atom number 14, is in group four in the periodic table and therefore has four valence electrons. These four electrons make up a crystal structure and forms covalent bonds, as illustrated in Figure 7 to achieve eight valence electrons.

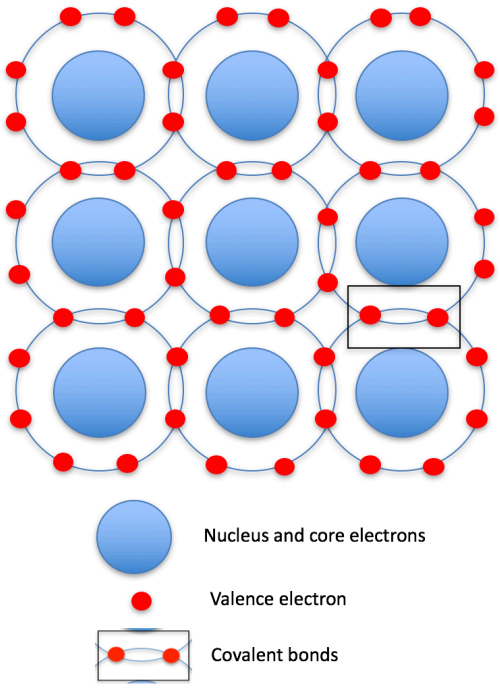

Figure 7: Crystal structure of Silicon. The nucleuses share electrons, forming covalent bonds and hence achieving eight valence electrons.

2.3.2 Doping of the solar cell

The silicon is then doped with materials from group three and five, which have three and five valence electrons respectively. The doped material is illustrated in Figure 8 and Figure 9. Most common is boron (B) from group three and phosphorus (P) from group five. When doped with materials from group three, the material has seven valence electrons and is missing one electron to achieve eight valence electrons. An electron is denoted e^- because it has a negative charge. The silicon is now a positive doped (p-type) material because of the missing electron. We say that the material has excess of "holes", and the holes are the majority charge carriers in the p-type material. The silicon doped with materials from group five gets nine valence electrons and an excess of electrons. The silicon is a negative doped (n-type) material because of the excess electrons. In n-type materials, the electrons are the majority charge carriers. The doped materials are then combined and form a metallurgical junction.

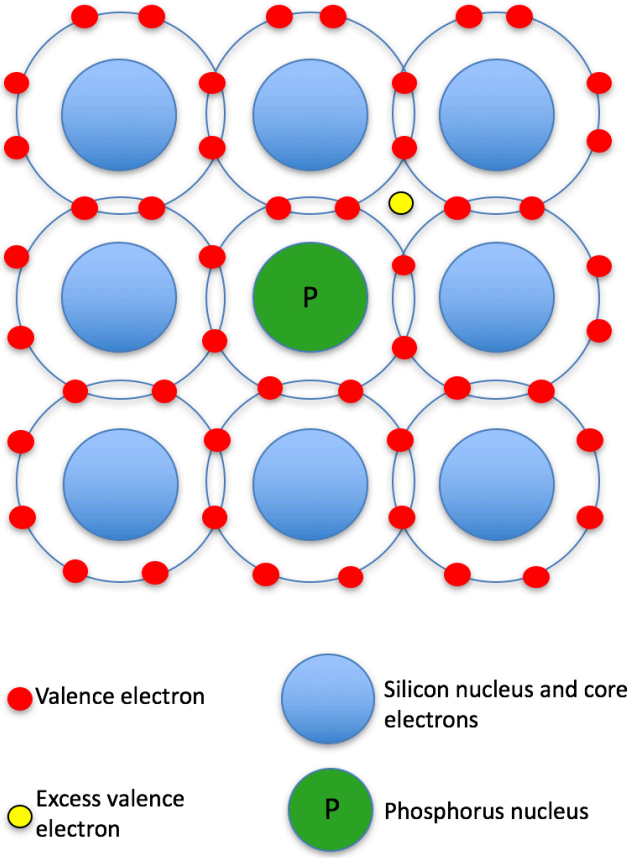

Figure 8: Silicon doped with Phosphorus from group five resulting in an excess valence electron.

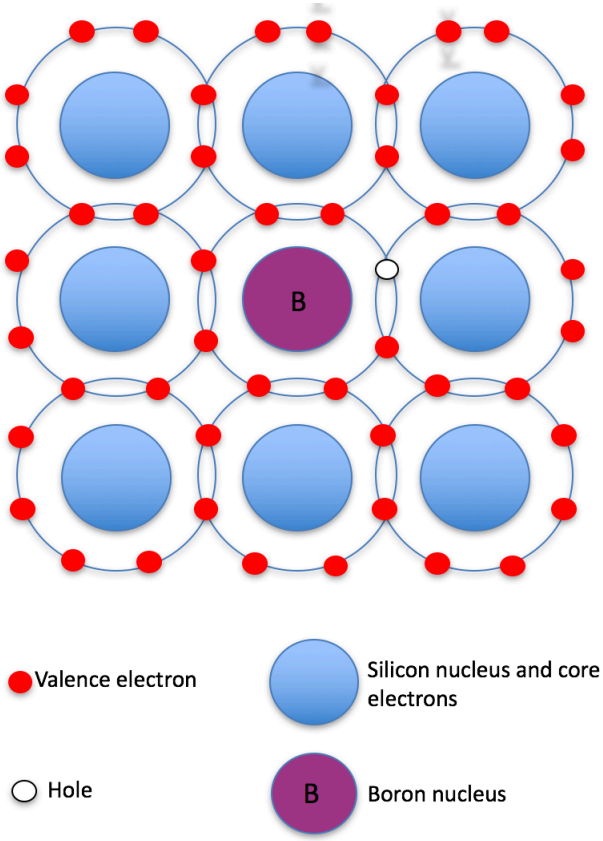

Figure 9: Silicon doped with Boron from group three resulting in one less valence electron and a hole in the crystal structure.

Because of the difference in concentrations of electrons and holes in the two materials, we get diffusion across the layers. The diffusion of holes in one direction and electrons in the other direction causes a diffusion gradient across the layers and a depleted region where there are almost no charge carriers. This is illustrated in Figure 10. In this area, an electric field is made, which works in the opposite direction of the diffusion gradient. These two effects will eventually equalize each other, there is no transport of charge carriers and the junction is in equilibrium. The electrons are now in their bound state and have a potential to conduct. It is first when the material is illuminated that the conduction of electrons can be used to produce energy, as we do with a photovoltaic system.

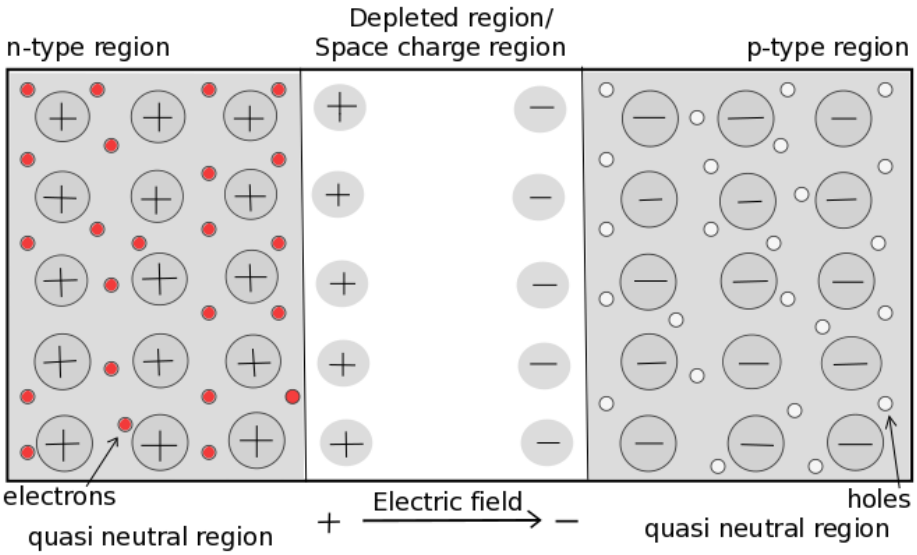

Figure 10: Illustrating the depleted region created between the doped materials caused by diffusion of holes and electrons and the opposite electric field caused by charge difference.

2.3.3 The band gap energy

The electrons in the silicon have a band gap energy, E_g, which is illustrated in Figure 11. E_g represents the energy necessary to release the electrons from its bound state in the valence band.

If the energy from the Sun absorbed in the material, E_{light}, is large enough to exceed the bandgap energy, the electron is excited from the valence band, E_v, to the conduction band, E_c, leaving a hole in the valence band. We say that the electron is excited from its bond state. If E_{light} is smaller than E_g, the energy will traverse the material. If E_{light} exceeds the bandgap energy the excess energy will convert to thermal energy.

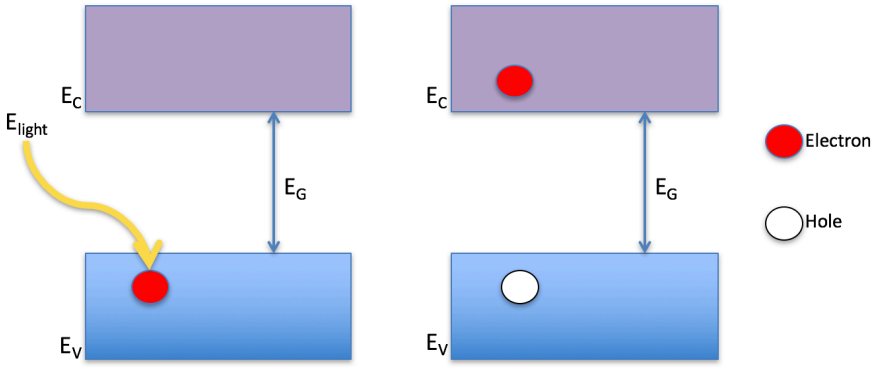

Figure 11: Illustrating the bandgap of an electron. The blue area is the valence band of the electron. The purple area represents the conduction band. The electron gets excited by the energy from the illumination and moves from the valence band to the conduction band, leaving a hole in the valence band.

2.4 The photovoltaic system

2.4.1 The composition of the solar cell

A silicon solar cell is made from a silicon wafer which is approximately between 100 and 300 µm thick [5]. Together with the silicon wafer there is back and front contacts, serial connections for connection to the next cell and antireflective coating.

The illuminated solar cell behaves as an ideal diode and can be described schematically with the equivalent circuit as in Figure 12.

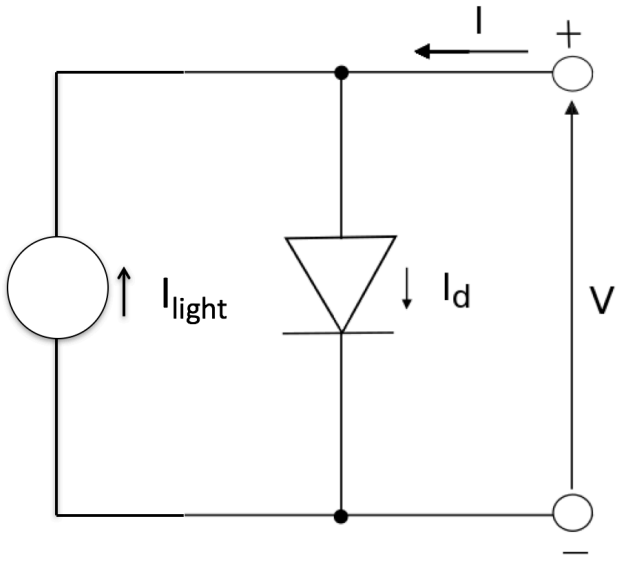

Figure 12: The solar cell as an equivalent circuit. I_{light} is the light induced current, I_d is the current through the diode, I is the total current of the circuit and V is the voltage across the cell.

2.4.2 The Modules

Several solar cells connected makes up a module, several modules connected makes up a panel and connected panels makes up an array, as illustrated in Figure 13. Most common is to connect the cells, modules and panels in series. When connecting cells in series the total current will be the same, while the total open circuit voltage is the sum of all the cells. The total current is the sum of the current in all the cells, while the open circuit voltage is the same when connecting cells in parallel.

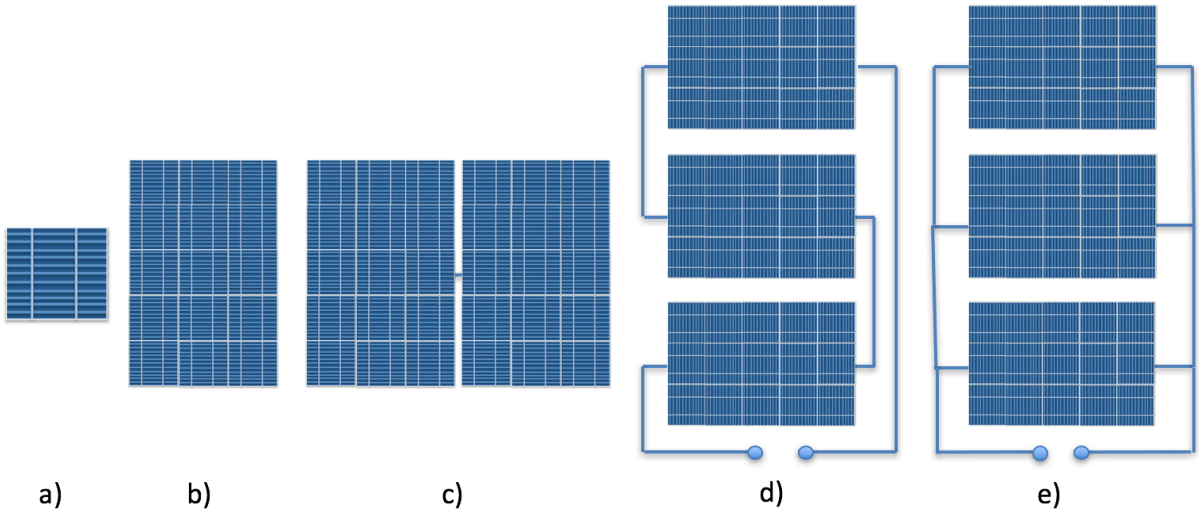

Figure 13: A cell (a), a module (b), a panel (c). Several panels connected together makes an array, here connected in series (d) and parallel (e).

2.4.3 The components of the photovoltaic system

The complete photovoltaic system consists of several components in addition to the modules. These are called the balance of system (BOS). We differentiate between grid connected systems and stand-alone systems. The stand-alone systems, or off-grid systems, often have a form of energy storage, but can also consist of only a module connected with a load. This thesis will only look at grid-connected systems. This type of system is illustrated in Figure 14. The most important BOS' for a grid-connected system are described below.

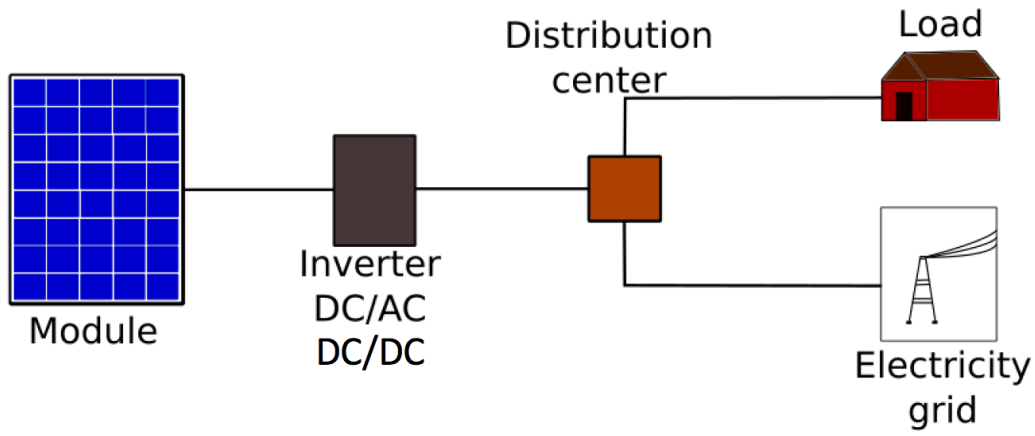

Figure 14: Illustration of the main components of a photovoltaic system.

Mounting structure

The mounting structure is the framework of the system. The panels are mounted on the framework and fixed in the optimal direction. They're often made of steel or aluminum.

DC-DC converters

The output voltage from the module varies and the DC-DC converters are used to convert the varying output voltage, so that the input voltage for the DC-AC converter is constant. The DC-DC converter also sets the operating point for the Maximum Power Point Tracker [5].

Maximum Power Point Tracker (MPPT)

The MPPT is not an actual component itself, it is a technique incorporated in the inverter. The MPPT is always connected to the DC-DC converter or a charge controller [5]. The MPPT optimizes the system so that it gets maximum output power. To find this point there are necessary to study the *I-V* curve and characterization of the modules.

The solar cell is characterized by an *I-V* curve, which is illustrated in Figure 15. On the *I-V* curve, the voltage and current are plotted. This curve is illustrated together with the corresponding *P-V* curve, where the voltage and power are plotted. On these curves the maximum power point (MPP) can be observed. The MPP is the point on the *I-V* curve that results in the maximum power output. The MPPT is finding the MPP either by indirect or direct maximum power point tracking. Indirect tracking estimates the MPP by using algorithms and direct tracking uses the actual *I-V* data [5].

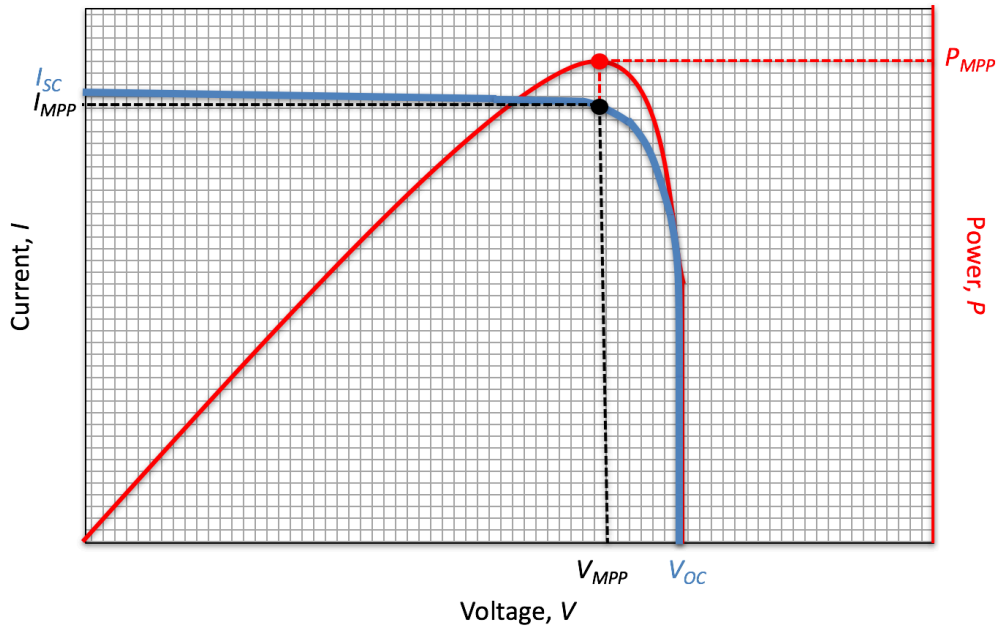

Figure 15: Illustrating an I-V and P-V curve. The operating points of the cell for the current and voltage are marked by the circles with an arrow. P_{MPP}, V_{MPP} and I_{MPP} are the output power, the voltage and the current for the maximum power point respectively. V_{oc} is the open circuit voltage and I_{sc} is the short circuit current. The MPP for the cell is marked on the P-V curve together with the associated point on the I-V curve.

Cables

A good cable structure is it necessary to connect the modules to the inverter and further to the loads and the grid. The cables have a resistance which leads to resistive losses given by formula 2:

$$P_{cable} = I^2 R_{cable} \tag{2}$$

where I is the current and the resistance in the cable, R_{cable} is given by

$$R_{cable} = \rho \frac{l}{A} = \frac{1}{\sigma} \frac{l}{A} \tag{3}$$

where ρ is the specific resistivity, σ is the specific conductance or conductivity, l is the length of the cable and A is the cross section of the cable [5].

For the cables in a PV system is it important that the system is designed to minimize the resistive losses.

DC-AC converter

Description and figures for this section are inspired by [5]. Converters are often called inverters. The term inverter is used for both the DC-AC converter and all the components for an actual power converter. It is possible to extract output data for the system from the inverter.

There are different types of inverters, all depending on their application. Four types of inverters are illustrated in Figure 16; the central inverter, the micro inverter, the string inverter and an inverter with optimizers.

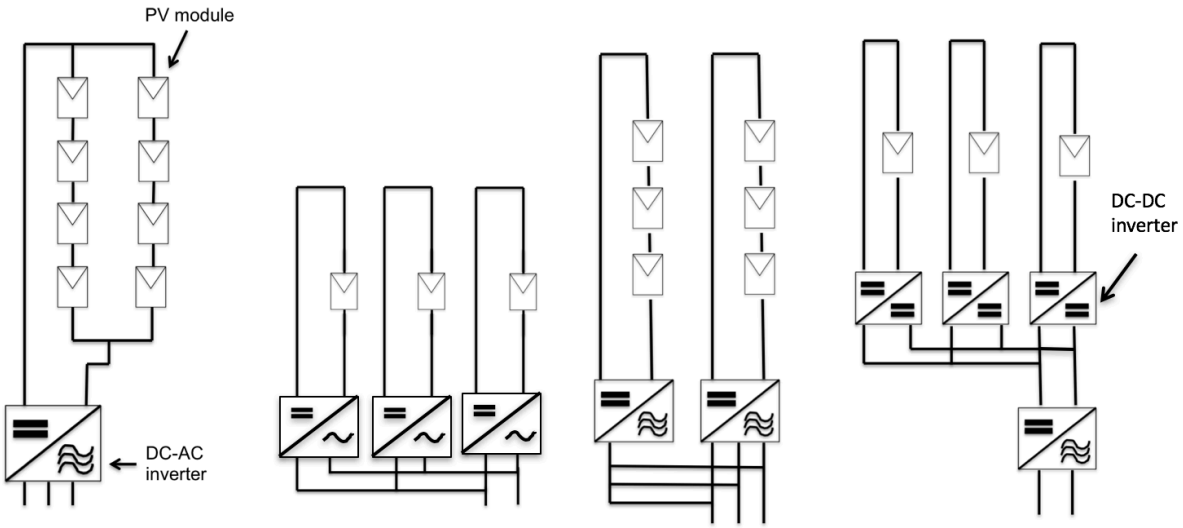

Figure 16: Illustrating (a) the central inverter, (b) the micro inverter, (c) the string inverter and (d) an inverter with optimizers. Inspired by [5].

The central inverter is used in large-scale PV systems. Several modules are connected in series, forming a string. These strings are connected in parallel forming an array. This array is connected to a central inverter. The central inverter has a low specific cost and has only few components, which make it easier to maintain. Though the central inverter also has some disadvantages. This type of inverter leads to a transferring of large amount of power and more insulation is required which leads to higher costs. Mismatch losses in the modules occur since they all need to operate at the same MPP and hence are limited by the lowest MPP. The mismatch losses will lead to a reduction in power output for the system. Also, it is difficult to extend the system in the future.

The micro inverter operates directly on the modules. It is more expensive to have one inverter on every module, but it is easier to increase or decrease the size of the system in the future. Because the inverters are directly mounted on the modules, they should be robust enough to operate in challenging weather condition.

The string inverter is combining the advantages of the central inverter and the micro inverter. As for the central inverter, the string inverter achieves high DC voltage. This inverter is often operating on small systems as systems mounted on private houses or office buildings. Each string has its own MPP and the mismatching losses decrease.

The central inverter with optimizers is a hybrid between a central inverter and a micro inverter. It has a box attached which contains a MPPT and a DC-DC converter and optimize the power output. Every module can operate at its own MPP to decrease mismatch loss.

2.5. Parameters that affect the solar cell and the PV system

There are several factors influencing the photovoltaic system and these factors are in each way affecting the efficiency of the system. Knowledge of these factors' impact on the system is important to achieve the best efficiency. For silicon, efficiencies of 26.3 % has been achieved in laboratories [9]. For commercial silicon solar cells, the efficiency is in the range from 16% to 24% [10]. Both for laboratory cells and commercial cells these maximum efficiencies are improving. Figure 17 is a simple illustration of the losses related to a PV system.

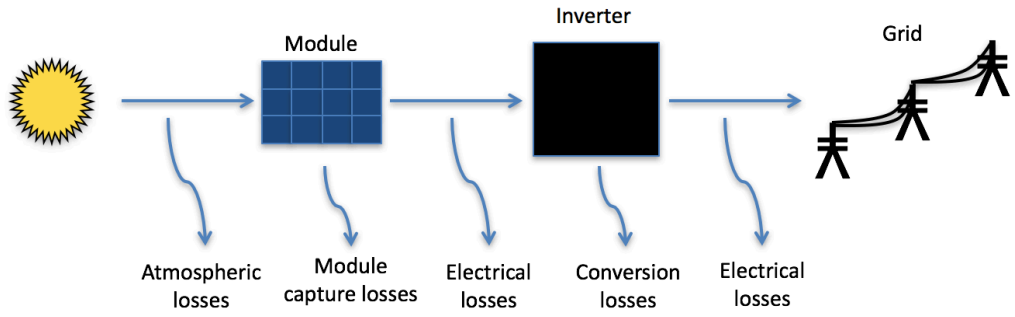

Figure 17: The losses related to a PV system.

2.5.1 Optical losses

Not all the irradiation on a solar cell can be exploited. The incident light on the absorption layer can be reflected, absorbed or transmitted as illustrated in Figure 18. It is only the absorbed light that can lead to the generation of electron-hole pair. The amount of absorbed irradiation depends on the properties of the material in the cell. To decrease the losses, it is possible to use antireflective coating, to texture the surface to reduce the reflection and to increase the absorption. For a polished silicon surface the reflection is over 30% [7].

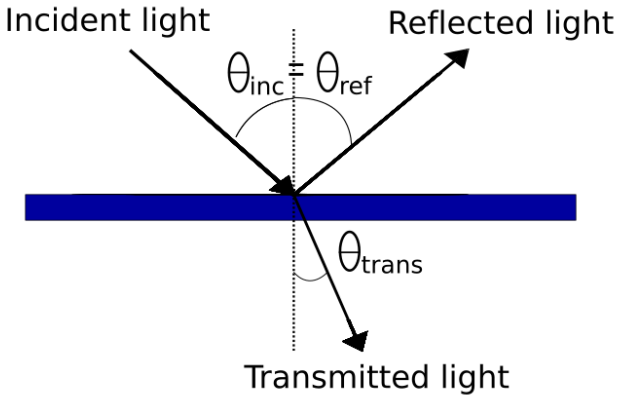

Figure 18: Illustrating incoming light on a surface. Some of the light will be reflected and some will be transmitted. The ratio of reflected and transmitted light depends on the properties of the surface.

2.5.2 Spectral mismatch

When the incident light is absorbed in the cell, not all of it is exploitable. As mention in section 2.3 the photon energy needs to match the cells band gap energy. If the energy of the photons is larger than the band gap energy, the electron will be excited and the excess energy will lead to thermalization. The photon will traverse the absorptive layer if the photon energy is smaller than the band gap energy and the unexploited energy will lead to thermalization. The losses due to spectral mismatch for crystalline silicon are approximately 50% [5]. To minimize this type of loss is it possible to use multi junction cells. These cells consist of two or several different semiconducting materials with different band gap. Each of the different semiconducting material can exploit different areas of the spectra.

2.5.3 Recombination and collection losses

When the energy of the photons has generated electron-hole pairs there is a chance that an electron could recombine with a hole before they can be exploited in a circuit. There are several types of recombination; direct recombination which occur when the cell is thicker than the diffusion length of the charge carriers , Shockley-Read-Hall recombination which occur due to impurities or lattice effects, Auger recombination which is a three particle process in indirect semiconductors (for indirect semiconductors there is also necessary with a change in momentum to move from the valence band to the conduction band) where the recombined electron and hole transfer their energy and momentum to another electron or hole, and surface recombination which occur in the surface of the semiconductor where the lattice of the silicon ends [5]. If the charge carriers don't recombine they also must be collected by the electrodes in the cell before they can contribute to conduction.

2.5.4 Quantum efficiency

The quantum efficiency is "the ratio of the number of carriers collected by the solar cell to the number of photons of a given energy incident on the solar cell" [7]. We can divide this efficiency in external and internal quantum efficiency. The external quantum efficiency includes what happens outside the solar cell, such as the optical losses. The internal quantum efficiency is only dealing with the photons that get absorbed in the solar cell.

2.5.5 Degradation

During its lifetime, a module will have a decrease in efficiency. This decrease is due to both the first expose of light and due to aging. The degradation of the first hour of exposition is called Light Induced Degradation (LID) and is approximately 1-3% [11]. The average degradation due to aging during the lifetime of the modules is caused by weather and possible damages to the module. This value is approximately 20% during the lifetime of the modules, or 0.8% per year [11]. It is normal that the manufactures give a warranty of 25 years for the modules, but many modules will have a potential for a lifetime of several more years. It is difficult to give an estimate of the lifetime of the modules, since the majority of the installed PV modules today have not exceeded their warranty period.

2.5.6 Mismatch losses

Mismatch losses of modules occurs when the modules have different properties or are experiencing different conditions [7]. In a worst-case scenario, the module efficiency can be limited by the module with the lowest current. Mismatch losses accounts for a considerable part of the system losses and a power loss of approximately 10% has been observed [12].

2.5.7 Shading of the modules

Shading is an example of an event where mismatch losses occur. There are two types of shading; near and far shading. Near shading occurs when near objects draw visible shades on the PV field or if something covers up the cell. Far shading is due to the horizon line. The simulation program PVsyst defines far shading as shading from objects located more than ten times the PV field size away from the PV system [11]. Shading of the cells in the modules could have an extreme impact on both the shaded cells and the total power production. Figure 19 a) illustrates a string of six cells in connected in series, where the first one is shaded by a leaf. The shaded cell will receive less irradiation and the whole string will be limited by the current produced by the shaded cell. The rest of the five cells will now act as a reverse bias source on the shaded cell and energy will dissipate energy in form of heat in the shaded cell. This case where heat is generated in a cell is called “hot spots”. These can lead to damages on the cell and lower power production due to higher temperature in the string.

The challenge with shaded cells can be solved by using bypass diodes, either over each cell as illustrated in Figure 19 b), or one bypass diode over a string of cells. The bypass diodes have a small resistance and the current will choose the path with less resistance, through the bypass diode. The bypass diode is conducting only in one direction and blocking flow of the current in the other. As illustrated in Figure 19 b), the bypass diode will lead the current past the shaded cell.

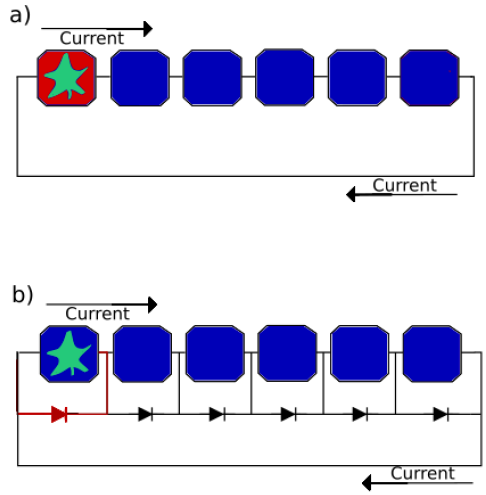

Figure 19: The illustration of the use bypass diodes. Figure a) has no bypass diodes and heat will dissipate in the shaded cell. The diode will lead the current past the shaded cell in figure b).

2.5.8 Temperature dependency

The module temperature has an impact on the efficiency of the system. The current will increase when the module receives more irradiation and the MPP will increase. The irradiation will thus lead to the increase of the module temperature. This leads to the decrease in efficiency of the module. This is illustrated in the *I-V* curve in Figure 20 where the current is slightly increasing, but this effect is completely assessed by the fact that the voltage is decreasing.

Higher temperature can also lead to damage on the module because of the expansion of materials with higher temperature. In Central Europe, on a clear summer day and a value of 1000 W/m^2 for the irradiation, the module temperature can reach 60°C [13]. A study [14] of 18 grid connected PV systems in Europe showed an annual loss due to module temperature of 1.7% to 11.3%.

The dependence of the different PV technologies varies. The variation is listed in the specifications as the Temperature coefficient. This coefficient is given in %/°C and describes the percentage reduction for the module output when the nominal operating cell temperature (NOCT) increases with one degree. The NOCT are defined [7] as the temperature reached by open circuited cells in a module under the following conditions

- Irradiation = 800 W/m2
- Air temperature = 20 °C
- Wind velocity = 1 m/s
- Mounting = open back side

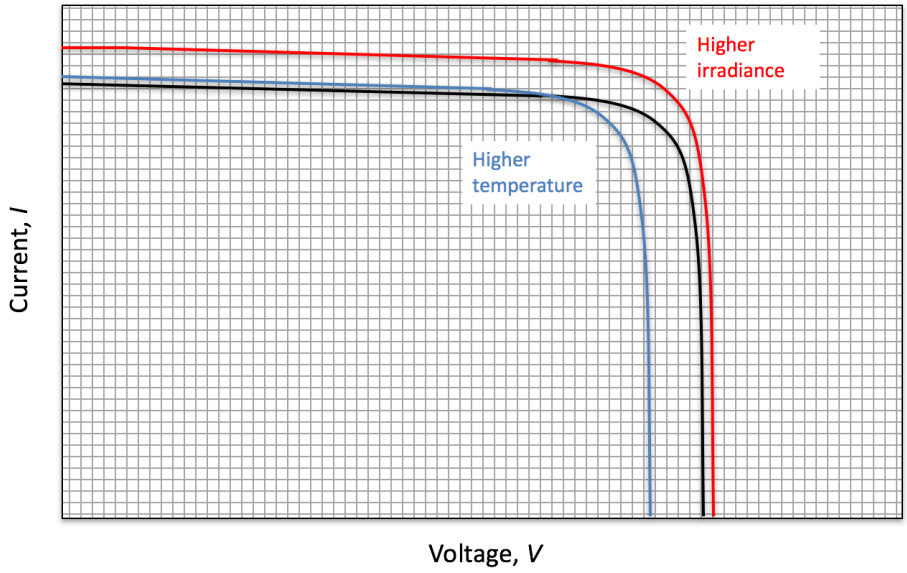

Figure 20: Illustrating the effect of higher irradiation and temperature on a solar cell. Inspired by [5].

2.5.9 Wind
Wind has a positive effect on the system. The cooling effect has been reported to be as much as 15 to 20°C [13]. The cooling effect can assess a part of the negative effect that the increase in temperature has on the system.

2.5.10 Soiling and snow
Soiling has an impact on the system because it covers up the modules and prevent the irradiation. Soiling is caused by dust and particles on the module surface. Rainfall will often be sufficient to clean the modules.

Snow is also a type of soiling. Snow cover in the surroundings of the PV system can have a positive effect on the amount of irradiation on the modules because the snow has a high albedo and thus reflects the light.

2.6. Conversion efficiencies

2.6.1 The efficiency of the DC-DC and DC-AC inverter
The efficiency of an inverter can vary from 50% to over 90%, even close to 100%. The different inverters are distinguished by the cost of the inverter. The choice of inverter will have a big impact on the power produced from the PV system, with such a range in efficiencies.

2.7. Different terms for the efficiencies of a PV system

2.7.1 Standard test conditions (STC)
The efficiency of a photovoltaic system varies with several factors. To compare the different photovoltaic cells and modules, there is a standard used in the solar industries called STC (standard test conditions). The manufacturers test their products under these conditions and make data sheets with the specification for the modules. These conditions are a cell temperature of 25 °C, an irradiation of 1000 W/m^2 and an AM of 1.5. The power generated by the modules under these conditions is given in watt peak (Wp) and is called nominal power [5]. The real conditions for a photovoltaic system will of course deviate from the STC.

2.7.2 Specific yield
Specific yield is given in kWh per kW$_p$ where kWh is the annual energy produced by the PV system. The annual energy generated per nominal power is often used to help determine the financial value of a system and compare operating results from different technologies and systems. The total installed nominal power for a PV system can be found using the data sheet. In the data sheet for the module the nominal power for *one* module is specified. To get the total installed nominal power for the system the number of modules is multiplied by the

nominal power for *one* module. The annual energy generated by the PV system is given by the output power (AC power) from the inverter.

2.7.3 Performance ratio (PR)

Performance ratio (PR) is also called "quality factor". The PR gives the product of all the loss factors or the utilization of an entire photovoltaic system. The PR are given by the following formula

$$PR = \frac{P_{\text{specific}}}{G_{\text{specific}}} \tag{4}$$

The specific yield, P_{specific} is given by

$$P_{\text{specific}} = \frac{P_{AC}}{P_{STC}} \tag{5}$$

where P_{AC} is the output yield from the inverter, delivered to the grid, and P_{STC} is the nominal power for the PV system.

The specific irradiation G_{specific} is given by

$$G_{\text{specific}} = \frac{G_{mp}}{G_{STC}} \tag{6}$$

where G_{mp} is the total irradiation in the module plane, and G_{STC} is the irradiation corresponding to the STC (1000 W/m^2). The G_{mp} is measured either by a reference cell or a pyranometer. The difference between a pyranometer and a reference cell is explained further in Chapter 2.9. To calculate the correct PR of a system is it necessary with parallel measurements of both the yield of the PV system and the irradiation at the site of the PV system. These data are not always available for all PV systems.

The typical range of the PR was in the late 1980 from 0.50 to 0.70. Nowadays many systems have a PR higher than 0.80. The reason for the rise in PR are less defects on the DC installations, better reliability and MPPT, shorter repair times and better design of the system in conjunction with shading [3]

2.8 Monitoring of the PV system

Monitoring of a PV system is necessary to determine if all the components of the system is working properly. Monitoring of a PV system can also give information of the behavior of a system under different conditions. This can give valuable information about the PV technology and the design of the system. Figure 21 illustrates the information necessary for good monitoring. PV systems well equipped normally does have instruments for measuring irradiation, ambient temperature, module temperature and wind speed. The following section describes the measuring of meteorological data and a method for monitoring of PV systems. The chapter about meteorological data focuses on irradiation, module temperature and ambient temperature.

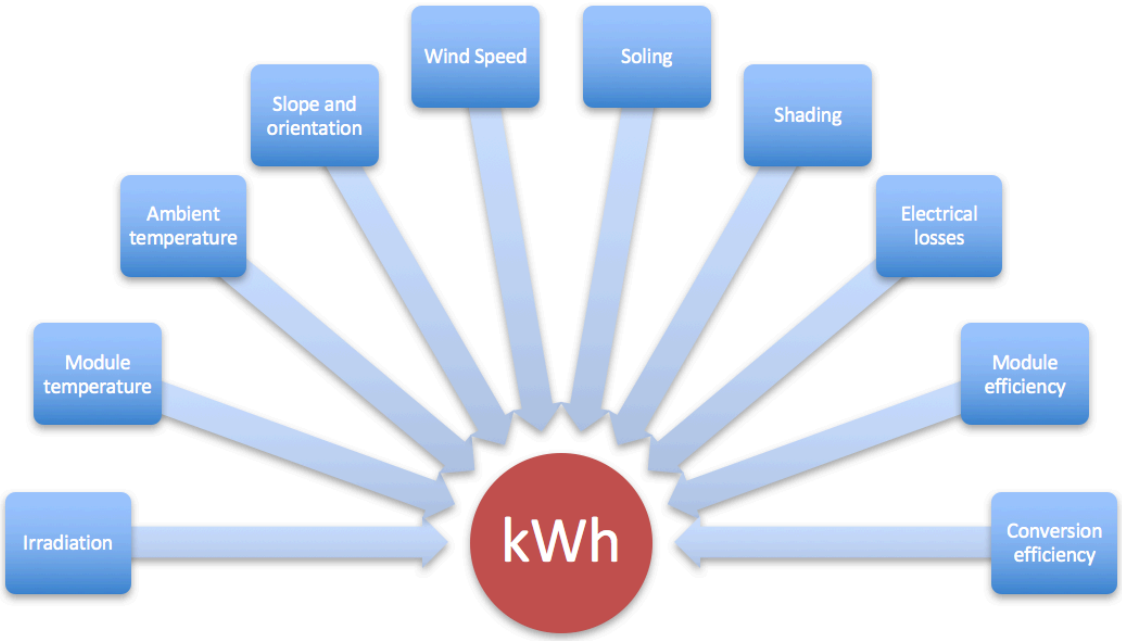

Figure 21: Good practice for the monitoring of PV systems demands good information flow from several factors illustrated in this figure.

2.8.1 Good practice for monitoring of PV systems

The report "Analytical Monitoring of Grid-connected Photovoltaic Systems – Good practices for Monitoring and Performance Analysis" [3] from The International Energy Agency (IEA) provides guidelines and descriptions of methods and modules used with analyzing grid-connected PV system performance. The report describes the best practices for PV monitoring and what kind of measurement equipment and parameters necessary to perform such an analysis. The best practices for hardware configuration and installation are described together with failure patterns.

The approach is based on linear-regression methodology for monitoring of PV systems. The approach can be used to analyze the influence of module temperature on system performance, the influence of wind speed and DC voltage deviations and their relation to module temperature, among others.

An example of monitoring is to plot the module temperature against the DC voltage. The DC voltage is linearly dependent on the module temperature and deviations from the linear regression indicate flaws in the system. This kind of plot can also say something about the degree of temperature dependence for the material of the PV system. The report suggests the following indicators for the operation

- Regression lines not changing significantly over time indicate that the system properties remained constant;
- Changing regression lines over time indicate a trend-wise change of system parameters;
- Samples suddenly significantly deviating from the regression lines hint towards exceptional operating points;
- Samples regularly deviating from the regression lines hint towards a design flaw.

Local data are necessary for monitoring of PV systems. Sometimes a pyranometer or a reference cell are too expensive to install, depending on the size of the PV system. The measurement instruments demand a certain expertise to install, operate and maintain. Questions has been asked whether it is possible to say something about the system performance without local meteorological data. For monitoring over a longer time period, satellite derived data can be sufficient, but for shorter periods, the satellite data has higher uncertainty and may not be suitable for accurate monitoring [3]. The paper “Measuring Degradation Rates without Irradiance Data” [15] describes a method for finding degradation rates without irradiance data. The method is based on finding a set of relative degradation rates that are determined by comparing daily AC final yields from a group of PV systems relative to the average final yield of all the PV systems. The difference between relative and absolute degradation rates is found using a Bayesian statistical analysis. The degradation values from this method were compared with degradation values found by utilizing irradiance data and the results coincided.

2.9 The meteorological factors and collection of meteorological data

2.9.1 Irradiation

The meteorological factors are continuously changing through the year for a given location, due to the factors explained in chapter 1. When planning a PV system, information of the expected irradiation on the chosen location needs to be provided. Simulation programs for PV systems are used to estimate the production of the PV system. The most important input of the simulation program is the irradiation on the location of the PV system. Usually information from different databases are used for this, when historical measurements on site not are available. The databases are based on satellite data, ground measurements and interpolations. When monitoring a PV system more accurate data for the irradiation is needed. The best option is if the system is equipped with instruments for measuring irradiation. Not all PV systems have instruments for measuring meteorological factors on the site. The instruments are expensive and needs to be installed, calibrated and operated correctly. The pyranometer has traditionally been used for measuring global horizontal irradiation and the reference cell has been introduced with the PV industry to measure the irradiation in the module plane.

2.9.2 Differences between the pyranometer and a reference cell

The pyranometer measure the irradiation indirectly by measuring temperature differences. The temperature differences are measured between a black covered surface that absorbs irradiation and one surface that does not absorbs the irradiation. The surfaces are encapsulated by two glass domes. The temperature is measured by a thermistor, where the resistance of the thermistor is dependent on temperature. The pyranometer gives a voltage signal that is proportional to the irradiation and the irradiation is calculated using the calibration of the pyranometer and given in watts per square meters (W/m^2) [16]. The pyranometer measure irradiation from all angles in a hemisphere, has a spectral response approximately from 400 to 2700 nm and is designed to minimize sensitivity to temperature [17]. Compared to the reference cell, the pyranometer is more expensive. The uncertainty of the pyranometer is also reported to be higher than for the reference cell when used in evaluation of PV array performance [16]. The response time for the pyranometer can be up to 30 seconds [16].

The reference cell is designed to measure the irradiation available for the PV modules and is mounted in the same angle and with the same orientation as the modules. The reference cell is working in the same way as a PV cell. If the energy from the Sun exceeds the band gap of the reference cell, the energy from the Sun will be converted to charges that can be collected in an external circuit. The voltage from the circuit is measured across a resistor in the reference cell. This voltage is converted to a value for the irradiation using the calibration of the reference cell [16]. The reference measures how much of the irradiation in the module plane that can be converted into electricity for a certain PV material. While the pyranometer measure irradiation from a view of 180 degrees, the reference cell will only measure irradiation in the mounted angle and orientation. The spectral response for the reference cell is approximately 300 to 1200 nm [16], considerably smaller than for the pyranometer. Both the temperature and time response for the reference cell are comparable with the response of the

PV system. The response time for the reference cell is typically in the magnitude of milliseconds [16].

2.9.3 Temperature

For monitoring of a PV system, it is important with information about the temperature, both the ambient temperature and cell temperature. Most common for measuring ambient temperature for PV systems is the thermistor which is based on resistance that changes with temperature. When measuring cell temperature, the thermistor is mounted on the back of the module.

2.10 Copper Indium Selenide (CIS)

The majority of the PV systems are based on silicon based material. In this thesis, an alternative to the silicon is evaluated. A Copper Indium Selenide (CIS) is a polycrystalline thin film solar cell. Sometimes Gallium is included in the semiconductor and is called Copper Indium Gallium Selenide (CIGS). The material easily absorbs sunlight and can be made so thin that they can be made flexible. The laboratory efficiency of CIS cells is lower than the efficiency of silicon cells [18], but the costs are lower than for the silicon cells. For commercial CIS cells the efficiency is between 12 and 14% [19]. The highest efficiency achieved in a laboratory under regular sun levels is 22.6% for CIGS [20].

3. Methodology

This section describes the methodology used for this thesis. The section is divided into four chapters:

- Description of the programs used for the work in this thesis
- Meteorological data – collection of data
- Inverter data from two comparative PV systems on Kjeller - collection of data
- Processing of meteorological data and inverter data

The different sites for gathering data for the thesis are listed below and described in the following sections. Figure 22 shows the locations of the stations in the vicinity of Oslo.

- Økern nursing home – meteorological measurements of a PV site
- Ås – meteorological weather station
- Blindern – meteorological weather station
- PVGIS – database
- NASA SSE– database
- Kjeller – two comparative PV systems

Figure 22: A screenshot from Google Maps showing the locations for the meteorological weather stations and the PV system on Kjeller. Screenshot from November 11, 2016.

3.1 Meteorological data – collection and processing of data

3.1.1 The meteorological weather station on Økern

One of the sources for meteorological data for this thesis is the station on Økern nursing home. The nursing home is located in Oslo and together with an upgrade of the building in 2014 a PV system of 130 kW_p was installed. The PV system is equipment for measuring weather data and mounted on the same roof as the PV system on Økern nursing home. The measurements can be monitored in real time and historical data can be downloaded from a web user interface. ITAS is responsible for the layout of the measurement system on the roof and the web user interface. Økern nursing home is owned by Omsorgsbygg Oslo KF. Relevant data for the system at Økern is listed below.

- Latitude: 59.931600
- Longitude: 10.809377
- Elevation: 115 m
- Operating time: August 21, 2015 -
- Building Azimuth: -5 degrees

The main parts of the measurement system are:

- One Campbell Scientific CR1000 – measurement and control datalogger
- One Campbell Scientific 109 – temperature sensor
- One Lambrecht 14577 – wind speed sensor
- Four Campbell Scientific 110PV - surface temperature sensor
- Four Ingenieurbüro Mencke & Tegtmeyer GmbH Si-01 TC-T – irradiance sensor

For this thesis, the focus is on the measurements for irradiation, module temperature and air temperature.

The Campbell Scientific datalogger is the system's control unit and it collects all the information from the sensors. The specifications for the datalogger can be found in the Appendix. It can be programmed to perform arithmetic, trigonometric and statistical calculations based on the measured data. The system is operated by a computer with a software package from Campbell Scientific called "LoggerNet".

The Campbell Scientific temperature sensor is measuring the air temperature. Chosen specifications for the sensor are given in Table 1. Detailed specification can be found in the Appendix. The air temperature is measured on the top of the building, approximately three meters above the PV system.

Table 1: Specifications for the air temperature sensor.

Measuring:	Range	Resolution	Accuracy	Unit
Air temperature	-50 to 70	0.01	±0.25 (–10 to 70)	(°C)

The Ingenieurbüro Mencke & Tegtmeyer irradiance sensor is measuring irradiation. This sensor is a reference cell for the PV system. The irradiation sensor is connected to a temperature sensor which is mounted on the back of the reference module. This sensor can give an approximate value for the module temperatures. Selected specifications are given in Table 2 and a full list of specification can be found in the Appendix. Figure 23 shows the reference cell number two.

Table 2: Specifications for the irradiation sensor, which also measure module temperature.

Measuring:	Range	Resolution	Accuracy	Unit	Response time (s)	Spectral response (nm)
Irradiation	0-1000	0.01	±5 W/m^2 ± 2.5% of measured value	W/m^2	0.15	350-1200
Module temperature	-35 - 80	0.01	±2 (-20 to 70)	°C	0.15	-

Figure 23:Reference cell number two on the PV system on Økern.

Updates on the measurements are given every hour in the web user interface. The data can be found at http://graf.itasdata.no/index.html, but requires username and a password. All information is given with a timestamp with the format "DD.MM.YYYY HH:MM:SS". The hourly values given are the average value for the last 3600 seconds. The station measures and calculates all the available variables every second. The intervals for the available stored data are 1 minute, 10 minutes or 60 minutes, where the intervals are a mean value of measurements of 60, 600 and 3600 seconds respectively. A list of the available relevant data can be seen in Table 1.

Table 1: Description of the available data possible to extract from the web user interface.

Data	Description	Unit	Best resolution available
Irr_grC_Avg(1)	Mean module temperature on reference cell 1	°C	1 minute
Irr_grC_Avg(2)	Mean module temperature on reference cell 2	°C	1 minute
Irr_grC_Avg(3)	Mean module temperature on reference cell 3	°C	1 minute
Irr_grC_Avg(4)	Mean module temperature on reference cell 4	°C	1 minute
Irr_Wpm2_Avg(1)	Mean irradiation on reference cell 1	W/m^2	1 minute
Irr_Wpm2_Avg(2)	Mean irradiation on reference cell 2	W/m^2	1 minute
Irr_Wpm2_Avg(3)	Mean irradiation on reference cell 3	W/m^2	1 minute
Irr_Wpm2_Avg(4)	Mean irradiation on reference cell 4	W/m^2	1 minute
LT_s_Avg	Mean air temperature	°C	10 minutes
LT_s_Max	Maximum air temperature	°C	10 minutes
LT_s_Min	Minimum air temperature	°C	10 minutes

A screenshot from the web interface is shown in Figure 24 and Figure 25. The positions for the measurement equipment are marked with the red dots. There are four reference cells on the roof with sensors for measuring irradiation and module temperature, four sensors for measuring surface temperature, one sensor for measuring air temperature and one sensor for measuring wind speed.

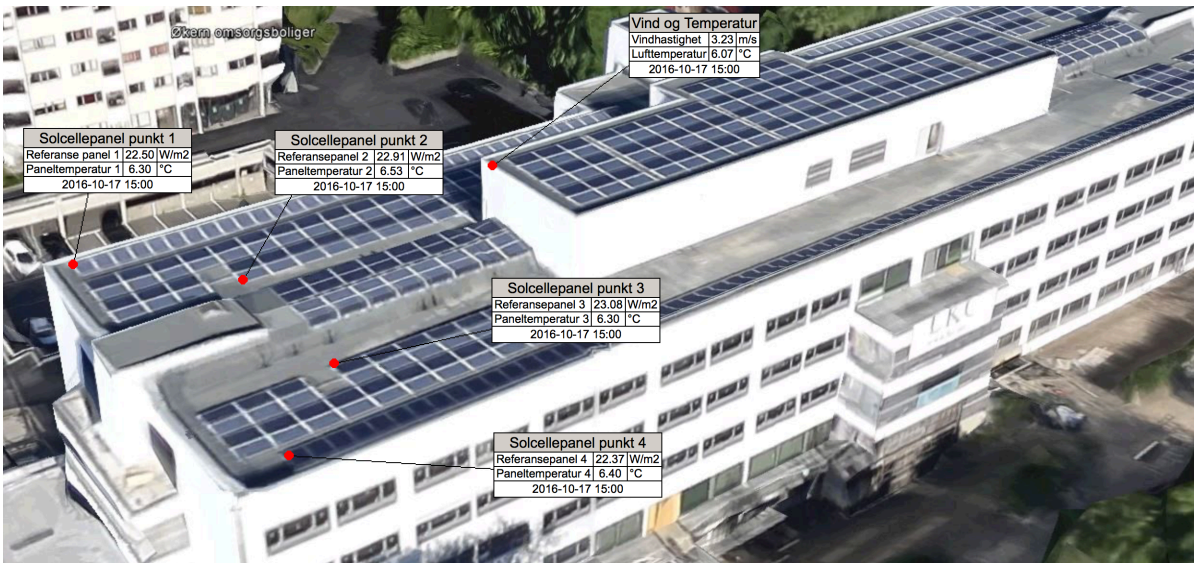

Figure 24: The system on the roof of Økern with the positions for the weather measurement equipment. The user interface gives an update every hour.

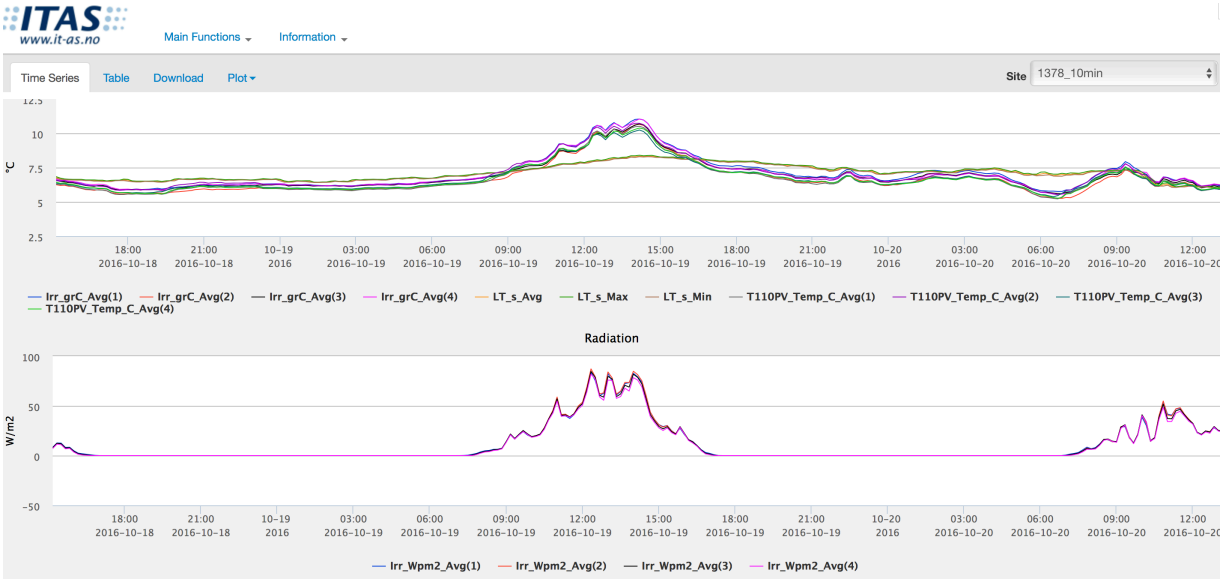

Figure 25: A screenshot from the interface showing one selection of real time display for the weather data. The first curve shows irradiation converted to panel surface temperature, minimum, maximum and average air temperature and the module temperature. The second curve shows irradiation on the four reference cells. Both curves show data from October 18 at 18.00 until October 20 at 12.00.

The nursing home on Økern is oriented approximately north south with an azimuth angle of minus five degrees. The system on the roof is facing east or west. The orientation and slope of the reference cells on their respective modules are illustrated in Figure 26, together with the motion of the Sun. Figure 27 is panoramic picture of the corner of the building facing south-west. The two main sources causing near shading on the PV system is the beige building to

the right in Figure 27. On the top of the building, there is a box, housing a technical room. This part of the building is also a source for near shading on the system.

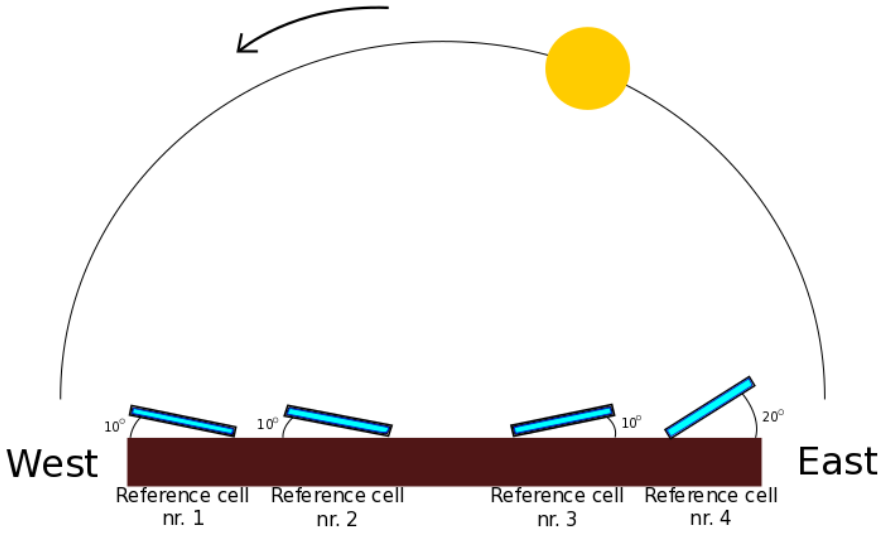

Figure 26: The illustration of the orientation and slope of the reference cells on Økern nursing home.

Figure 27: Illustrating the south-west corner of the building and one of the main sources for shading on the system. The picture is taken December 1, 2016 at 14.15. At this time a year the Sun sets before it reaches the building to the right.

3.1.2 The meteorological measurement station in Ås

The station in Ås is operated by The Norwegian Institute of Bioeconomy Research (NIBIO). The project is in Norwegian called "Landbruksmeteorologisk Tjeneste" (LMT) and historical meteorological data can be obtained from a web user interface at http://lmt.bioforsk.no/. Some chosen values can be monitored in real time from the interface, either as listed values or in a graphic format. Figure 28 and Figure 29 shows a screenshot from the web user interface, the graphic presentation and the table values. The data is updated every hour and the available intervals are hourly, daily or monthly values. All information is given with a timestamp with the format "DD.MM.YYYY HH:MM:SS". The hourly values given are the average values for

the 3600 seconds after the given hour. The station has several measuring equipment including equipment for measuring temperature, wind, precipitation and irradiation. The relevant equipment for this thesis is described in this section. Relevant data for the station are listed below.

- Latitude: 59.660468
- Longitude: 10.781989
- Elevation: 94 m
- Operating time: August 28, 1991 -

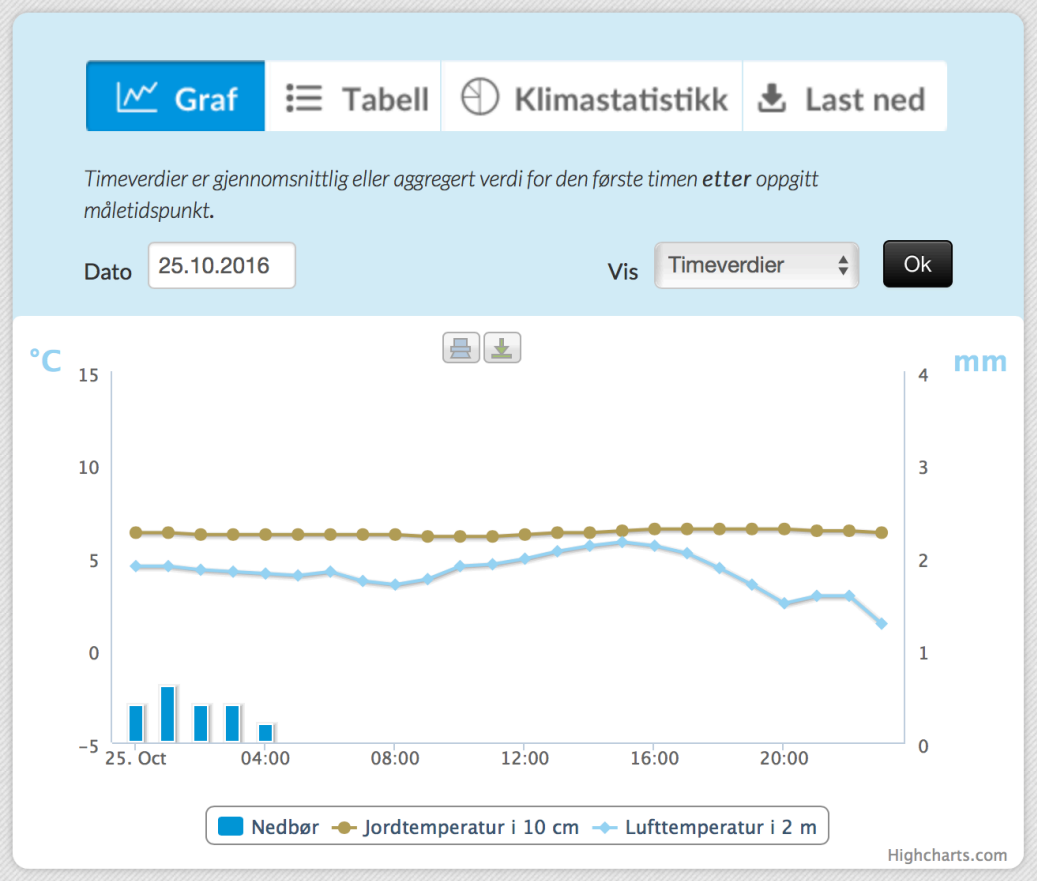

Figure 28: A screenshot from the graphical presentation. The presentation shows precipitation, earth temperature and air temperature for October 25, 2016 with hourly values.

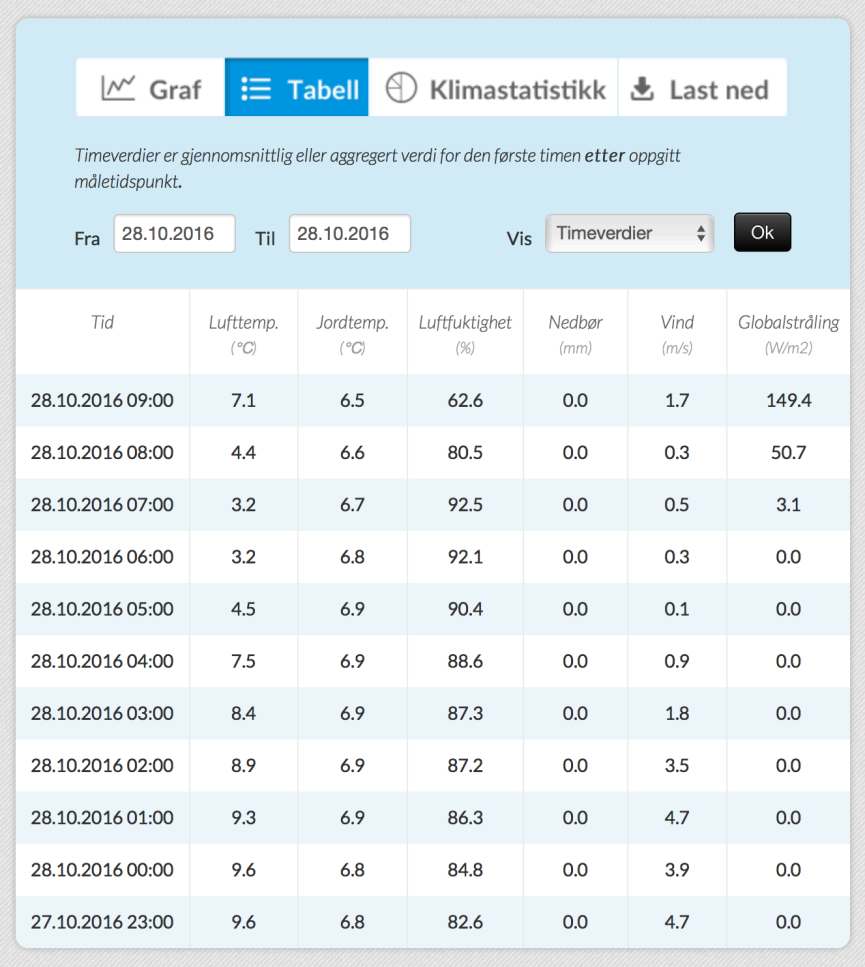

Tid	Lufttemp. (°C)	Jordtemp. (°C)	Luftfuktighet (%)	Nedbør (mm)	Vind (m/s)	Globalstråling (W/m2)
28.10.2016 09:00	7.1	6.5	62.6	0.0	1.7	149.4
28.10.2016 08:00	4.4	6.6	80.5	0.0	0.3	50.7
28.10.2016 07:00	3.2	6.7	92.5	0.0	0.5	3.1
28.10.2016 06:00	3.2	6.8	92.1	0.0	0.3	0.0
28.10.2016 05:00	4.5	6.9	90.4	0.0	0.1	0.0
28.10.2016 04:00	7.5	6.9	88.6	0.0	0.9	0.0
28.10.2016 03:00	8.4	6.9	87.3	0.0	1.8	0.0
28.10.2016 02:00	8.9	6.9	87.2	0.0	3.5	0.0
28.10.2016 01:00	9.3	6.9	86.3	0.0	4.7	0.0
28.10.2016 00:00	9.6	6.8	84.8	0.0	3.9	0.0
27.10.2016 23:00	9.6	6.8	82.6	0.0	4.7	0.0

Figure 29: A screenshot from the table presentation. The presentation shows air temperature, earth temperature, humidity, precipitation, wind and global irradiation for some hourly values on October 28, 2016.

To measure irradiation a pyranometer from Kipp & Zonen is used. The model is CM3 and its detailed specifications are given in the Appendix. Table 4 gives selected specifications. The pyranometer is mounted two meters above the ground.

Table 4: The specifications for the pyranometer.

Measuring:	**Range**	**Resolution**	**Accuracy**	**Unit**	**Response time (s)**	**Spectral response (nm)**
Irradiation	0-2000	0.01	±10% of daily sums	W/m^2	18	305-2800

To measure air temperature a sensor from Reissmann is used. The model is Pt100 and its specifications can be found in the Appendix. Selected specifications are described in Table 5. The sensor is mounted two meters above the ground and gives minimum, maximum and average air temperature.

Table 5: The specifications for the temperature sensor.

Measuring:	Range	Resolution	Accuracy	Unit
Temperature	-50 - 230	0.01	±0.1 °C	°C

The measured values are given for the time after the given interval and can be obtained for each either hour, day or month. Table 6 gives available relevant data for the station.

Table 6: The relevant data available from the web user interface for the station in Ås.

Data	Description	Unit	Best available resolution
TM	Average air temperature	°C	Hourly values
TX	Maximum air temperature	°C	Hourly values
TN	Minimum air temperature	°C	Hourly values
Q0	Global irradiation	W/m^2	Hourly values

3.1.3 The meteorological measurement station on Blindern

The Norwegian Meteorological Institute operates the meteorological station on Blindern. The station has been operating since 1931 and is located on Blindern in Oslo. The data for air temperature is first available from 1937 and data for global irradiation available in 1996. Relevant data for the station are listed below.

- Latitude: 59.9423
- Longitude: 10.7200
- Elevation: 94 m
- Operating time: air temperature from 1937 and global irradiation from1996

The data from the station is available on a web user interface with a free user account at http://sharki.oslo.dnmi.no/portal/page?_pageid=73,39035,73_39049&_dad=portal&_schema=PORTAL. It is possible to download data for a chosen time series from the web user interface. All information is given with a timestamp with the format "DD.MM.YYYY HH:MM:SS". The hourly values are given as an average value for the hour after the given measurement point. A screenshot from the web user interface is shown in Figure 30.

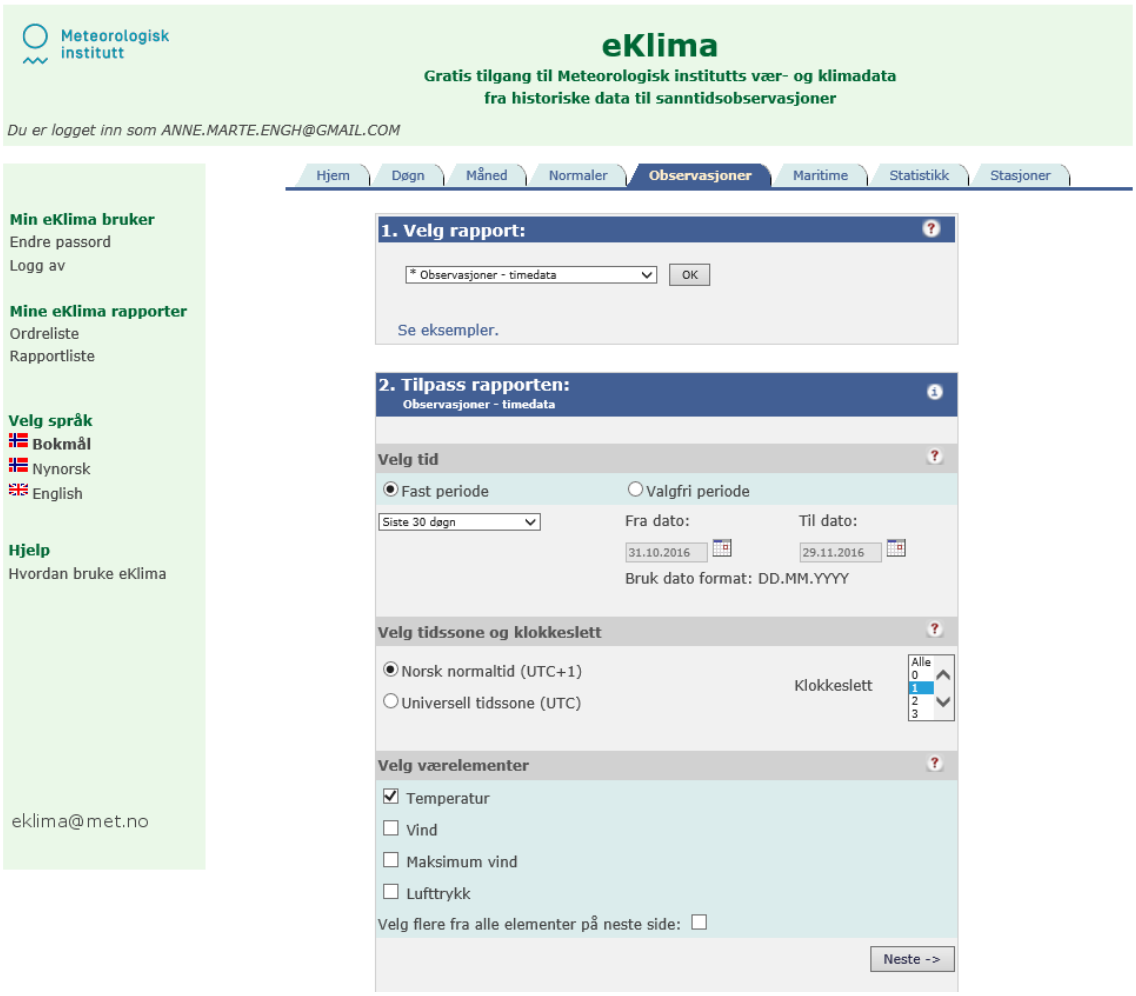

Figure 30: A screenshot from the web user interface. It is possible to choose time series, time interval, time zone and data.

To measure irradiation a pyranometer from Kipp & Zonen is used. The model is CMP21 and its detailed specifications are given in the Appendix. Table 7 gives selected specifications for the pyranometer. The pyranometer is mounted two meters above the ground.

Table 7: The specifications for the pyranometer at Blindern.

Measuring:	Range	Resolution	Accuracy	Unit	Response time (s)	Spectral response (nm)
Irradiation	0-4000	0.01	<2% of daily sums	W/m^2	5	285-2800

To measure air temperature a Pt100 sensor is used. Specifications can be found in the Appendix. Selected specifications are described in Table 8. The sensor is mounted two meters above the ground.

Table 8: The specifications for the temperature sensor at Blindern.

Measuring:	Range	Resolution	Accuracy	Unit
Temperature	-50 - 230	0.01	±0.1	°C

The measured values are given for the time after the given interval and can be obtained for each either hour, day or month. Table 9 gives available relevant data for the station.

Table 9: The relevant data available from the web user interface for the station at Blindern.

Data	Description	Unit	Available stored interval
QSI	Global irradiation	W/m^2	Interval: in minutes, hourly and monthly
TA	Air temperature	°C	Interval: in minutes, hourly and monthly

3.2 Databases for meteorological information

In this thesis, the measured meteorological data are compared with meteorological data from databases. The two databases used in this thesis are the databases from PVGIS and NASA.

3.2.1 PVGIS

PVGIS (Photovoltaic Geographical Information System) is a web-based database for solar energy resources available at http://re.jrc.ec.europa.eu/pvgis/apps4/pvest.php. The service is provided by the Joint Research Center, which is the European Commission's science and knowledge service. Two types of databases are available from PVGIS: Classic PVGIS and CM-SAF PVGIS. The Classic PVGIS is based on ground measurements from meteorological stations and interpolations between the stations. The CM-SAF PVGIS is based on calculations from satellite data performed by The Satellite Application Facility on Climate Monitoring. The Classic PVGIS are based on data from 1981 to 1990. The CM-SAF PVGIS is based on data from 1998 to 2005 and from June 2006 to 2011. The spatial resolution for the data are 1,5 arc-minutes which is equivalent to three kilometers right below the satellite at 0° N and 0° W [21]. The CM-SAF PVGIS more accurate, according to [21] and is the preferred database in this thesis. The data from CM-SAF PVGIS has been compared to quality measurements from ground stations and the error was in most places found to be less than 5% [21]. Figure 31 gives a screenshot from the web user interface for PVGIS. For a chosen location, it is possible to download information about daily and monthly solar energy resources. Additionally, it is possible to get an estimation of the PV production for a system at the chosen location.

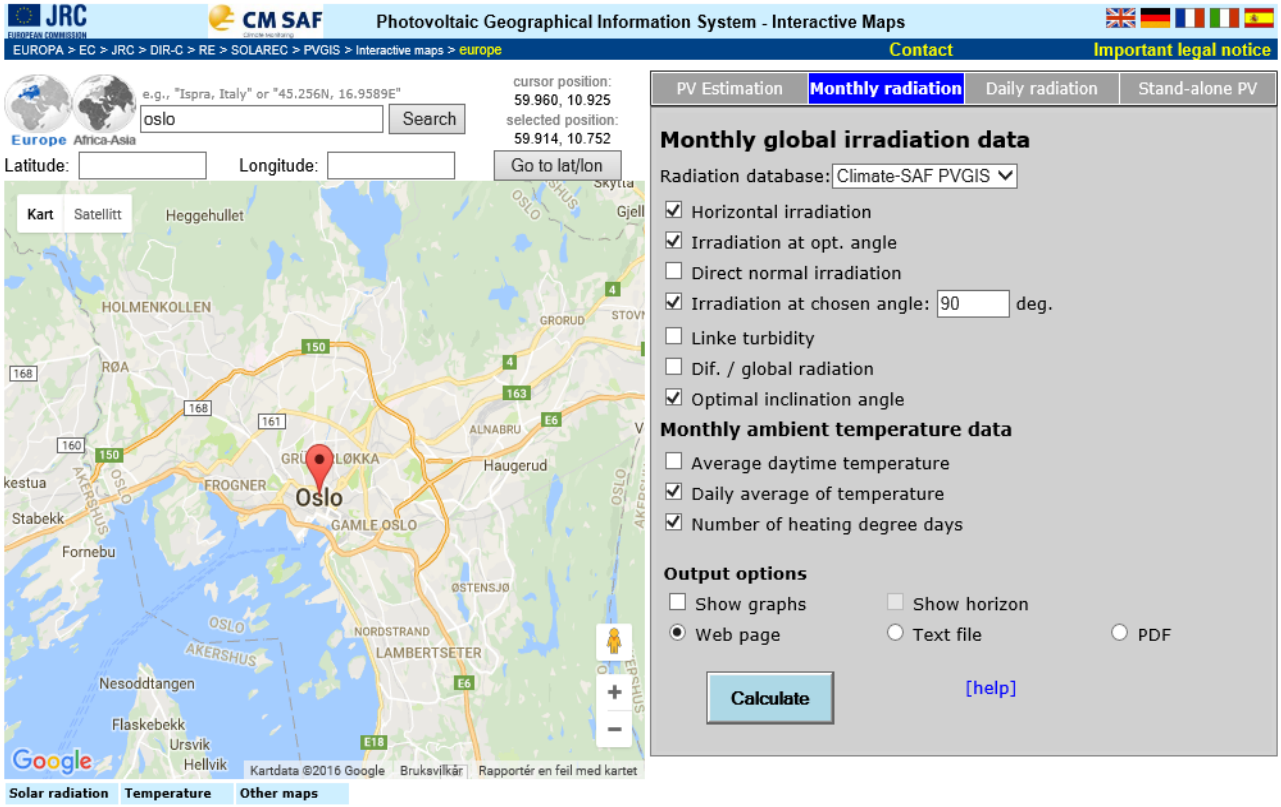

Figure 31: A screenshot from the web user interface for PVGIS database.

3.2.2 NASA

NASA SSE (National Aeronautics and Space Administration Surface meteorology and Solar Energy) is a web-based database for solar energy resources and surface meteorology. The data from the database is available at https://eosweb.larc.nasa.gov/cgibin/sse/daily.cgi?email=skip@larc.nasa.gov. The data is based on calculations from satellite data from a 22-year period from July 1983 to June 2005. The spatial resolution for the data is 1° latitude by 1° longitude. This means that for the southern part of Norway the resolution is 50 km by 100 km. The error for the monthly values has been estimated to 13-16% [22]. Figure 32 shows a screenshot from the web user interface for the database from NASA SSE

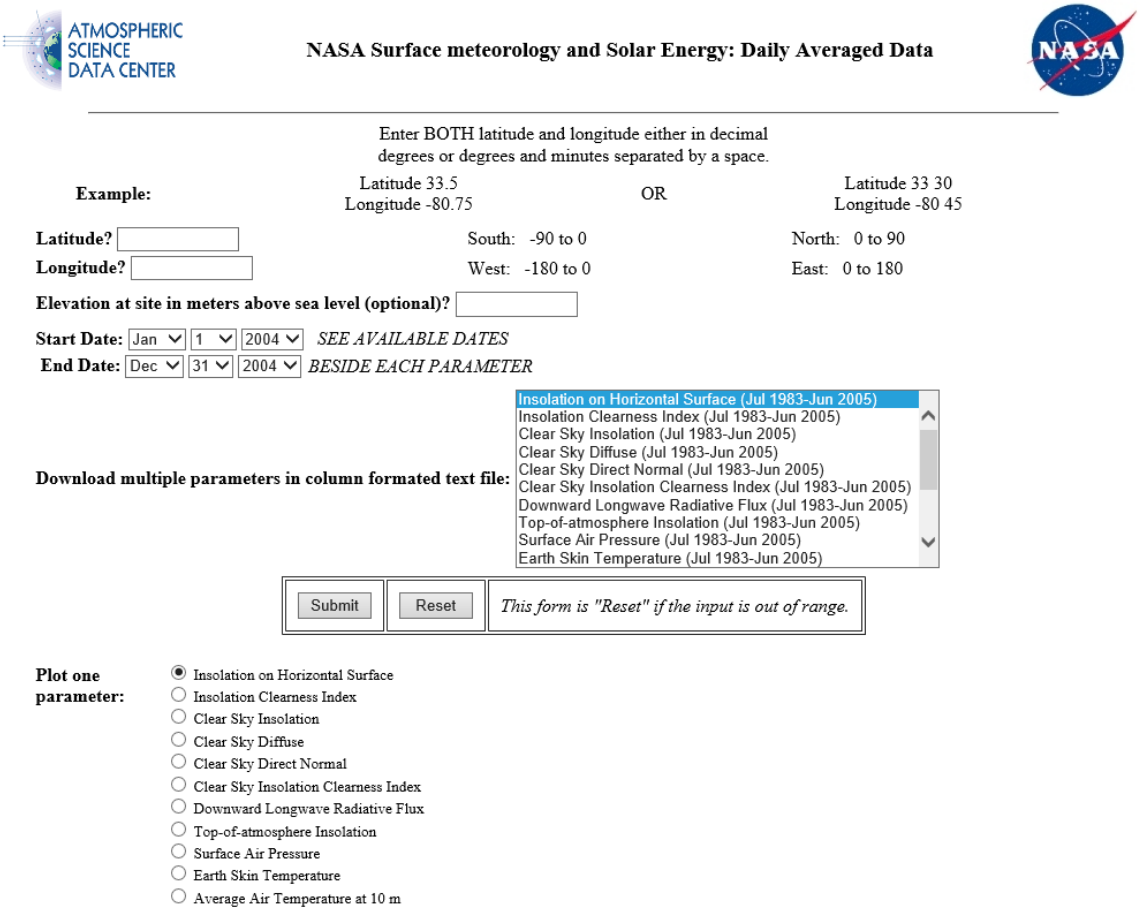

Figure 32: A screenshot from the web user interface for The NASA SSE database.

3.3 Two comparative PV systems on Kjeller - collection of inverter data

3.3.1 The PV system on Kjeller

The two different PV systems studied in this thesis is located on Kjeller, close to Lillestrøm. The systems are attached to the building of the Solar Department on The Institute for Energy Technology (IFE). Relevant information about the systems is listed below. It is no meteorological data measured at the location for this system.

- Latitude: 59.973341
- Longitude: 11.051184
- Elevation: 100 m
- Operating time: December 2015
- Building azimuth: 13 degrees

There are two different systems on Kjeller, one of them with silicon-based modules and the other system with thin-film modules. Both the systems are connected to a string inverter. The two systems are illustrated in Figure 33. The thin-film system is to the left and the silicon-based system to the right. The systems are mounted with the same slope of 90 degrees and is assumed to receive approximately the same amount of irradiation. The modules are not building integrated, but mounted on the wall. This leads to less convection for the modules compared to free standing systems and the result is a higher module temperature. The building seen in Figure 33 is located on a top of a small hill. The building will experience little shading in the morning, but in the evening will the neighbor building cause some shading on the modules.

Figure 33: Picture of the two PV systems mounted on the roof on Kjeller. The picture was taken on November 9, 2016 at 12.30. To the left is the thin-film system and the silicon-based system is to the right.

For the silicon-based system modules from IBC Solar is used. The type of modules is the PolySol 260 CS which is a solar cell made of poly crystalline silicon. For the thin-film system modules from Solar Frontier is used. The type of module is the SF 165-S which is a CIS solar cell. Relevant information for the two systems is listed below. Detailed specifications can be found in the Appendix.

PV technology: CIS

- Number of modules: 8
- Nominal module power: 165 W_p
- Total nominal power: 1.32 kW_p
- Module efficiency: 13.4%
- Area of the module: 1.32m^2
- Temperature coefficient for P_{MPP}: -0.43%/°C

PV technology: CIS

- Number of modules: 5
- Nominal module power: 260 W_p
- Total nominal power: 1.3 kW_p
- Module efficiency: 15.9%
- Area of the module: 1.67m^2
- Temperature coefficient for P_{MPP}: -0.31%/°C

Both of the string inverters are from Delta and of the type RPI H3. The inverter has a maximum power point tracker (MPPT). Selected specifications for the inverter is listed below. Detailed specifications can be found in the Appendix.

Inverter specifications for Delta RPI H3:

- Nominal power: 3.13 kW
- Max efficiency: 97.0%
- EU efficiency: 96.2 %

3.3.2 Inverter data

Data from the inverter can be downloaded from a web user interface at https://monitoring.solar-inverter.com/, but requires a username and password. The web user interface Solvia Monitor 2.0 is created by Delta. A graphical solution is available, where the available data is plotted. The historical data are available for downloading. Figure 34 shows a screenshot from the user interface. It is possible to choose between the two different systems. Available data from the user interface are listed in Table 10.

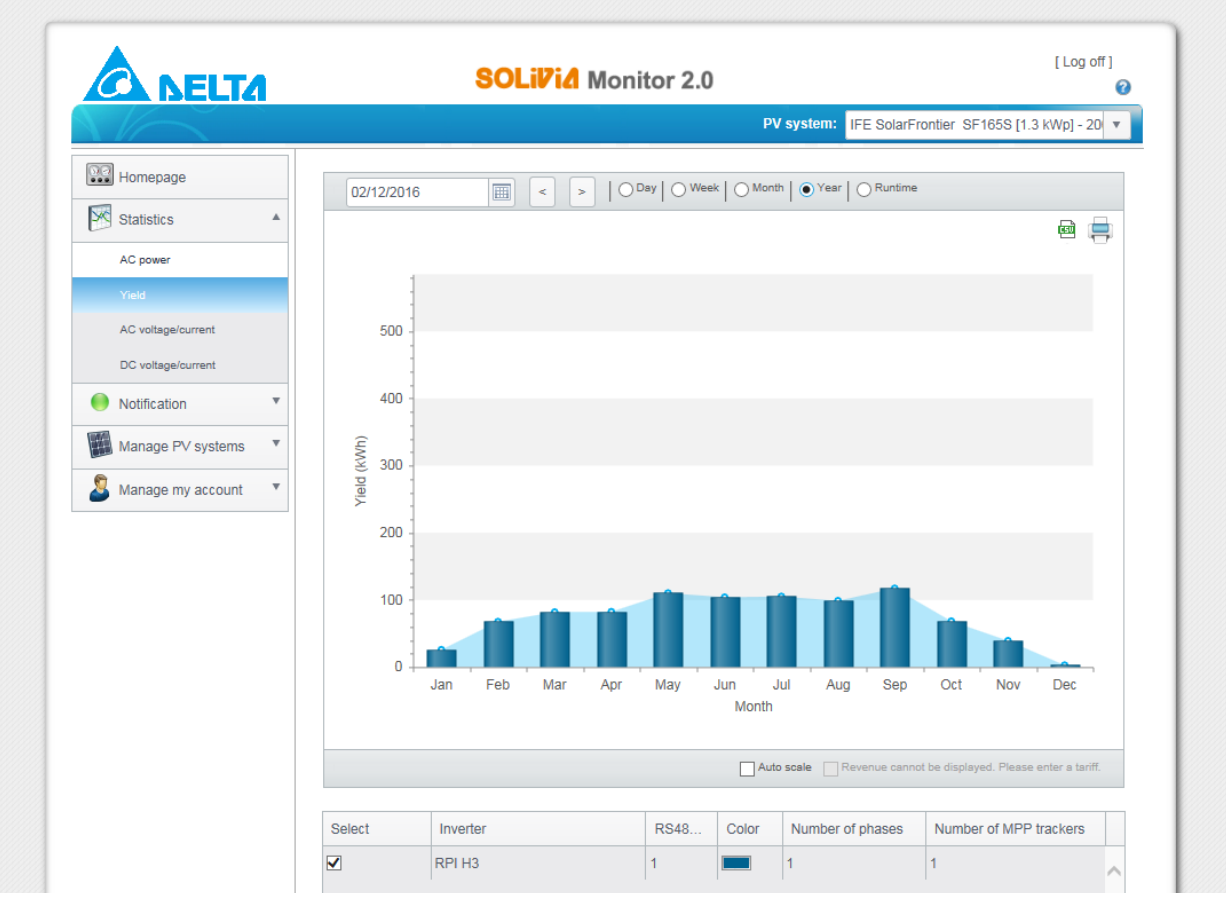

Figure 34: A screenshot from the web user interface from Delta. The figure shows monthly produced yield for 2016.

Table 10: Available data and corresponding units from the web user interface.

Available data	Unit
AC power	kW
Yield	kWh
AC voltage/current	V/A
DC voltage/current	V/A

3.4 Processing of meteorological data and inverter data

3.4.1 Meteorological data

To be able to compare the available data, processing and quality control of the data was necessary. Because the thesis original was going to use Økern as a main source for both meteorological data and inverter data, was the chosen time series dependent on the availability of Økern data. The first reliable measurement of irradiation on Økern was on August 21, 2015. The year from August 21 2015 to August 20, 2016 was chosen to get an

overview of the annual available irradiation at Økern. The corresponding time series for Blindern and Ås were collected and processed.

To get an impression of the monthly irradiation, a resolution of hourly values was considered sufficient enough to extract from the web user interfaces. The missing data points for every time series were found and listed in a table.

To compare the different time series, it was adjusted for the fact that the time series have different definitions of the average hourly values. For the time series from Ås and Blindern, the average hourly value is the value for the first hour after the given hour, i.e. the value given at 12.00 is the average value for the hour 12.00-13.00. For Økern is the average hourly value the value for the hour before the given hour, i.e. the value given at 12.00 is the average value for the hour 11.00-12.00. This difference was adjusted so that the Excel spreadsheet gave the hourly average value for the same time interval. All the time series are in Norwegian Mean Time (NMT) and not adjusted for Daylight saving time (DST).

The irradiation data for Ås and Blindern showed negative values at night time. These negative values are due to the temperature difference between the domes of the pyranometer and the pyranometer sensor and the pyranometer body. The domes will cool faster than the body and the sensor. The dome will then attract heat from the body by conduction and from the sensor by infrared radiation, resulting in negative irradiation output from the pyranometer [23]. The negative values were removed from the time series for Ås and replaced with a value of zero irradiation.

Annual irradiation data from NASA and PVGIS were compared with the annual data for Ås, Blindern and Økern. The challenges with comparison of irradiation measured with a pyranometer and irradiation measured with a reference cell are exanimated and discussed.

For three different scenarios, a more accurate analysis was performed. From the hourly values, three days with different weather conditions were found. The different scenarios analyzed with a higher resolution on the irradiation data were

- A day with fully overcast
- A day with varying cloud coverage
- A sunny day

Data with a resolution in minutes was downloaded from the web user interfaces for Blindern and Økern. For irradiation data in Ås, only a resolution in 10 minute-intervals was available. These data were provided by Signe Kroken at the Norwegian University of Life Sciences (NMBU). Excel was used to find 10 minute-intervals for Blindern to be able to compare these time series.

The three different scenarios for Økern were compared with module temperature. The three scenarios for Ås and Blindern were compared with air temperature.

The difference between the irradiation data for the different sources were analyzed for

- Local sources: the four sensors on Økern
- Remote sources: Blindern and Ås

The value and relevance of using data from databases are discussed for

- Monitoring of PV systems
- Estimation of PV production

Different approaches for replacing missing values are analyzed and the error of replacing missing data points with existing point from other sources is exanimated. For periods where data points were missing, they were replaced by data point from the best suited source. Missing data points at Blindern were replaced with existing data points from Ås. Missing data points at Ås were replaced with existing data points at Blindern. To find an approximate error of replacing the missing data point with data points from another source, the same procedure was performed for a reference month. The reference month had complete datasets for both locations. This made it possible to compare the irradiation for the original monthly value of the reference month with the monthly value were the missing data points were replaced.

3.4.2 Inverter data and system monitoring

The data for the total yield for each month of 2016 was collected from the web user interface. Because inverter data from the whole month of December not was available at the end of this thesis, the yield from December was estimated with irradiation data from PVGIS, the total area of the modules, the module efficiency and the efficiency of the inverter. The slope of 90 degrees, the material of the PV system and the azimuth angle were used as inputs in PVGIS to find the irradiation in the module plane. The azimuth angle was found using the compass application for iPhone.

The PR and specific yield were calculated for the two systems. Necessary for the calculation of the PR is the irradiation in the module plane at the given location. PVGIS was used to estimate the irradiation at Kjeller, due to the lack of local measurement of the irradiation. The slope of 90 degrees and the azimuth angle and the nominal power were used as input in PVGIS.

The estimated values for the monthly yield were also found by PVGIS. The estimated values are compared with the actual yield for both of the PV systems. PVGIS gives an estimated value for both system losses. No profile for shading is used as input in the PVGIS database.

The daily yield was extracted from the web user interface for the two systems at Kjeller. The daily values were divided by the nominal power of the systems, to be able to compare the yield of the different technologies.

The daily specific yield was plotted with data for mid-day temperature and daily irradiation measured at Blindern. Data from Blinder was used because no local measurements of module temperature or air temperature was available at the PV site.

March 23 and July 2 had the same amount of daily irradiation, but different hourly temperatures during the day according to irradiation data and temperature data from Blindern. These two days were compared to illustrate the temperature dependency of the PV technologies. The AC power from the inverters at Kjeller was extracted from the web user interface. The AC power was divided with the nominal power and the specific AC power from these two days were compared for the two systems at Kjeller.

4. Results and Discussion

4.1 Available Irradiation Data

For a theoretical PV system, or a planned PV system, it is necessary with an overview of the available irradiation at the given location. Prediction of the weather is challenging and historical data is used to predict what the future meteorological conditions will be. When estimating the yield of a planned system it is normally sufficient with an average value for the irradiation. Such an estimate gives a good indication for what the following years will look like, but the meteorological data varies from year to year. This average value can, be extracted from a database such as NASA [24] or PVGIS [25]. This estimated value is necessary for dimensioning and designing the system so that it produces the required power for the purpose of the system.

For detailed monitoring of a PV system, more precise information about the irradiation and most preferably other meteorological factors is necessary. Especially the module temperature is an important factor when monitoring a PV system. Temperature is considered the most important factor, after the amount of irradiation. The motivation for monitoring a PV system is to be able to say something about the performance of the system. Is it designed correctly? Does it produce the expected amount of power? If not, then why? In which part of the system does the failure occur? It is convenient if the monitoring can tell you something about the degree of the failure in the system. Is the failure caused by natural meteorological reasons, like snow or leaf coverage of the modules? Is it a failure in the PV system, like a heat damaged module, power loss of the inverter or a dislocated cable? The monitoring should give an indication of the importance of the failure. Will the failure pass after short time or is it necessary to fix the problem right away? Can the problem be fixed from an operation center or does it requires a physical visit on the site?

The question is how exact does this meteorological information needs to be to give a good explanation of the changes and failures in the system. This section takes a closer look on the available irradiation in the Oslo area for the reference year August 21, 2015 to August 20, 2016. This interval was chosen because the meteorological data from Økern are available from August 21, 2015. It can be convenient to use the interval of one year to compare the data with data for a typical average year. The irradiation is chosen as an example because it is the most important of the meteorological factors, when saying something about the performance of a PV system. When local measurements are not available, is it possible to use irradiation data from somewhere close by? Not all PV systems have good equipment for measuring meteorological data, since this equipment demands a certain expertise to install, operate and maintain. The price of such equipment is also a reason why they are not installed at the site. It is often the case for small PV systems that it seems too expensive and time demanding to install and operate such equipment.

Figure 35 shows the available irradiation for some chosen locations in and near Oslo.

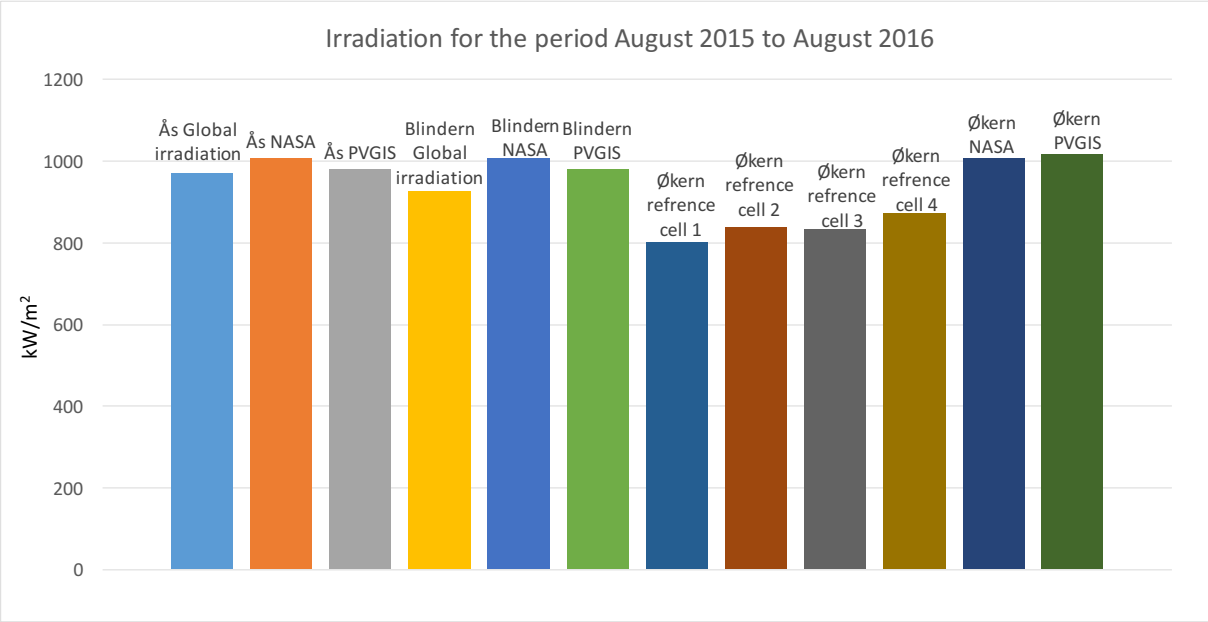

Figure 35: The irradiation for the chosen locations in the Oslo area for the time series August 21, 2015 to August 20, 2016. Both measured irradiation and irradiation from databases are illustrated.

The data presented above represents the variation in irradiation data for the Oslo area. For both the meteorological stations at Ås and Blindern, the measured annual irradiation is lower than for the estimated annual values from NASA and PVGIS. This means that for the reference year the annual irradiation was lower than the annual average that the databases represent. Because of the on the spatial resolution of the data from NASA with 1° latitude by 1° longitude, the annual irradiation from NASA for all the locations is precisely the same. The measured irradiation for the four reference cells on Økern is lower than the other locations. This is due to the fact that the irradiation on Økern is measured with reference cells mounted with the same slope as the modules. They receive less irradiation than the pyranometer that measures irradiation from 180°. The spectral response of the reference cells is narrower than for the pyranometer. Due to these reasons, the reference cells will receive less irradiation than the pyranometers at Ås and Blindern. A comparison of the measurements from the reference cells and the pyranometer is handled later in the following chapter.

4.2 Missing data points

Unfortunately, some data points were missing for the time series. To compare the different time series, the intervals where data was missing were removed from all the time series. Table 11 shows the missing data points for the different locations. Missing data points will be a problem when monitoring a PV system. For the total annual irradiation, missing data points in the summer, with typical higher irradiation, will have bigger impact on the total annual sum than for missing data points in the winter, with typical low irradiation values. The error of

replacing missing data points with existing data from other sources close by will be discussed in late a later chapter.

Table 11: Shows the missing data points for the locations in Oslo.

Location	Period for missing data points	Number of days missing
Økern, reference cell no. 4	January 10-26, 2016	17
Økern, reference cell no. 4	March 3, 2016	1
Økern, reference cell no. 4	March 7-9, 2016	3
Ås	January 17-22, 2016	6
Blindern	October 21-24, 2015	4

Figure 36 is illustrating the same time series as in Figure 23, only with intervals with missing data points removed.

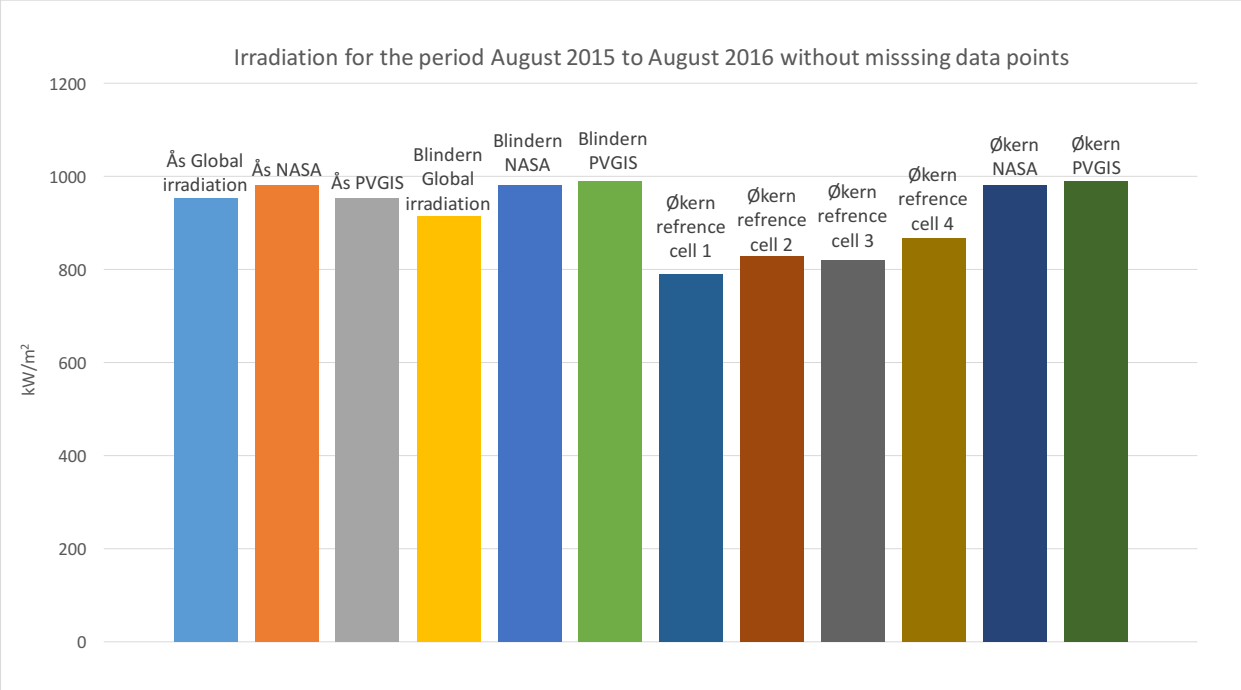

Figure 36: The irradiation for the chosen locations in the Oslo area for August 21, 2015 to August 20, 2016 where the missing data points are removed for all the data sets. Both measured irradiation and irradiation from databases are illustrated.

The datasets show different annual irradiation and some of the explanation can be found in the uncertainty of the instrumentations. As listed in the Methodology, the accuracy for the instruments is varying. The accuracy for the irradiation measurements at Økern, Ås and Blindern is listed in Table 12, together with the accuracy for the PVGIS data base. A more

detailed accuracy for the database from NASA are listed in Table 13. The data from NASA is presented with a minimum and maximum deviation from the average value for each month. The variation is also naturally due to varying cloud coverage. On a day with shifting cloud coverage it is natural to assume that the cloud coverage will be different for Ås and Blindern. This is examined in later chapters.

Table 12: The location for the measured irradiation and the accuracy of the measurements. The accuracy is for the daily sum of irradiation and supplied for the pyranometer from the instrument specifications. The accuracy for irradiation computed in the database PVGIS is listed. The accuracy is supplied by PVGIS and found by comparing the computed PVGIS values with a selection of measured data from ground stations.

Location	**Blindern**	**Ås**	**Økern**	**PVGIS**
Accuracy (%)	±2 of daily sums	±10 of daily sums	±2.5 of daily sums	±5 from annual ground measurements

Table 13: The percentage maximum and minimum deviation from the monthly average irradiation over 22 years for NASA database.

Month	**Jan**	**Feb**	**Mar**	**Apr**	**May**	**Jun**	**Jul**	**Aug**	**Sept**	**Oct**	**Nov**	**Dec**
Monthly average (W/m^2)	0.39	1.09	2.31	3.70	5.32	5.54	5.51	4.23	2.76	1.30	0.54	0.24
Minimum difference (%)	-18	-28	-24	-15	-17	-20	-17	-17	-21	-38	-20	-13
Maximum difference (%)	21	28	29	16	18	24	19	28	20	26	13	17

4.3 The reference cell versus pyranometer

The difference between the irradiation measured with a pyranometer and the irradiation measured with a reference cell can be seen in both Figure 35 and Figure 36, where the annual irradiation for all the sensors on Økern are lower than for the other sources. It is important to keep in mind that the modules on Økern are not mounted in the optimized angle, but are mounted to exploit the sunlight for more hours during the day and to minimize module shading.

The hemisphere of the pyranometer is measuring irradiation from all angles and both the direct and diffuse irradiation from the angles that reach the sensor. The reference cell which is mounted in the same angle and orientation as the PV module will have some time during the day where it doesn't receive direct irradiation. The amount of diffuse irradiation will also be less for the reference cell, because the back of the reference cell doesn't receive any irradiation. The difference will vary during the year because of the varying ratio of diffuse to global irradiation. This ratio is available for extraction from the PVGIS database. When calculating the irradiation for a specific location, PVGIS provides an overview of both the diffuse and direct component of the total horizontal irradiation. PVGIS is also calculating the ratio of diffuse to global irradiation, which are illustrated in Table 14.

Table 14: The varying ratio of diffuse to global irradiation throughout the year. The values extracted from PVGIS.

Month	**Jan**	**Feb**	**Mar**	**Apr**	**May**	**Jun**	**Jul**	**Aug**	**Sept**	**Oct**	**Nov**	**Dec**
Ratio of diffuse to global irradiation	0.69	0.61	0.48	0.45	0.43	0.43	0.45	0.45	0.48	0.58	0.64	0.68

The spectral response is also different for a pyranometer and a reference cell, since the reference cell is made to match the spectral response for the PV modules. As an example; the pyranometer at Blindern measures the light from 285 to 2800 nm, while the reference cell at Økern measures from 350 to 1200 nm.

The meteorological stations with a pyranometer and measured irradiation are often located far apart. With the number of PV systems increasing and thus the amount of reference cells, it would have been of good use to be able to exploit the information from these reference cells, both for design, dimensioning and monitoring of PV systems. To be able to do this, an efficient and simple way to convert the data for an angled surface is necessary. Today it is possible to make calculations for a specific hour with the help of different online calculators, but it is not practical to use datasets with hourly values for irradiation on a tilted surface as input and get horizontal irradiation as output. The calculations are highly complicated and it is necessary to calculate the correction for both the direct and diffuse component of the irradiation.

A PV system well equipped with meteorological instruments has a great advantage when it comes to monitoring of the system. With the growing PV industry, it has been more common to install PV reference cells. The reference cell has several advantages compared to the pyranometer when the purpose is to measure irradiation in the module plane. The reference cell is cheaper than the pyranometer and the reference cell is designed to match the spectral

response of the modules of the system. It is still necessary with knowledge about installation, operation and maintenance of both of the irradiation measurement instruments. The pyranometer can also be mounted with the same slope as the modules, but still it will have another spectral response than the reference cell. When using a pyranometer it is necessary to consider deviating spectral response and difference between the slope of the module and the horizontal pyranometer when calculating the amount of irradiation available for the modules. This adds more uncertainty to the values from the pyranometer. The reference cell will give a value for the available irradiation more close to the amount that the PV modules receive. The pyranometer is designed to have low dependence of temperature. The reference cell is more dependent of temperature changes in the instrument, as are the PV modules. The response time for the reference cell does match the response time of the modules better than the response time for the pyranometer, which has a longer time response. For detailed monitoring with resolution of seconds, this can be an advantage. But then it can be discussed how high the resolution for the data must be, to have a sufficient monitoring of the PV system. There are also advantages of using a pyranometer over a reference cell. The pyranometer has been used for measuring irradiation longer than the reference cells. The methods for calibration of the instruments are well known and the calibration factors are known to be stable. The pyranometer with its hemisphere domes also requires less cleaning compared to the pyranometer which has a plane surface. When dealing with several types of cells in a PV system is it necessary with different reference cells for all the different types of PV cells. When using a pyranometer it is only necessary with one instrument. Could it be good solution to place horizontal reference cells together with the reference cell in the module plane? This information could be available in a database with the possibility to see what information is available for a given location. However, this will require a system for handling a tremendous amount of data. With a good tool for converting the horizontal irradiation to the wanted plane of the modules, it could be convenient both for dimensioning PV systems and for monitoring of them. Still this information will only be valid for the modules with equal material as the reference cell. To make calculations for the efficiencies of different PV technologies it is necessary with a standard for how to measure irradiation, to be able to compare the different technologies on the same basis.

4.4 A comparison of two "remote" sources – Ås and Blindern

This section will take a closer look at the irradiation sources at Blindern and Ås. How coinciding are the irradiation values at Ås and Blindern? The annual irradiation for Ås and Blindern in the period of August 2015 to August 2016 are illustrated in Figure 37.

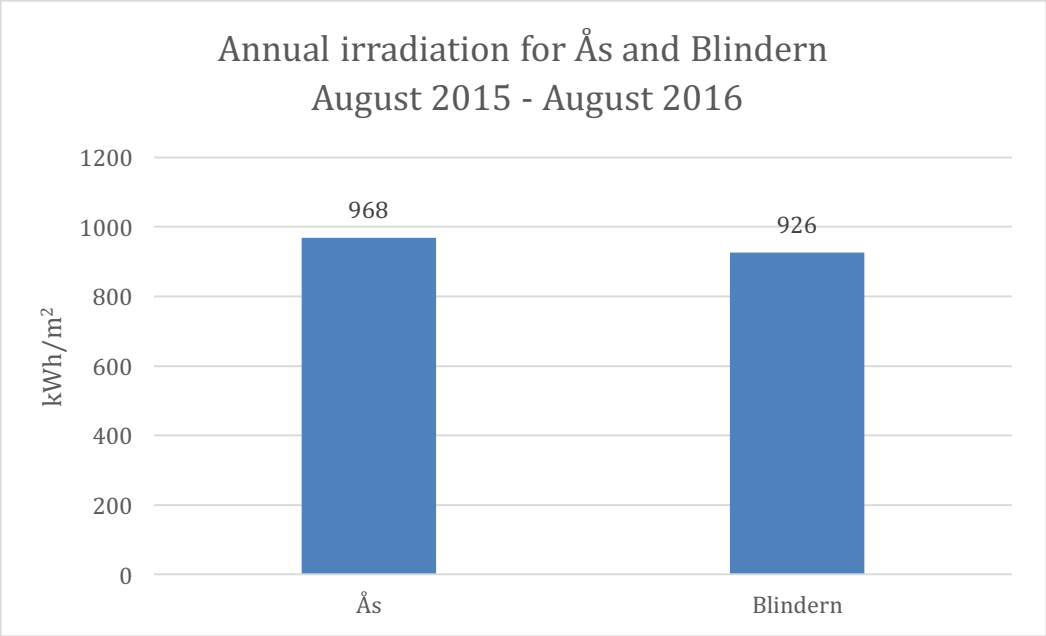

Figure 37: Annual irradiation at Ås and Blindern for the period August 21, 2015 to August 20, 2016.

Figure 37 shows that the annual irradiation for the two locations does varies. The annual difference is approximately 42 kWh/m^2, or 4.3% more annual irradiation at Ås compared with the irradiation at Blindern. This result is not that surprising. A lot of factors will influence the total irradiation, as changing cloud coverage. It is natural to see a difference here. Still, due to the lack of more local data, information from meteorological measurement stations far away from the PV system site is used for estimation of PV production.

4.5 A comparison of four "local" sources - The four reference cells on Økern

This section will take a closer look at the irradiation data sources at Økern. How coinciding are the irradiation values for the four reference cells? The annual irradiation for Økern in the time period of August 2015 to August 2016 are illustrated in Figure 38.

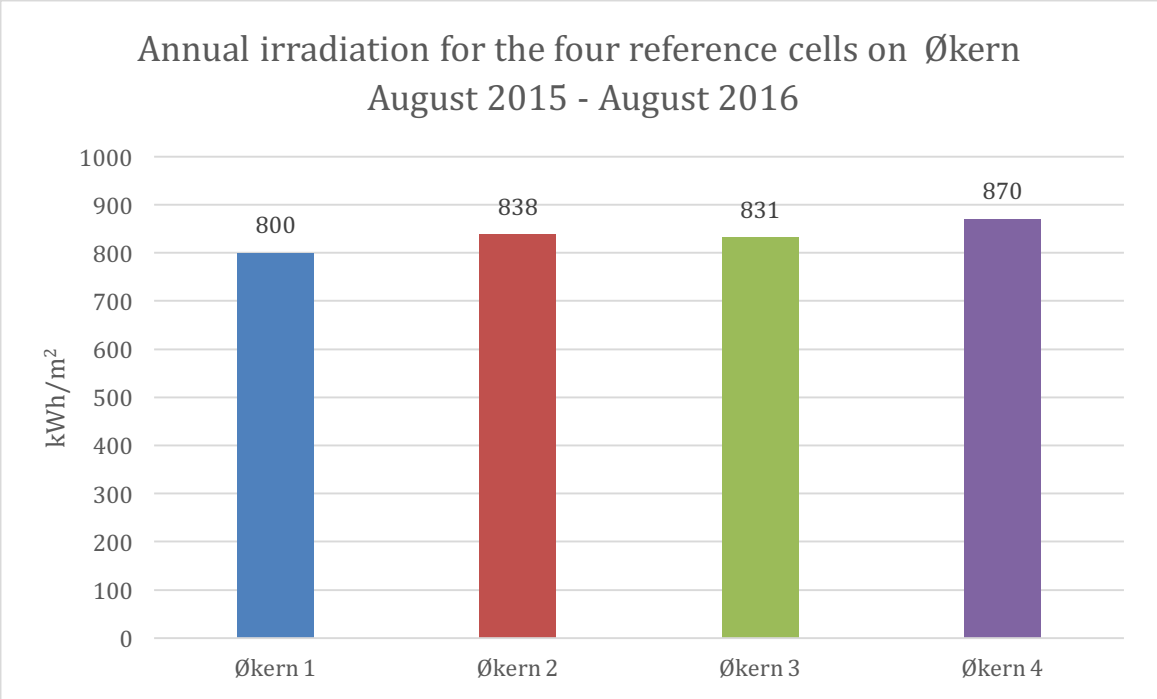

Figure 38: Annual irradiation for the four reference cells at Økern for the period August 21, 2015 to August 20, 2016.

This result is more interesting than the previous one. Here we have got four reference cells mounted on the same roof, only with the spacing of a few meters. The location of the reference cells is at the south end of the building and will not be affected by shading from the technical room in the middle of the roof. In the summer the reference cells will probably be affected by shading from the tall building located west of Økern. In the winter the Sun will set before reaching the building, but in the summer the Sun will set somewhere behind the tall building. The differences in total irradiation can be explained by the different slopes and orientation. Reference cell number four, Økern 4, has a slope of 20 degrees compared to the three other which has a slope of 10 degrees. It is a good explanation of why Økern 4 has a higher annual irradiation than the other three cells. Økern 1 and Økern 2 both have the same slope and orientation and should have approximately the same output. The annual difference between Økern 1 and Økern 2 is 38 kWh/m^2. The difference is less for Økern 2 and Økern 3. For these two cells, the annual difference is only 7 kWh/m^2. These differences can indicate that there is some sort of shading of the reference cells. When inspecting the roof at Økern on December 1, it was only some leaf trees that could contribute to shading on the reference cells, in addition the tall building in the west. The difference in annual irradiation for the reference cells can also occur due to soiling of the cells, different amount of snow coverage in the winter or varying leaf coverage.

The next section will examine the data from the reference cells on Økern in a better resolution. Figure 39 illustrates the plot of the irradiation on the four reference cells on August 23, 2015.

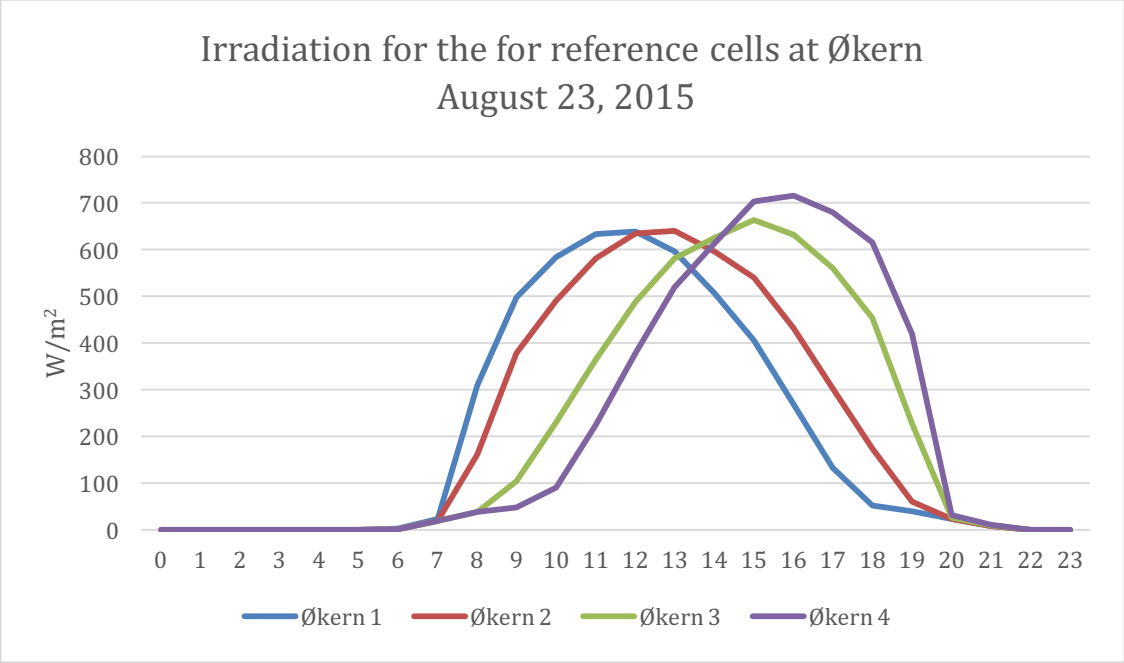

Figure 39: Irradiation for the four reference cells at Økern on August 23, 2015.

From Figure 39 it is obvious that Økern 4 receives more irradiation during the day. The amplitude of Økern 4 reaches approximately 70 W/m^2 over the other three reference cells. This is due to the slope of 20 degrees. All the curves have gentle slopes at the beginning and at the end of the curves. This can be due to diffuse irradiation before the Sun rises above the horizon in the morning and after it sets in the evening. The steep curves occur when the cells receive direct irradiation. Økern 1 is the first cell to receive irradiation. The curves for the three other cells are shifted towards right of the curve of Økern 1. It is a time, approximately at 14.00 that the reference cells receive approximately the same irradiation. The shift of the curves to the right can be due to the orientation of the reference cells. The Sun rises in the east and sets in the west. Økern 1 and Økern 2 are oriented towards east and will therefor receive direct irradiation some time before Økern 3 and Økern 4. Økern 3 and Økern 4 are oriented towards west and will be facing away from the rising Sun. To explain the time shift between Økern 1 and Økern 2, and the time shift between Økern 3 and Økern 4 is more challenging. It can be due to the elevation of the roof at the southern end of the building or if the trees in near distance are shading the modules. The fact that the time shift occurs both at the start and the end of the steep curve, can indicate that it is the same object responsible for the shading both when the Sun is on its way up and when it is on its way down during the day. Two arbitrary days was chosen to see if the same pattern was repeating. Figure 40 and Figure 41 shows the

irradiation for Økern 1 and Økern 2 at March 3, 2016 and May 25, 2016, and shows the same pattern for these two days.

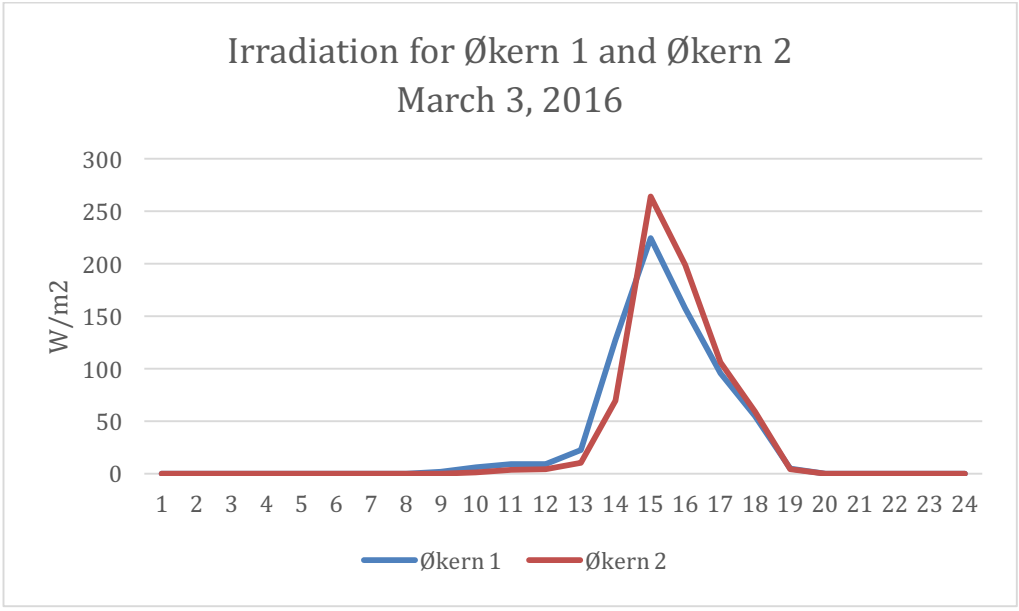

Figure 40: Irradiation for Økern 1 and Økern 2 at March 3, 2016.

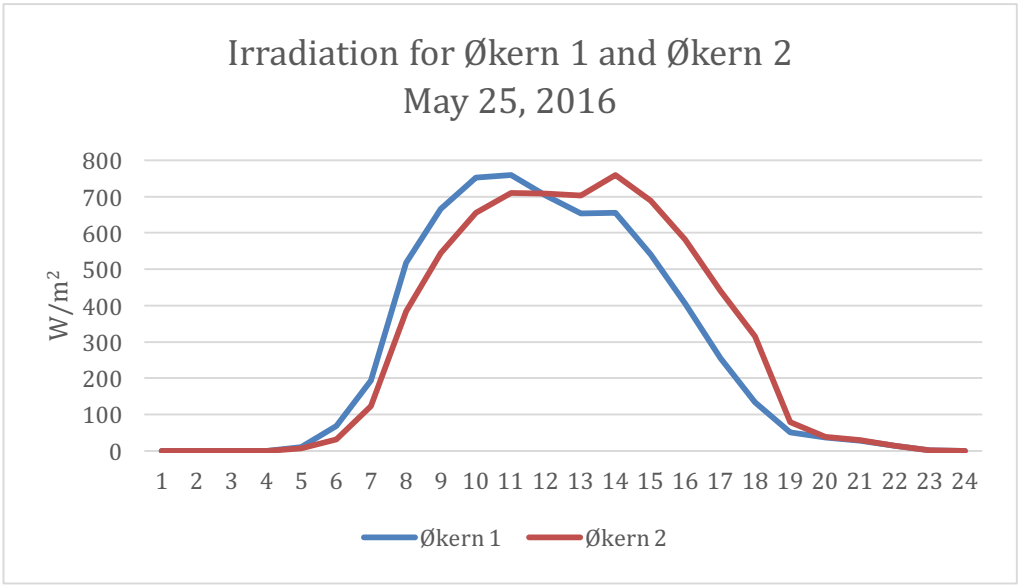

Figure 41: Irradiation for Økern 1 and Økern 2 at May 25, 2016.

This next section will be a comparison of Økern 1 and Økern 2, which are the only ones completely comparable of the four reference cells, with the same slope and orientation. Figure 42 illustrates the same day as Figure 39, but only showing the curves for Økern 1 and Økern 2.

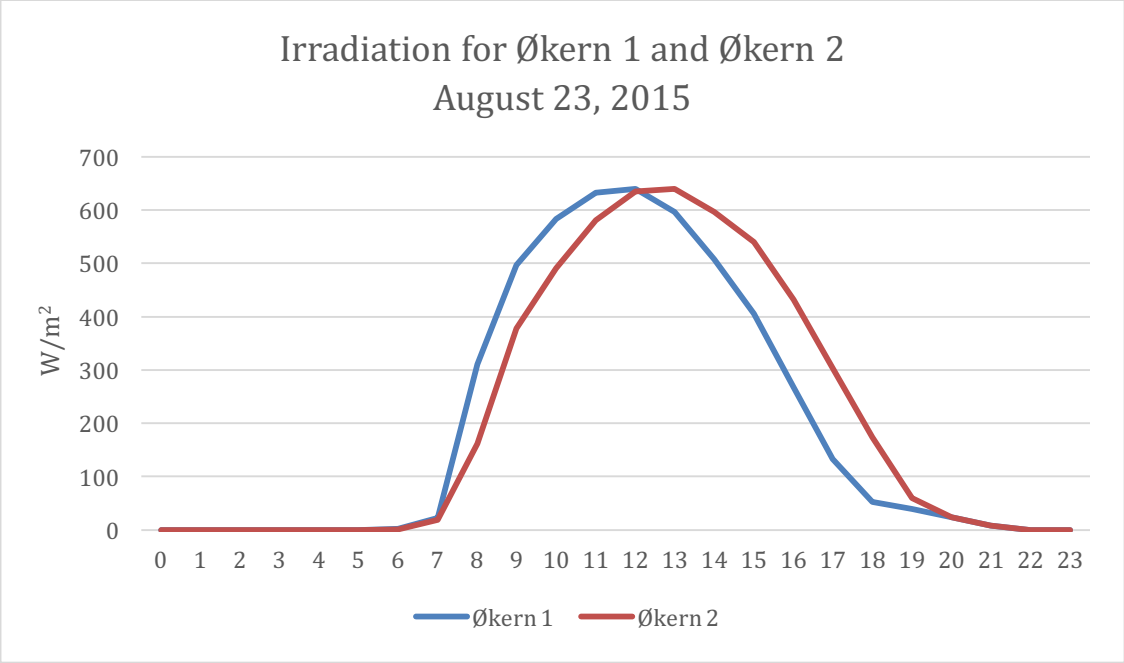

Figure 42: Irradiation for Økern 1 and Økern 2 at Økern. August 23, 2015.

The time shift between the two curves is approximately one hour. Meteorological factors as cloud coverage can change a lot in one hour. Figure 42 is from a clear day, with little or no clouds. For a day with a lot a cloud cover the time shift will have higher impact on the total daily irradiation.

4.6 The impact from varying weather

The following section will study the irradiation at Økern, Ås and Blindern with better resolution for the irradiation data. Additionally, the module temperature for the reference cells are compared with the data for the irradiation on Økern. The following scenarios are examined for all the locations:

- A day with varying cloud coverage
- A day with clear sky
- A fully overcast day

4.6.1 Økern

Case 1: A day with varying cloud coverage

Figure 43 shows the irradiation for Økern 1 and Økern 2 on June 10, 2016 with hourly resolution. The module temperature for the reference cells is plotted on the secondary axis. The dips on the curves are due to varying cloud coverage. Figure 8 shows the irradiation for Økern 1 and Økern 2 on June 10, 2016 with resolution in minutes.

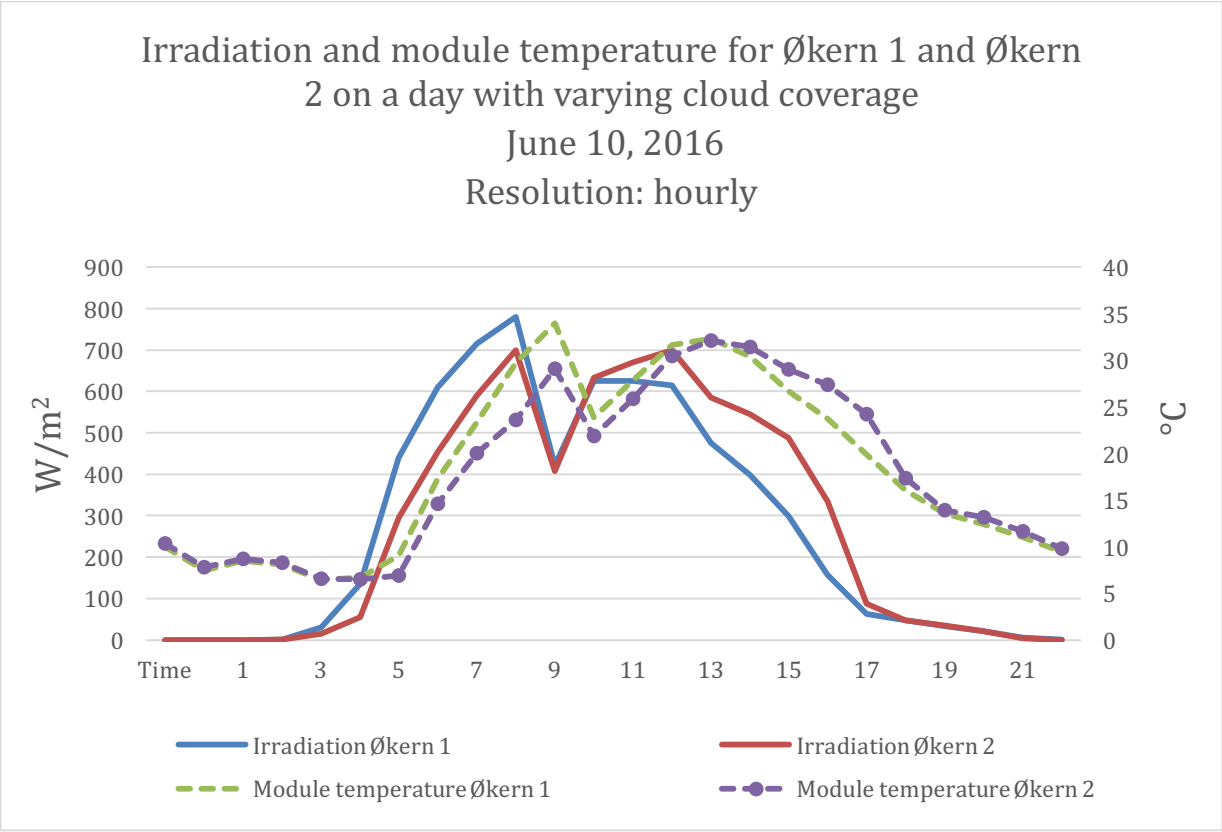

Figure 43: The irradiation for Økern 1 and Økern 2 on June 10, 2016. Resolution: hourly. Module temperature is plotted on the secondary axis.

Again, we can see the time shift when the Sun is on its way up and on its way down. Approximately between 09.00 and 11.00 there is almost perfect concurrence between the two curves. The module temperature is following the curves of the irradiation, with some delay. It takes time from the module receives irradiation to the heating of the materials. The maximum module temperature reaches over 30 degrees during the day. Figure 44 gives a more detailed illustration of the impact of the clouds.

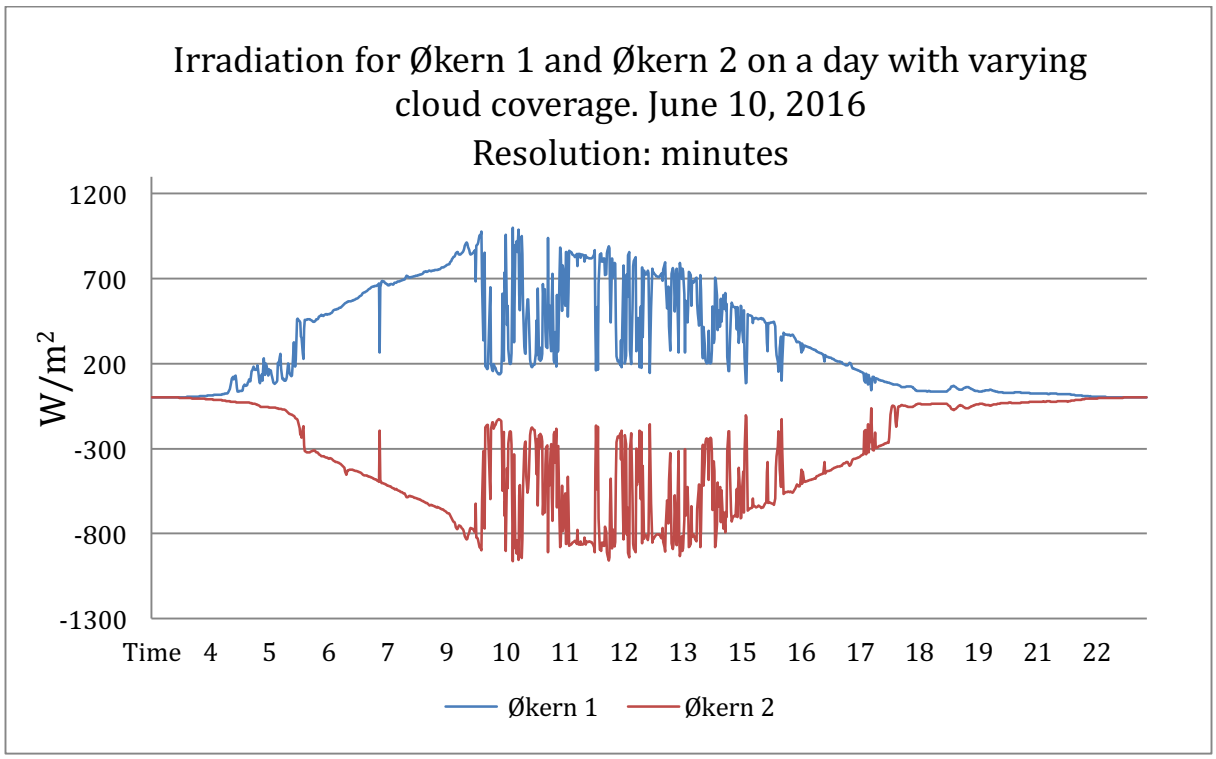

Figure 44: The irradiation for Økern 1 and Økern 2 on June 10, 2016. Resolution: minutes.

Notice that the timescale for Figure 8 has been adjusted, so that the most interesting part of the day is more visible. The hours without irradiation is removed. The time series for Økern 2 has been rotated on the x-axis to get a better picture of the impact of the clouds on the irradiation measurements. The concurrence of the dips is almost identical, as expected. The distance between the reference cells will count for equal impact from the varying cloud coverage. Values for the horizontal irradiation from Blindern are plotted together with the values from Økern 1 and Økern 2 in

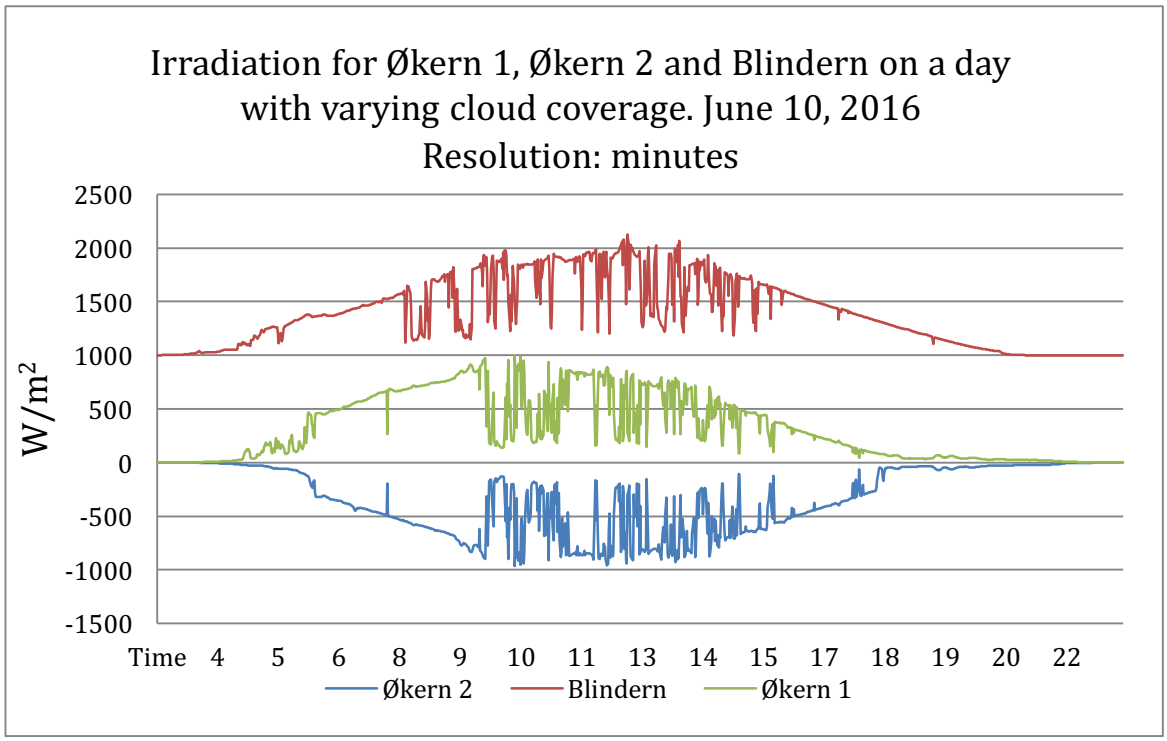

Figure *45*. 1000 W/m^2 has been added to the values for the irradiation at Blindern, to separate the time series from each other and avoid overlap of the curves.

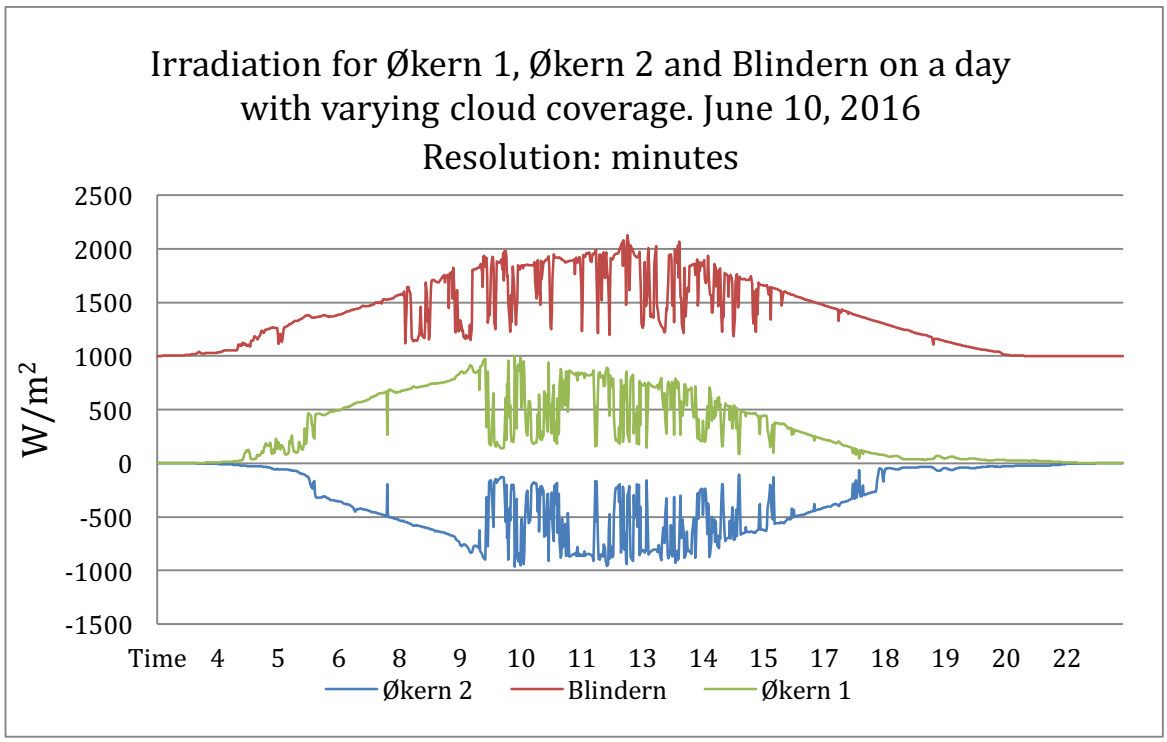

Figure 45: The irradiation for Økern 1 and Økern 2 on June 10, 2016. The irradiation for the reference cells are plotted together with the horizontal irradiation from Blindern. Resolution: minutes.

Figure 46 shows a section of the time series approximately from 09.00 to 11.00 on June 10, 2016.

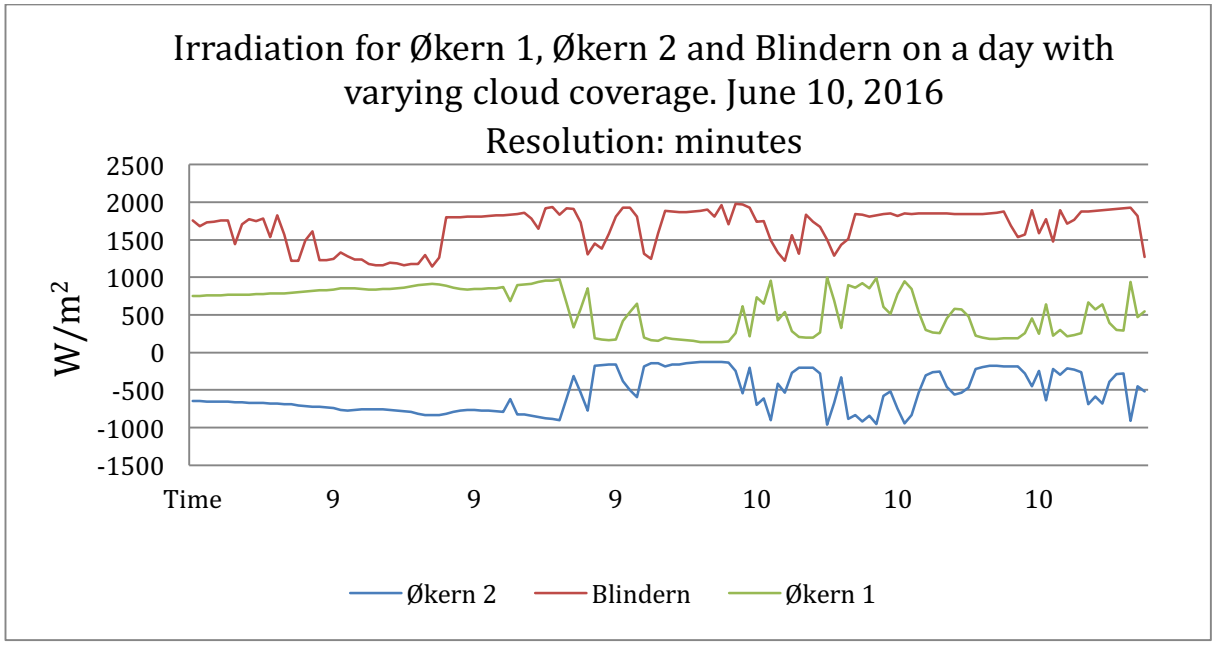

Figure 46: The irradiation for Økern 1 and Økern 2 on June 10, 2016 approximately from 09.00 to 11.00. The irradiation for the reference cells are plotted together with the horizontal irradiation from Blindern. Resolution: minutes.

The linear distance from Økern to Blindern is approximately 5 km. The pyranometer at Blindern is clearly affected by different clouds than the reference cells on Økern, according to the curves in Figure 46.

Case 2: A day with clear sky

Figure 47 shows the irradiation for Økern 1 and Økern 2 on August 22, 2015 with hourly resolution. The module temperature for the reference cells is plotted on the secondary axis.

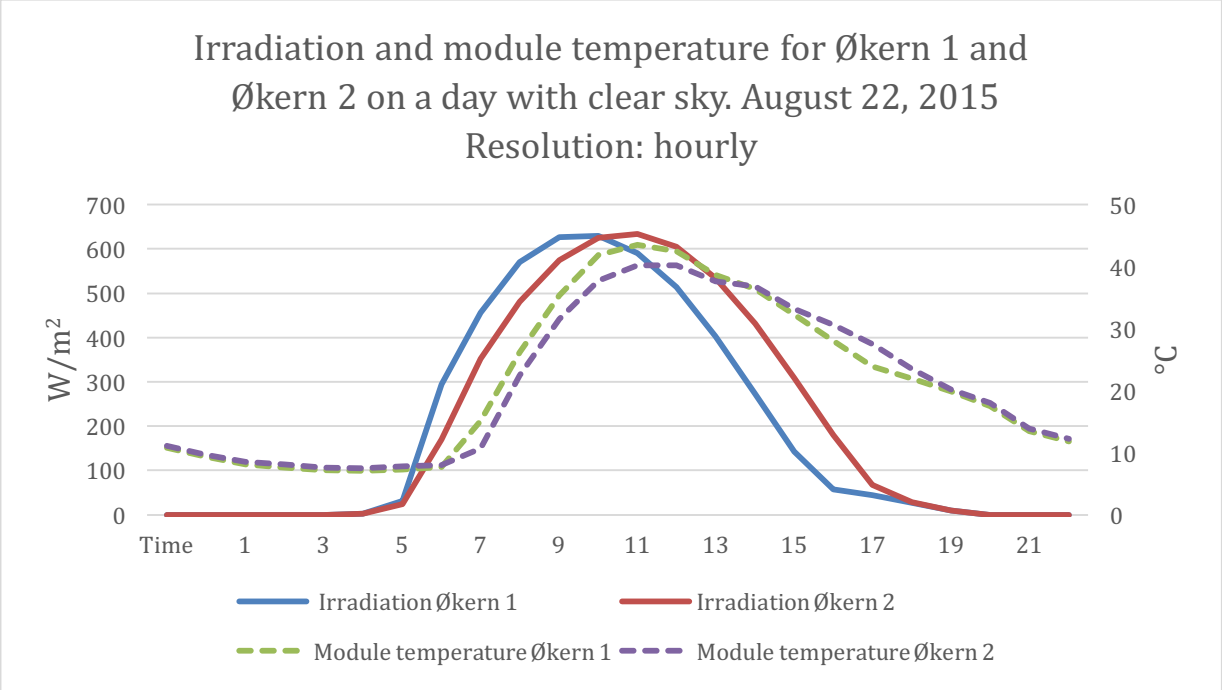

Figure 47: The irradiation at Økern 1 and Økern 2 on June 10, 2016. Resolution: hourly. Module temperature is plotted on the secondary axis.

Again, we can see the time shift when the Sun is on its way up and on its way down. Approximately at 10.00, there is almost perfect concurrence between the two curves. This is probably where the Sun is at its highest point in the sky that day. At this point the reference cells are minimally affected by shadowing from modules and the environment. The module temperature is following the curves of the irradiation, with some delay. It takes time from the module receives irradiation to the heating of the materials. When the Sun is on its way down and the reference cells are receiving less irradiation, it takes time before the material of the module is cooled. The curve of the module temperature will, due to thermal equilibrium, move toward the air temperature some time during the evening or in the night. The maximum module temperature reaches over 45 degrees during the day. The module temperature varies from seven degrees early in the morning to the maximum temperature at 45 degrees in the middle of the day. Figure 48 gives a more detailed illustration of the impact of the clouds.

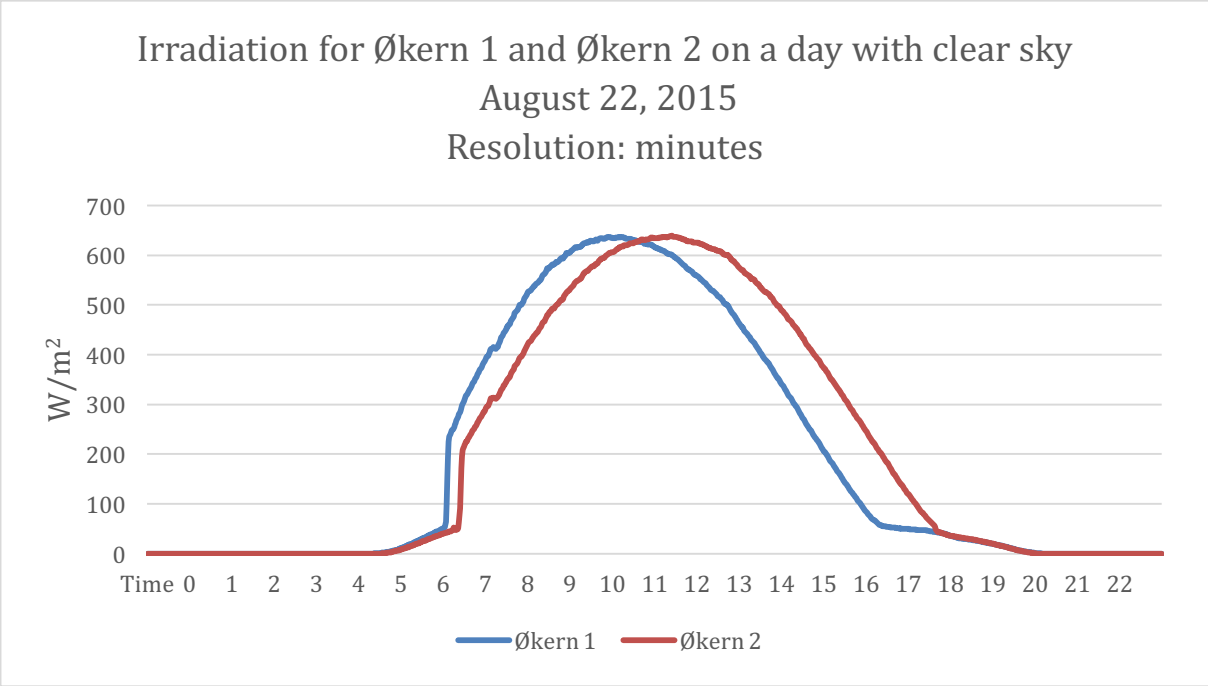

Figure 48: The irradiation at Økern 1 and Økern 2 on June 10, 2016. Resolution: minutes.

The changes in irradiation on a clear day are not varying during the day like on a day with varying cloud coverage. Better resolution of the data may not be as necessary on days with a clear sky as for days with varying cloud coverage. Figure 48 gives a better illustration of the transition between diffuse and direct irradiation received by the reference cells both in the morning and in the evening. This transition between direct and diffuse irradiation is on August 22, 2015 happening around 17.30 for Økern 1. On this date the Sun went down at 20.49 in Oslo, according to [26]. The gentle part of the curve at the end of day in Figure 48 can be caused by far shading or by the tall building west of Økern, resulting in only diffuse irradiation on the reference cells.

Case 3: A day with fully overcast

Figure 49 shows the irradiation for Økern 1 and Økern 2 on September 1, 2015 with hourly resolution. The module temperature for the reference cells is plotted on the secondary axis.

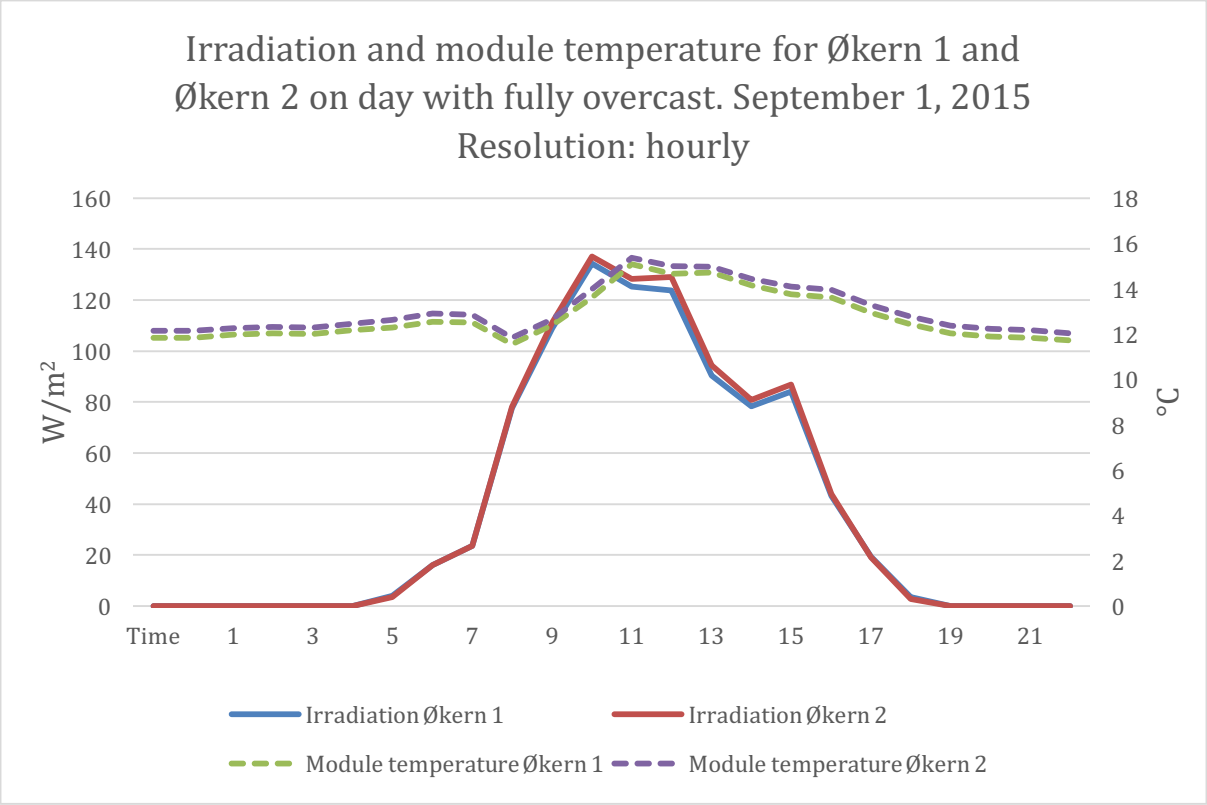

Figure 49: The irradiation at Økern 1 and Økern 2 on September 1, 2015. Resolution: hourly. Module temperature is plotted on the secondary axis.

Figure 49 have the same form of the curve as for a clear day, with the peak of the curve in the middle of the day were the Sun is at its highest. The curves for Økern 1 and Økern 2 does not reach the same maximum as for a clear day. The maximum value for the two curves reaches a value somewhere right below 140 W/m^2. This low value for the daily maximum is due to the lack of direct irradiation. The amount of irradiation received by the reference cells is due to diffuse irradiation. The module temperature is more stable for a day with fully overcast, only varying between twelve and 15 degrees. The reference cells and the modules receive less irradiation and thus less heat is generated in the material. It is good concurrence for the two irradiation curves. Figure 50 shows the irradiation for September 1, 2015 with resolution in minutes.

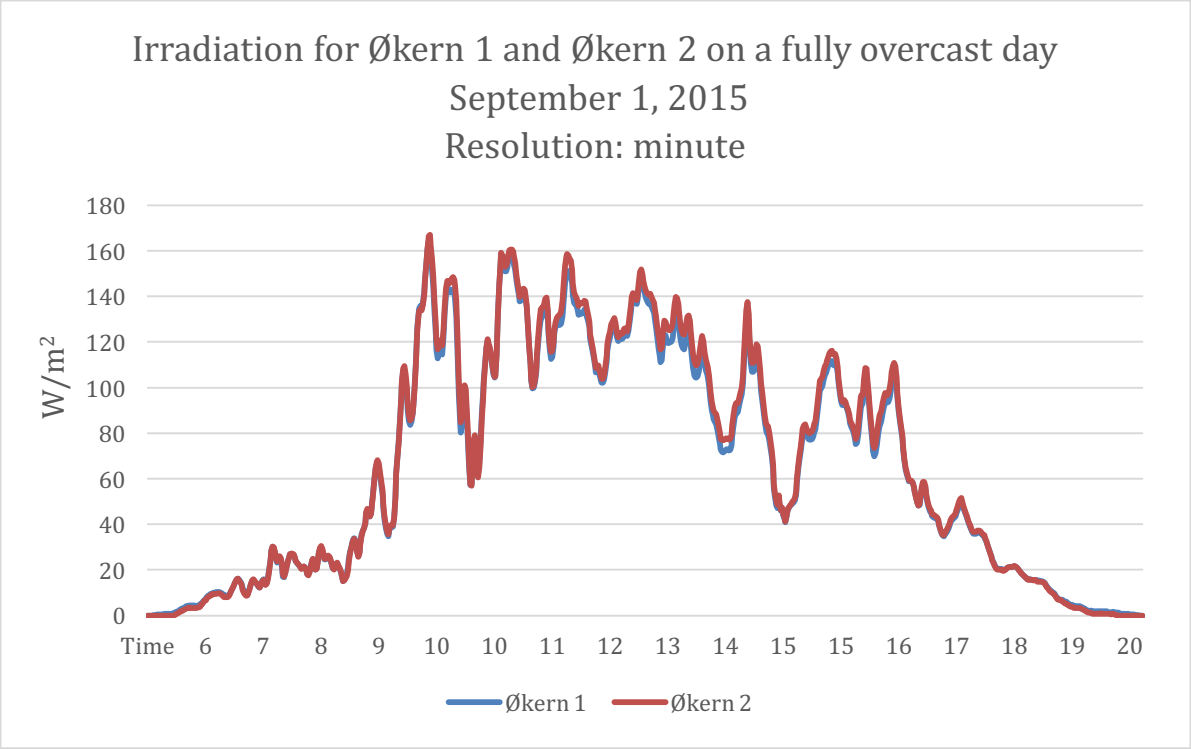

Figure 50: The irradiation at Økern 1 and Økern 2 on September 1, 2015. Resolution: hourly. Module temperature is plotted on the secondary axis.

The concurrence of the curves is even clearer in Figure 50. The time axis is adjusted to get a better picture of the irradiation curves and the time of the day without irradiation is removed. The difference in the two curves is minimal and they do not have the same time shift as in the previous scenarios. This can indicate that the time shift in the previous scenarios, which both included more direct irradiation, is due to shading. The problem with shading is less prominent for days with mainly diffuse irradiation. For an overcast day with diffuse irradiation, the irradiation has a more uniform distribution across the PV site, compared to days with direct irradiation where shading can have a varying impact on the different modules due to the position of the module.

4.6.2 Ås and Blindern

Case 1: A day with varying cloud coverage

Figure 51 shows the irradiation at Ås and Blindern on June 10, 2016. This is a day with varying cloud coverage.

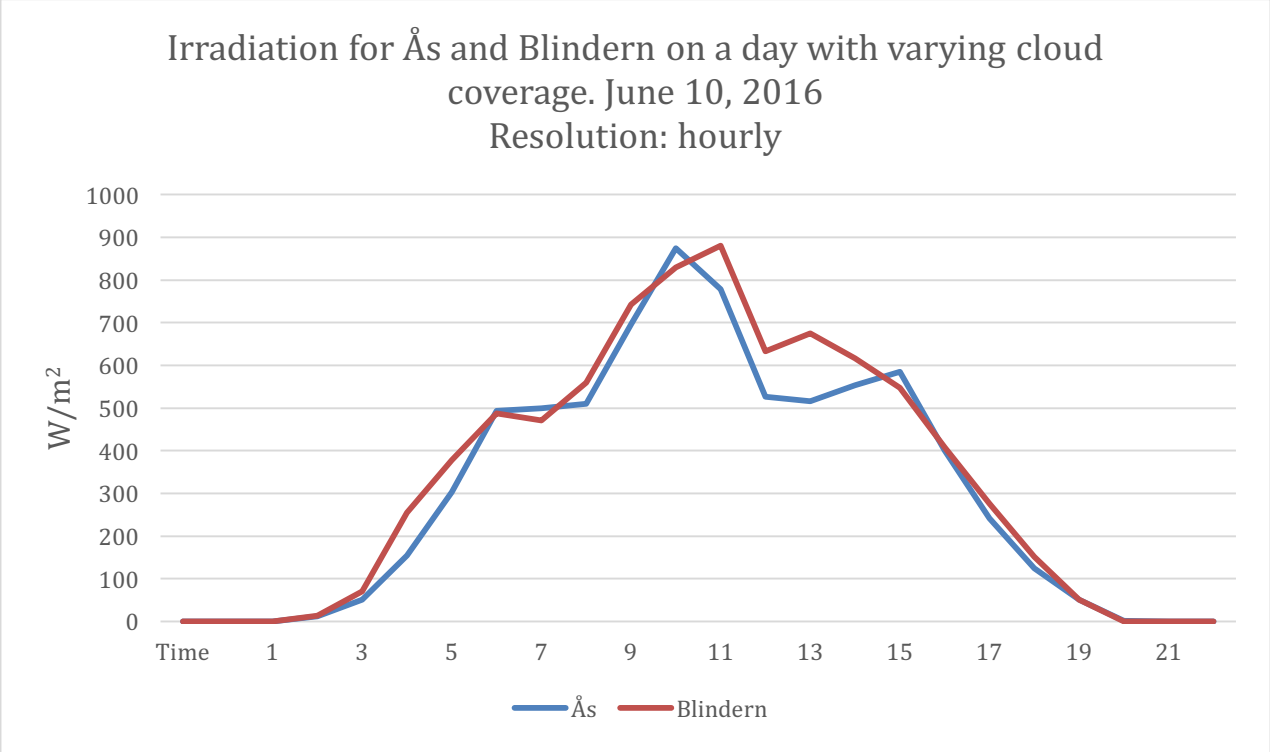

Figure 51: Irradiation for Ås on a day with varying cloud coverage, June 10, 2016. Hourly resolution.

The distance between Ås and Blindern is approximately 36 kilometers. The curves for the hourly irradiation values for Blindern and Ås deviates, but follows approximately the same path for the hourly values. It is especially from 10.00 to 15.00 that the curves deviate from each other. This difference in the irradiation curves for a day with varying cloud coverage indicates that the pyranometers are affected by different cloud conditions. Figure 52 shows irradiation for Ås and Blindern at June 10, 2016 with resolution of ten minutes to give a more detailed picture of the clouds impact on the irradiation measurements.

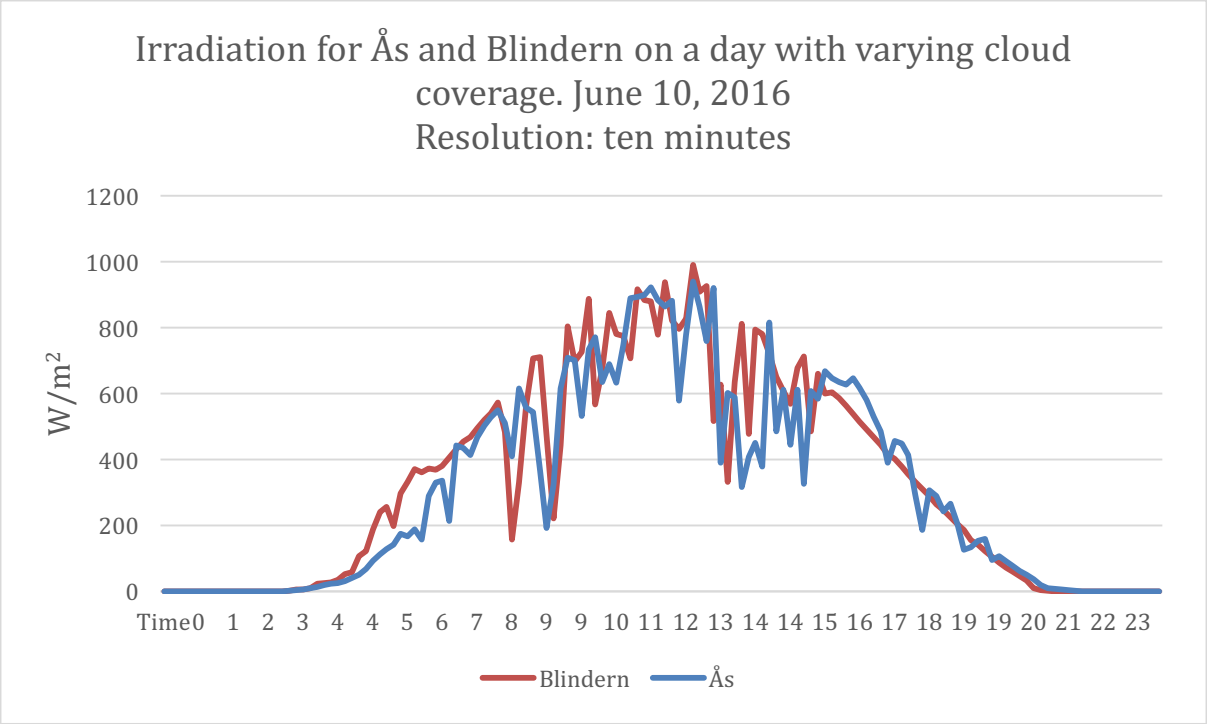

Figure 52: Irradiation for Ås on a day with varying cloud coverage, June 10, 2016. Resolution of ten minutes.

Figure 52 illustrates how the pyranometers at Blindern and Ås are affected by different cloud conditions. The result is not very surprising, considering the distance between the two meteorological stations.

Case 2: A day with a clear sky

Figure 53 shows the irradiation at Ås and Blindern on August 22, 2015. This is a day with a clear sky.

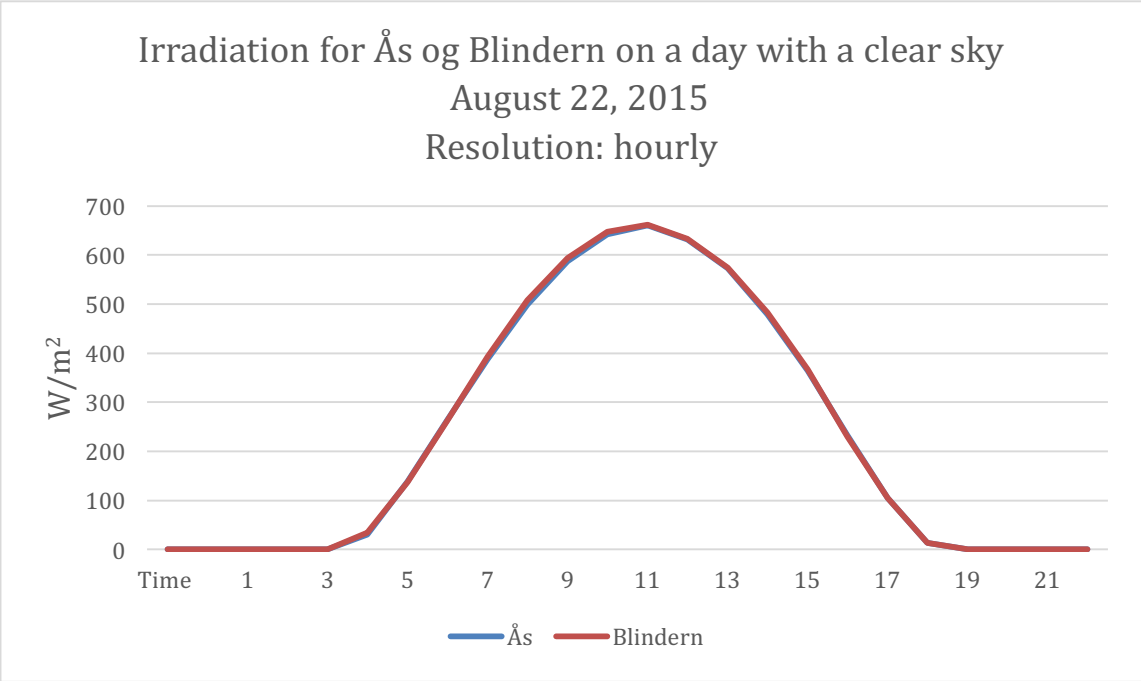

Figure 53: Irradiation for Ås on a day with a clear sky. June 10, 2016. Hourly resolution.

The hourly values for the irradiation are identical through the whole day. The curve for Blindern is almost perfectly covering the curve for Ås. This result is as expected. The distance between the meteorological stations is not enough to expect great variation in horizontal irradiation. The two stations are located 36 kilometers apart, but is still located at approximately the same longitude and latitude. Figure 54 shows the measured irradiation at Ås and Blindern for the day with a clear sky, with resolution of ten minutes for the data.

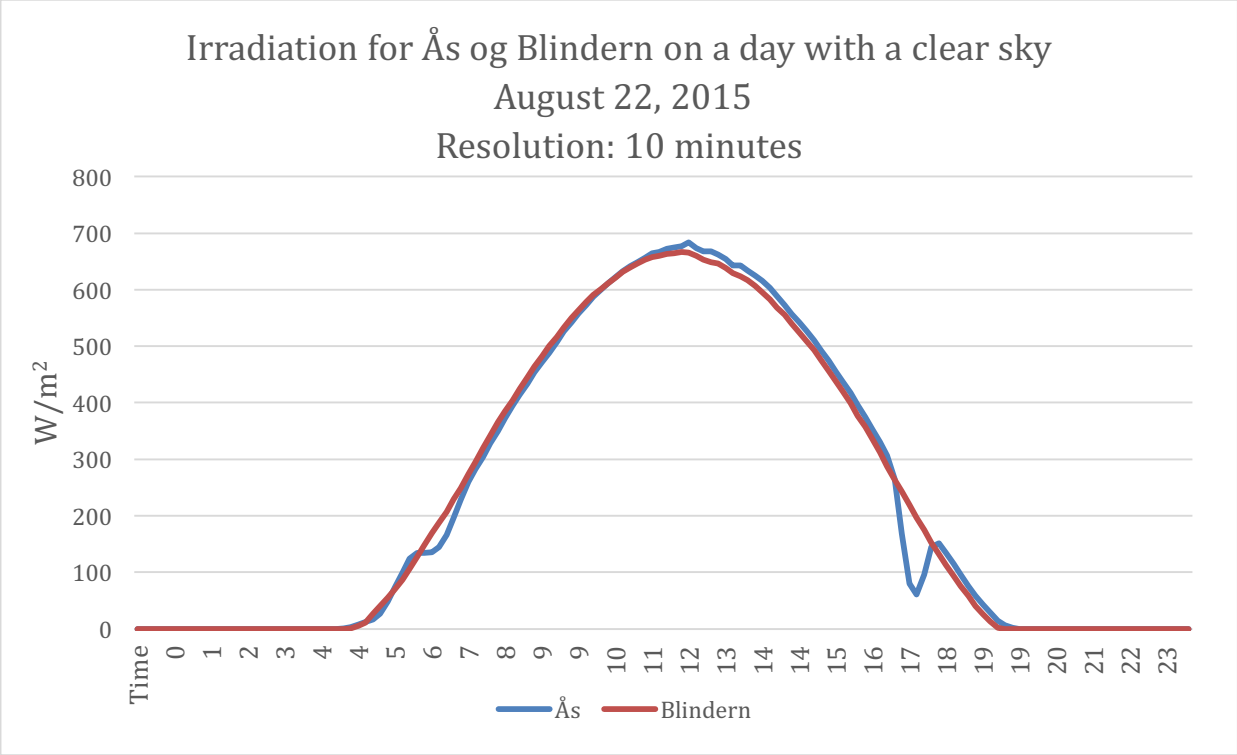

Figure 54: Irradiation for Ås on a day with a clear sky. June 10, 2016. Resolution of ten minutes.

The curves are still similar to each other, except for the two dips in the curve for the irradiation at Ås. These two dips can be caused by small, local clouds. Changes in the irradiation values over short intervals will not show, because of the low resolution of the data and the fact that each value is an average value of ten minutes. Because the span of the dips are approximately 15 minutes for the first one and 40 minutes for the second one, they are not likely to be caused by something covering up the pyranometer, like a bird or leafs.

Case 3: A day with fully overcast

Figure 55 shows the irradiation at Ås and Blindern on September 1, 2015. This is a day with fully overcast.

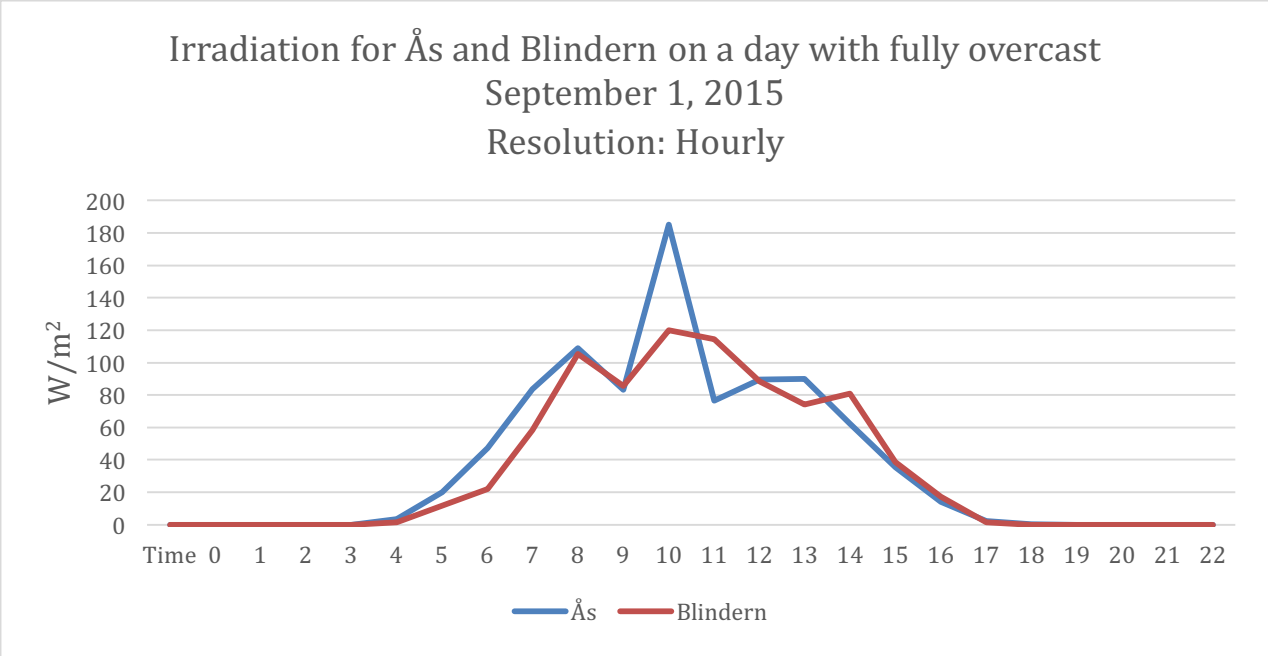

Figure 55: Irradiation for Ås and Blindern A day with fully overcast. September 1, 2015. Hourly resolution.

The curves have peaks in the middle of the day, like for days with a clear sky, but the amplitude is smaller for this day. The curve for irradiation at Ås reaches a maximum of approximately 180 W/m^2 and the curve for Blindern reaches a maximum of approximately 120 W/m^2. This indicated a day with fully overcast. It can look like the cloud coverage for Ås was smaller than for Blindern in the middle of the day, when the peak of the curves reached their maximum values. Figure 56 shows the same curves with a better resolution of the data, to get a better picture of the effect of the clouds on the irradiation measurement.

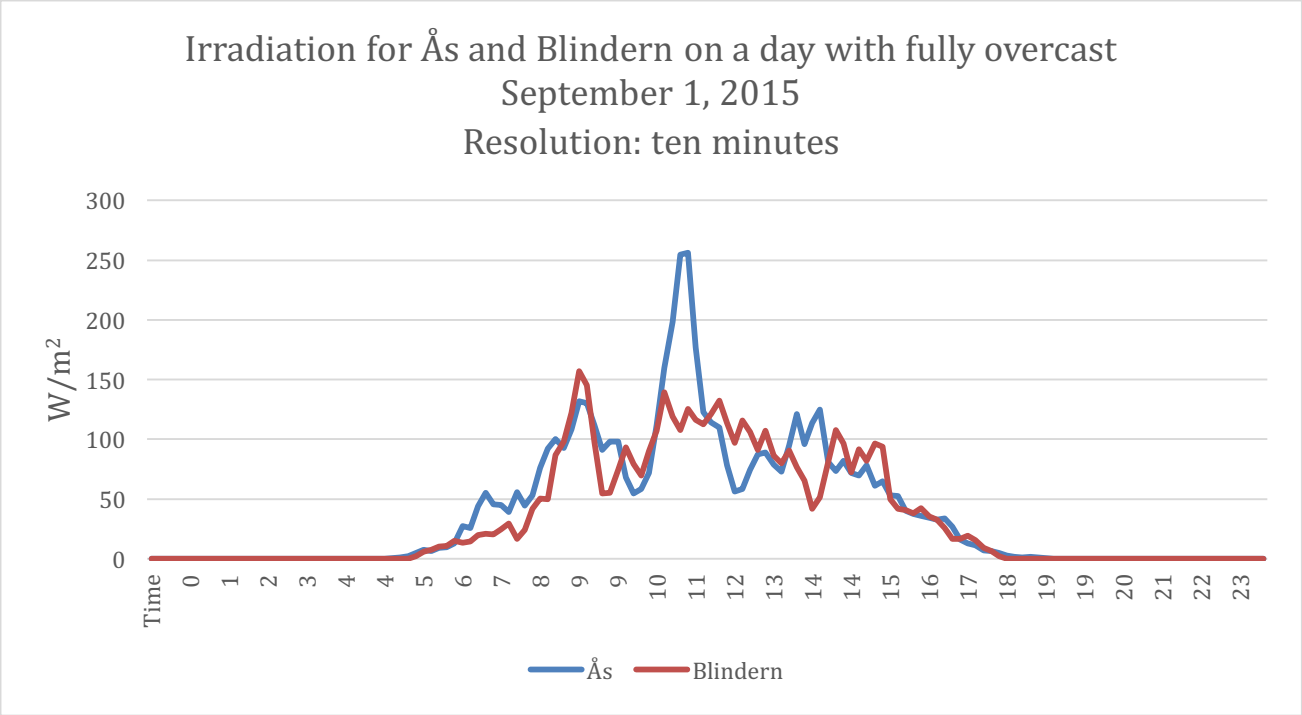

Figure 56: Irradiation for Ås and Blindern on a fully overcast day. September 1, 2015. Hourly resolution.

The curves are quite similar from midnight to 09.00 and from 18.00 to the end of that day. It is clear that during the rest of the day, the pyranometers are affected by different cloud conditions.

4.7 Comparison of Databases

This section takes a closer look at the databases from NASA and PVGIS. This section deals with the correlation between the databases and the measured values for the reference year August 2015 to August 2016, the uncertainty of the measurements and the error occurring when replacing missing data point with measured values from another location.

Figure 57 shows the annual irradiation for the databases from NASA and PVGIS and the measured values from Blindern and Ås.

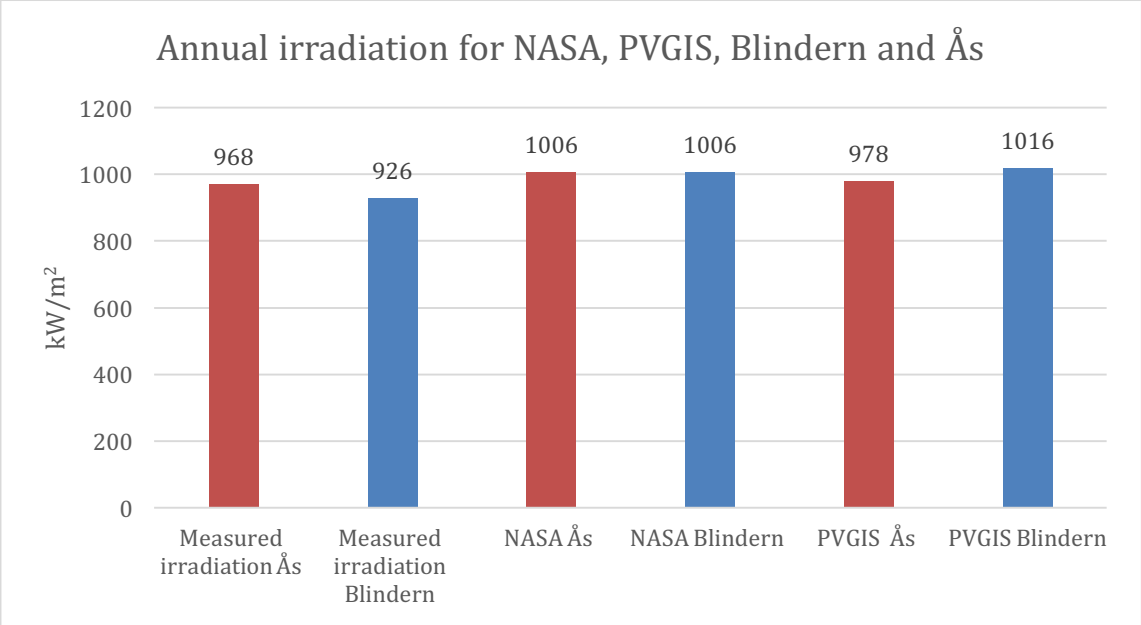

Figure 57: The annual irradiation for the databases from NASA and PVGIS and the measured values from Blindern and Ås for the reference year August 2015 to August 2016.

Figure 57 shows that the annual measured values for both Blindern and Ås are lower than the estimated annual values from NASA and PVGIS. The annual irradiation from the NASA database is equal for Blindern and Ås, due to the spatial resolution of the data. PVGIS has better spatial resolution and the annual results are different for Ås and Blindern, where the annual irradiation for Blindern is 38 W/m^2 higher than for the annual irradiation for Ås. PVGIS estimates the annual irradiation for Blindern to be higher than the annual irradiation for Ås, but the measured values for the two locations shows the opposite result, where the measured irradiation for Ås are higher than the measured irradiation for Blindern, with 42 W/m^2, or 4,5%. The annual estimates from PVGIS deviates from the actual annual irradiation measured at Ås with only 10 W/m^2. Estimates from PVGIS for Blindern has the highest annual deviation from the measured values, with 90 W/m^2.
PVGIS specifies a yearly error of less than 5%. NASA specifies a more detailed difference in irradiation, given for each month as a minimum and maximum difference from the average value. When calculating the maximum and minimum monthly irradiation from NASA, it is clear that the maximum and minimum deviation, from the average year from the 22 years period, is high. The results are represented in Figure 58.

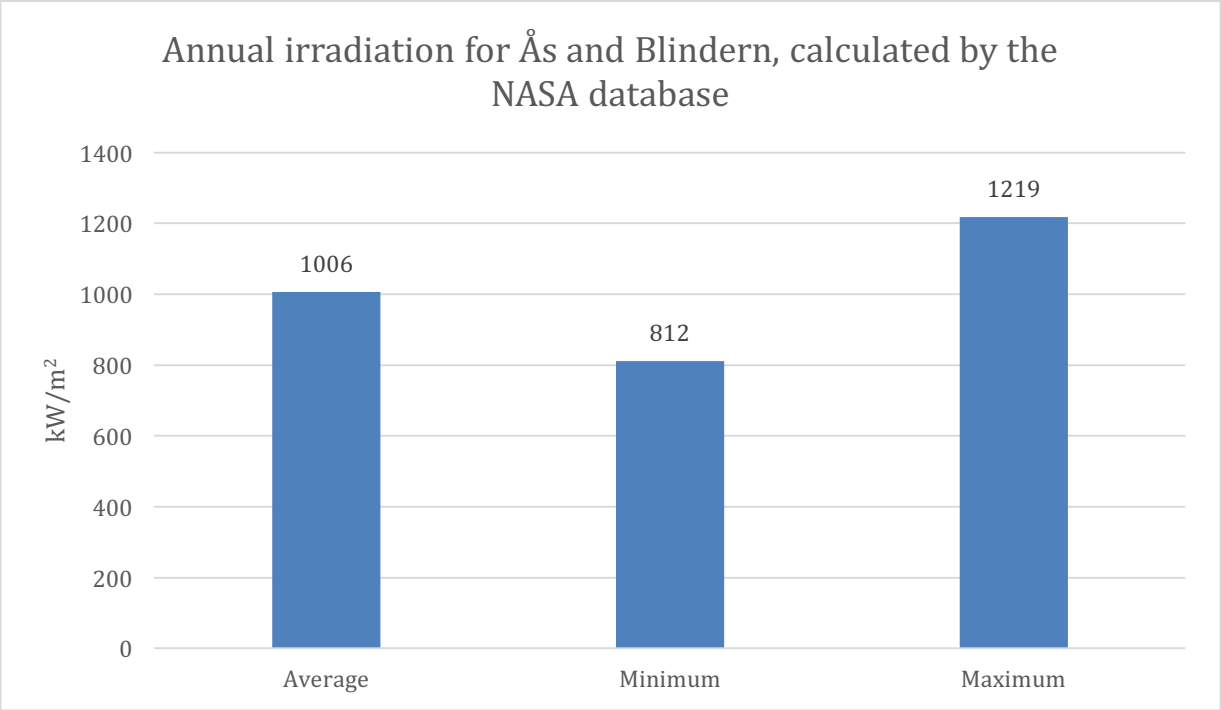

Figure 58: The difference from the estimated average annual irradiation from a 22-years period, given as a minimum and maximum value of annual irradiation.

The minimum value of 812 W/m^2 has an annual irradiation that is 194 W/m^2, or 19.3%, lower than the average year. The maximum value of 1219 W/m^2 has an annual irradiation that is 213 W/m^2, or 21.2%, higher than for the average year. A difference as big as the minimum and maximum value will give a big difference in the annual yield of a PV system.

4.8 Replacement of missing data points

What when meteorological data are missing? This can either be if no meteorological data are available for the PV site, or if the available data sets are missing data for shorter periods. When data points are missing from a data set and the value for the missing points are set to zero, will this lead to an underestimation of the irradiation. If the irradiation is used for calculation of the PR, then the underestimated irradiation value will give an overestimated value of the PR. This section takes a closer look at the error of replacing missing data point with available data sets from other locations. The missing data points examined are the ones missing in the data sets from Ås and Blindern. The only sensor at Økern that is missing data is Økern 4. This sensor has no comparable sensor, due to the fact that this sensor has a slope of 20 degrees, which none of the other sensors on Økern have. The annual irradiation for Blindern are different than the annual irradiation for Ås both measured for the reference year August 2015 to August 2016 and for estimated values by PVGIS. How big will the error be when replacing only the missing data points from the data sets for Blindern and Ås?

4.8.1 Missing data points at Ås

Table 15 shows the total irradiation for January, where the six missing data point from Ås are replaced with values from Blindern.

Table 15: Irradiation for Ås and Blindern in January, where six data points for Ås are missing. The missing data points are replaced with data points from Blindern.

	Ås	Blindern
Total irradiation for January 2016 where six data points for Ås are missing	8346 W/m^2	8891 W/m^2
Total irradiation for January 2016 where the six missing data points for Ås are replaced with values from Blindern	10374 W/m^2	8891 W/m^2

Both Ås and Blindern have complete data sets for February. Table 16 shows the total irradiation for February, where the same six data points are replaced with values from Blindern.

Table 16: Irradiation for Ås and Blindern in February, where the equivalent missing data points from January are replaced with values from Blindern.

	Ås	Blindern
Total irradiation for February 2016	63212 W/m^2	56164 W/m^2
Total irradiation for February 2016 if the equivalent dates with missing data points where replaced with values from Blindern	62594 W/m^2	56164 W/m^2

The calculated value was compared with the actual value for the monthly irradiation for Ås in February, and the result is presented in Table 17.

Table 17: The difference between the actual value for Ås in February and the calculated value with six data points replaced with values from Blindern.

Month	February
Difference	-618 W/m^2
Difference	-1 %

The difference between the actual value for Ås and the calculated value with values from Blindern was found to be -1%. The estimated value for Ås in January are presented in Table 18, where the difference from February has been taken into the calculations.

Table 18: The estimated irradiation for Ås in January, with the difference from February taken into the calculations.

Month	January 2016
Total irradiation for January in Ås with six data points replaced by values from Blindern	10374 W/m^2
Calculated error from replacing data point equivalent to the missing data points for February	-1%
Total irradiation for January in Ås with six data points replaced by values from Blindern, considered calculated error	10477 W/m^2

When considering the -1% difference, the estimated irradiation for Ås in January was 10477 W/m^2.

4.8.2 Missing data points at Blindern

Table 19 shows the total irradiation for October, where the four missing data points for Blindern are replaced with values from Ås.

Table 19: Irradiation for Ås and Blindern in January, where four data points for Blindern are missing. The missing data points are replaced with data points from Ås.

	Ås	Blindern
Total irradiation for October 2015 where four data points for Blindern are missing	40540 W/m^2	37168 W/m^2
Total irradiation for October 2015 where the four missing data points for Blindern are replaced with values from Ås	40540 W/m^2	40567 W/m^2

Both Ås and Blindern have complete data sets for September. Table 20 shows the total irradiation for September, where the same four data points are replaced with values from Ås

Table 20: Irradiation for Ås and Blindern in September, where the equivalent missing data points from October are replaced with values from Ås.

	Ås	Blindern
Total irradiation for September 2015	73498 W/m^2	70706 W/m^2
Total irradiation for September 2015 if the equivalent dates with missing data points where replaced with values from Ås	73498 W/m^2	70986 W/m^2

The calculated value was compared with the actual value for the monthly irradiation for Blindern in September, and the result is presented in Table 21.

Table 22: The difference between the actual value for Blindern in September and the calculated value with four data points replaced with values from Ås.

Month	September
Deviation of the calculated value from the original value	280 W/m^2
Deviation of the calculated value from the original value	0.4%

The difference between the actual value for Blindern and the calculated value with values from Ås was found to be 0.4%. The estimated value for Blindern in October is presented in Table 23, where the difference from September has been taken into the calculations.

Table 23: The estimated irradiation for Blindern in October, with the difference from September taken into the calculations.

Month	October
Total irradiation for Blindern with four data points replaced by values from Ås	40567 W/m^2
Calculated error from replacing data point equivalent to the missing data points for September	0.4 %
Total irradiation for October at Blindern with four data points replaced by values from Ås, considered calculated error	40405 W/m^2

When considering the 0.4% difference, the estimated irradiation for Blindern in October was 40405 W/m^2.

The annual measured irradiation for Ås are higher than for Blindern, and as expected is it necessary to tune up the replaced value for Ås and the replaced value for Blindern needs to be tuned down.

The uncertainty in this kind of replacements increases if the missing data point occur on days with varying cloud coverage. These days can lead to a difference in the daily irradiation, even for stations located within a small radius. For days with a clear sky, the result of replacing missing values will deviate less from the actual daily value.

Databases are suitable for estimating yield when designing a PV system, or to say something about the annual yield of a PV system. It is necessary with better resolution data for real time monitoring.

4.9 Two comparative PV systems at Kjeller without meteorological data available

The two systems at Kjeller are compared in the following chapter. The data from the two string inverters is available with resolution, but unfortunately is it no meteorological data available at the PV site. No source for irradiation are available from other sources close by, without having to do a comprehensive calculation of the irradiation to make it representative for the irradiation in the module plane for the systems at Kjeller.

Figure 59 shows the monthly yield for 2016 for the two PV systems at Kjeller. It is important to keep in mind that the value for December is an estimated value found by using monthly yield per square meters in the module plane estimated from PVGIS, the area of the modules, the module efficiency and the efficiency of the inverter. The CIS modules are producing more power than the silicon modules every month of 2016.

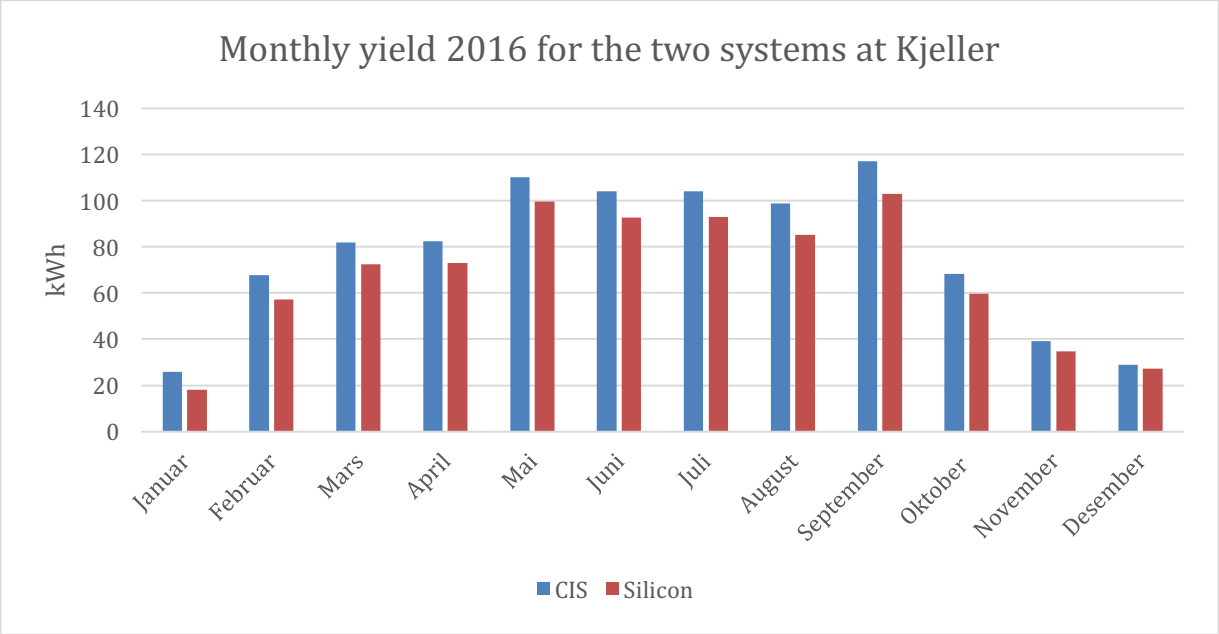

Figure 59: Monthly yield for the two PV systems at Kjeller. The yield for December is an estimated value.

For modules with a slope of 90 degrees, the amplitude of the yearly yield is reduced. The high peak of production during the summer months are reduced. On the other side, the modules with a steep slope will have a more even production approximately from March to October. The curve that follows the distribution for the yearly yield is wider than for the modules with less steep slopes. The production in the winter months will be higher for modules with steeper curves. PVeducation has a good animation where the effect of the module slope is illustrated. The animation can be found at [7]. The shape of the curve is mostly as expected, except the yield for two months. The yield for May and September are higher than for all the summer months in between. The efficiency of the modules is highly dependent of module temperature. Both May and September are months with irradiation lower than the summer months, but still

relatively high irradiation and these months often have lower temperatures. This can be a reason why the yield is higher for these months.

To be able to compare the two systems and their performance it is necessary to compare the specific yield, which is considering the nominal power of the systems. Figure 60 shows the monthly specific yield for the two systems at Kjeller.

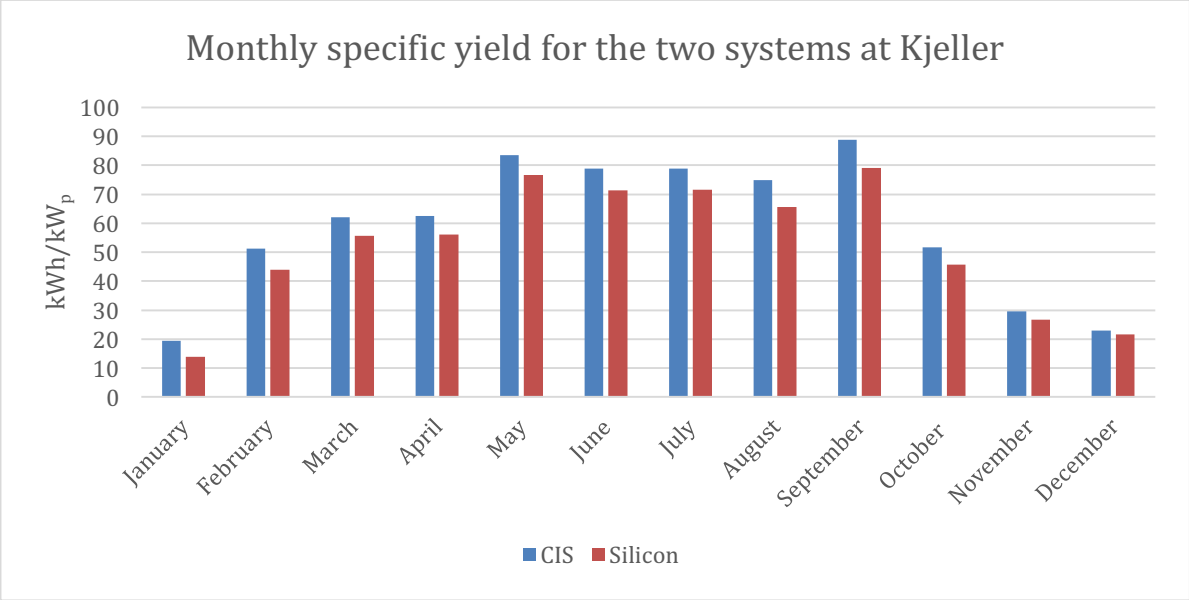

Figure 60: Monthly specific yield for the two PV systems at Kjeller. The specific yield for December is an estimated value.

Because the two systems have almost the same nominal power (1.3 kW_p for the silicon and 1.32 kW_p for the CIS modules), we see that the difference in the monthly specific yield between the two systems is approximately the same as the difference for the monthly yield. Even though the CIS modules have higher nominal power, the monthly specific yield is still higher for the CIS modules than for the silicon modules. This result is surprising considering the fact that the systems have almost equal nominal power and the efficiency of the silicon modules have an efficiency of 15.9%, while the CIS modules have an efficiency of 13.4%. Another important factor to consider is the total area of the modules at Kjeller. The total area of the CIS modules at Kjeller is 8.84 m^2 and the area of the silicon modules are 7.75 m^2. When space is an issue, for instance at small roofs, is it important to know how areal effective the modules are. The CIS modules on Kjeller have higher specific yield than the silicon modules but takes up more space compared to the silicon modules.

It is important to keep in mind that the efficiencies of the different technologies are calculated under STC. According to the web page for the manufacturer of the CIS modules, Solar Frontiers [4] the CIS modules do perform better under "real-world conditions". The CIS modules have the following advantages, according to the manufacturer

- Better performance in hot conditions
  CIS has a lower temperature coefficient than crystalline silicon.

- The “light-soaking” effect
  CIS modules increase in power output after exposure to light during the first few days of operation.

- Low light behavior
  CIS modules performs better under sunrise, sunset and under cloud cover. They also perform better under less ideal conditions, such as when facing west, north or when installed flat

- Better tolerance for shadows
  The uncovered part of the CIS module under the cast of perpendicular shadow will perform normally.

It would have been convenient to have data for measured irradiation in the module plane for the two systems. Since that kind of data is not available, estimated values from PVGIS are used. Figure 61 shows the monthly irradiation per square meters for each month, estimated by PVGIS.

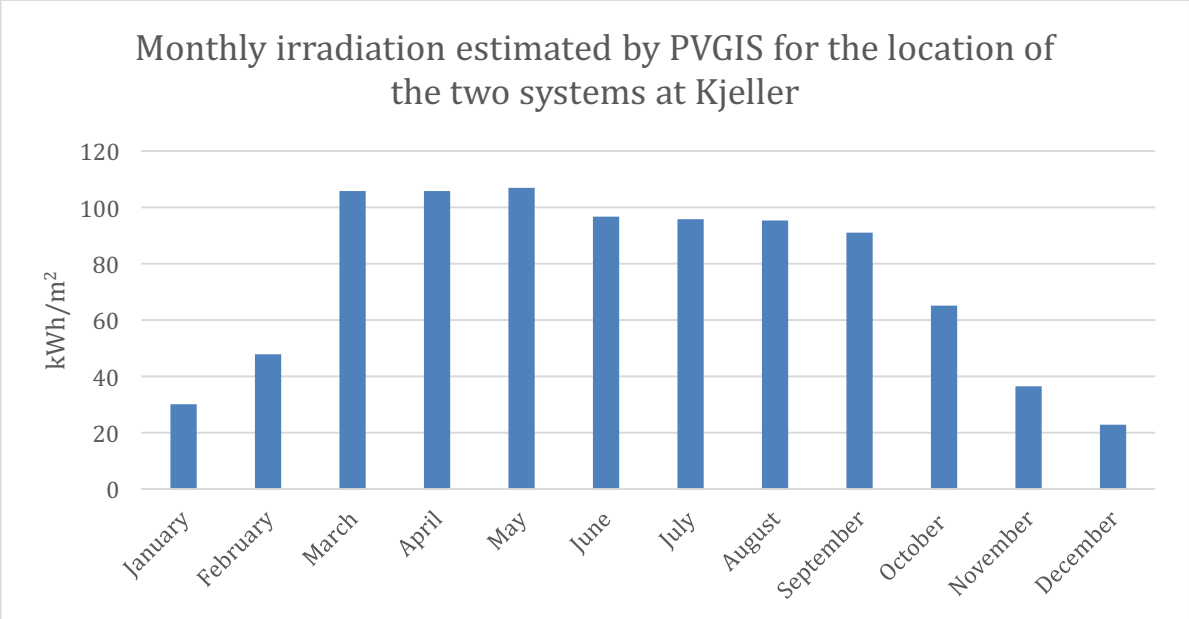

Figure 61: The monthly irradiation per square meters for each month, estimated by PVGIS.

The monthly irradiation estimated by PVGIS shows a curve of an unexpected form, where March, April and May have higher monthly yield than the summer months. The irradiation on the modules will be less in the summer months due to the Sun’s high position in the sky during the day and the slope of the modules. When the modules have a slope of 90 degrees,

they will receive less irradiation than if they had a less steep slope. The monthly irradiation estimated by PVGIS was investigated for different module slopes and that showed that for horizontal values the curve was as expected, with the monthly peak during the summer months. As the slopes was made steeper, the irradiation values for March, April and May were continuously higher.

Figure 62 shows the monthly yield estimated from PVGIS for the two system at Kjeller. For the months with high yield, the difference between the systems is higher than for the months with lower yield. The same pattern as for the monthly irradiation is shown. March, April and May have higher monthly yield than the summer months.

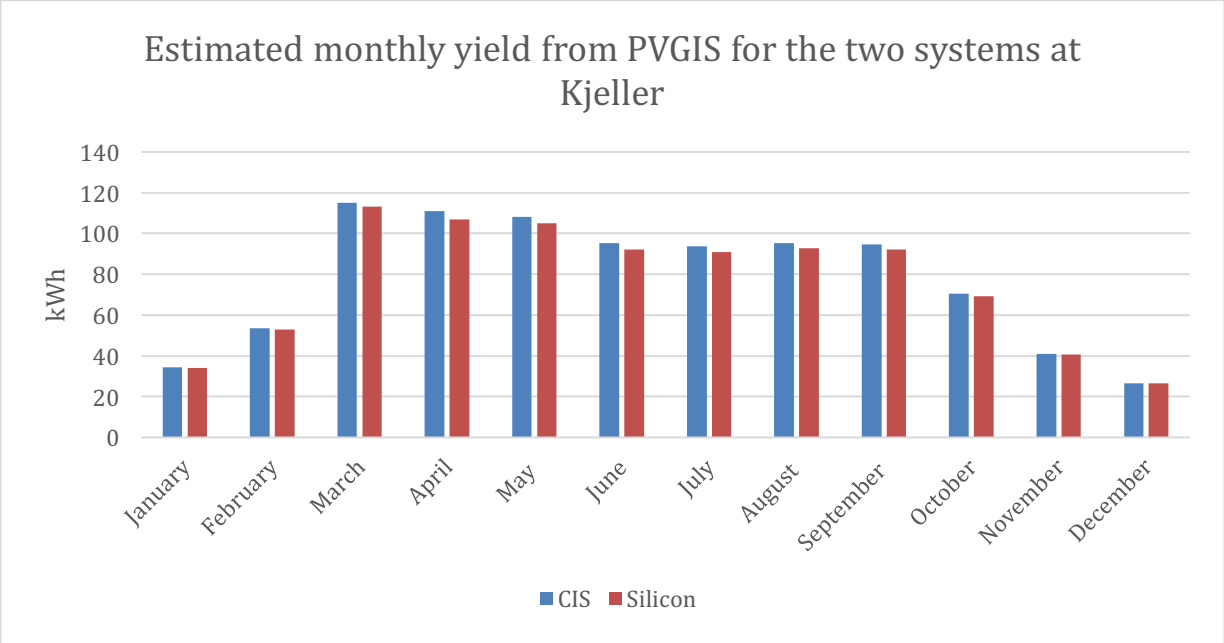

Figure 63: The monthly yield estimated from PVGIS for the two system at Kjeller.

The estimated monthly yield shows less difference between the two different systems than what the values for the actual yield shows. Figure 64 shows estimated monthly yield versus the actual monthly yield for the CIS modules.

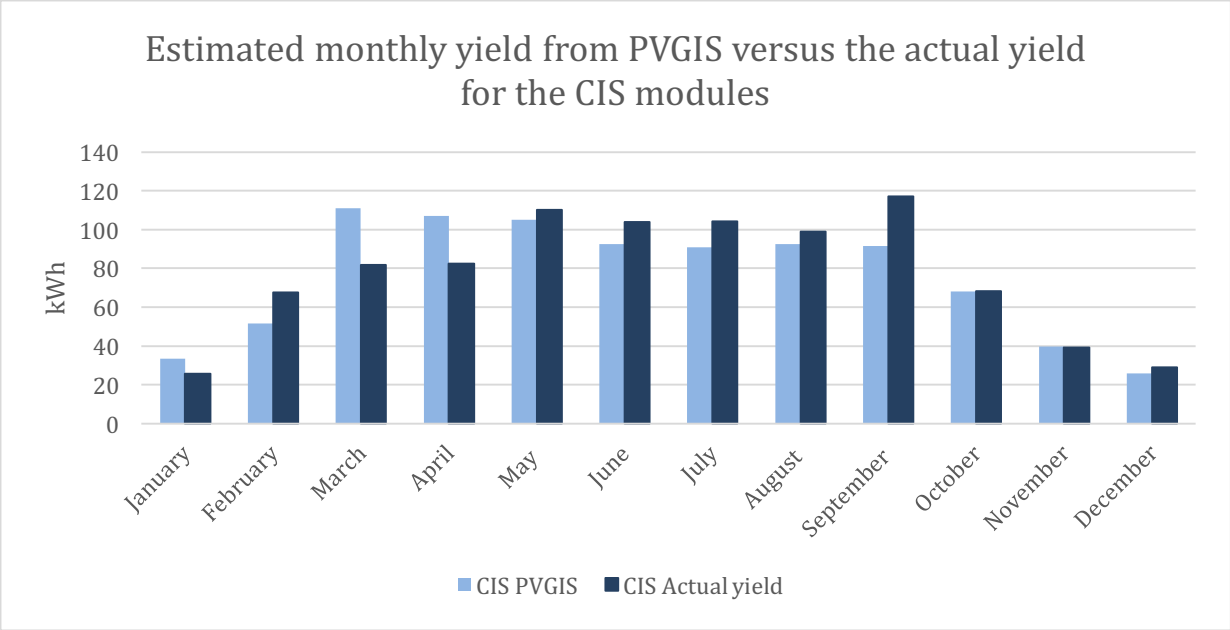

Figure 64: The estimated monthly yield versus the actual monthly yield for the CIS modules.

PVGIS overestimates the monthly yield for January, March and April. March and April are highly overestimated. For February, May, June, July, August and December the values are underestimated from PVGIS. September is highly underestimated. For October and November are the estimated values coinciding with the actual yield.
Figure 65 shows estimated monthly yield versus the actual monthly yield for the silicon modules.

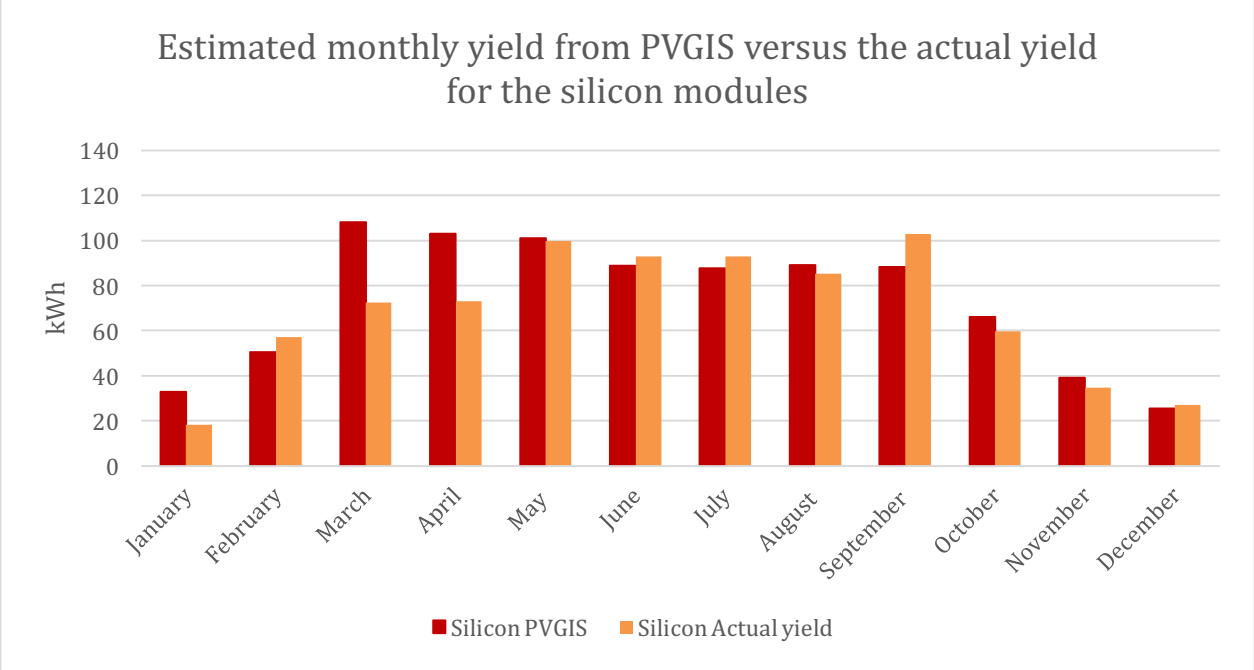

Figure 65: The estimated monthly yield versus the actual monthly yield for the silicon modules.

PVGIS overestimates the monthly yield for January, March, April, May, October and November. March and April are highly overestimated. For February, June, July, August, September and December the values are underestimated from PVGIS. September are highly underestimated.

The estimations from PVGIS does not include shading losses. This means that the estimated values from PVGIS probably are overestimated for every month.

The estimated losses from PVGIS for the two systems at Kjeller are listed in Table 24 and Table 25.

Table 24: The estimated system losses for the CIS modules.

Estimated loss due to temperature (using ambient temperature)	7.3 %
Estimated loss due to angular effects	3.8 %
Other losses (cable, inverter etc.)	14.0 %
Combined PV system loss	23.3 %

Table 15: The estimated system losses for the silicon modules.

Estimated loss due to temperature (using ambient temperature)	8.9 %
Estimated loss due to angular effects	3.8 %
Other losses (cable, inverter etc.)	14.0 %
Combined PV system loss	26.4 %

Figure 66 shows the monthly specific irradiation for the location of the two systems at Kjeller.

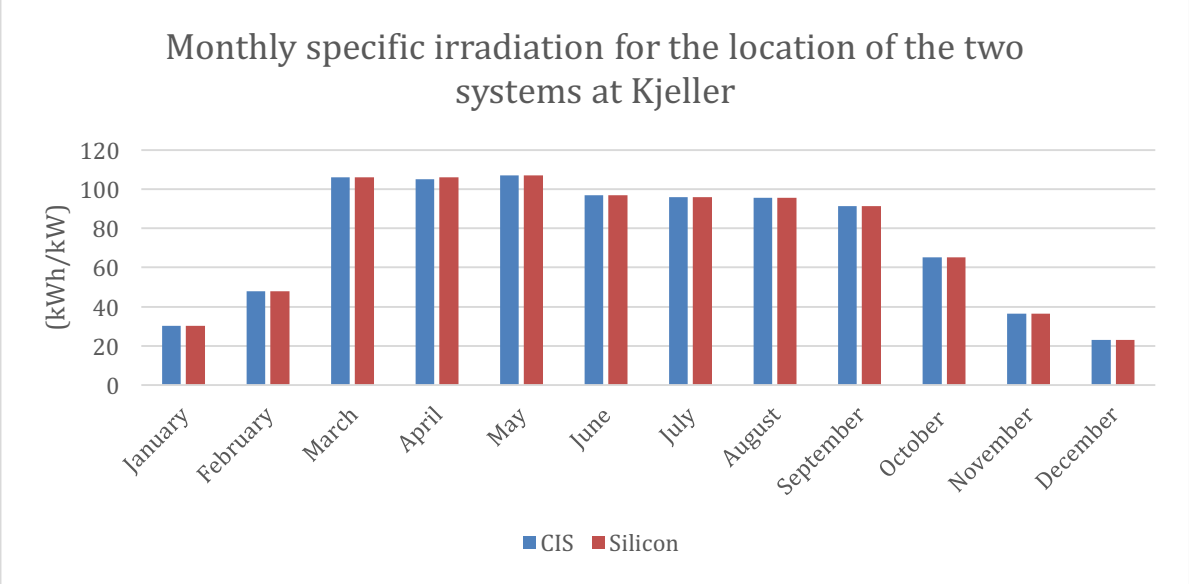

Figure 66: The monthly specific irradiation for the location of the two systems at Kjeller.

The monthly specific irradiation and the monthly specific yield was used to calculate the monthly performance ratio for the two systems at Kjeller. The monthly performance ratio is illustrated in Figure 67, together with the annual performance ratio. Typical range for the PR value nowadays is somewhere above 0,80 [3] The use of estimated values for the irradiation results in some unnaturally high values for the PR. The PR for the CIS modules in January, February September and December are higher than expected. The PR for the CIS modules even exceeds 1.0 in February, which should not be possible. In December and September, the PR is close to 1.0. The PR for the silicon modules is unnaturally high in February, September and December.

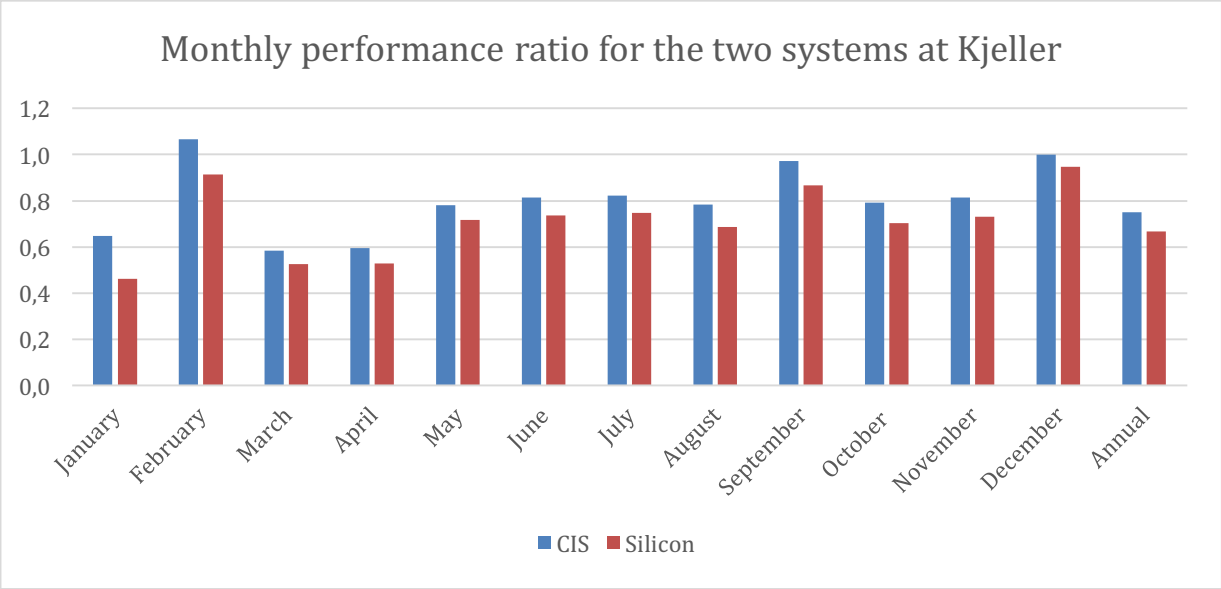

Figure 67: The monthly performance ratio for the two systems at Kjeller. The annual performance ratio for the two systems are also illustrated.

Figure 68 to Figure 78 shows the daily yield for the two systems at Kjeller for the months January to November.

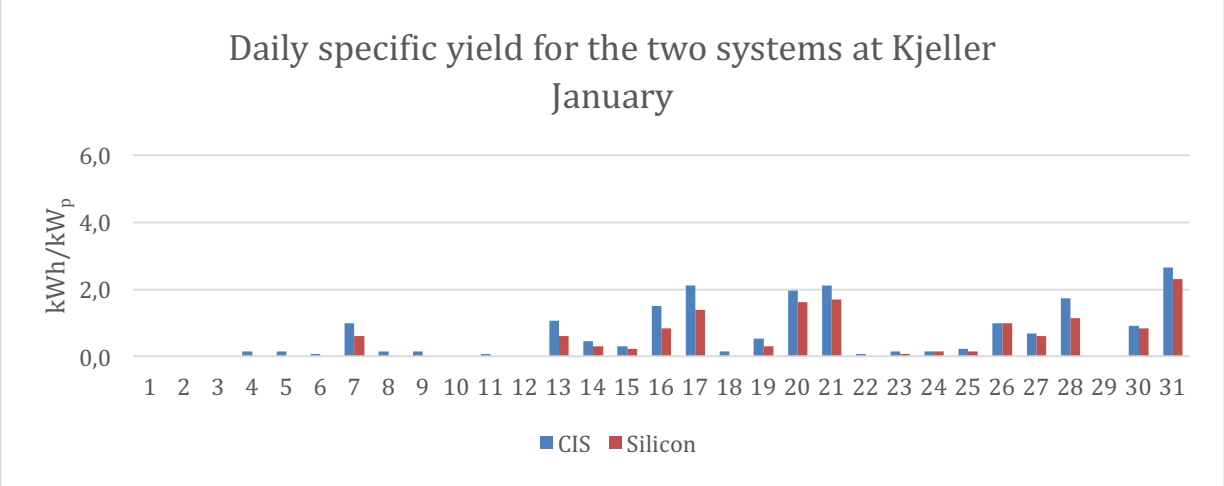

Figure 68: Daily specific yield for the two systems at Kjeller in January.

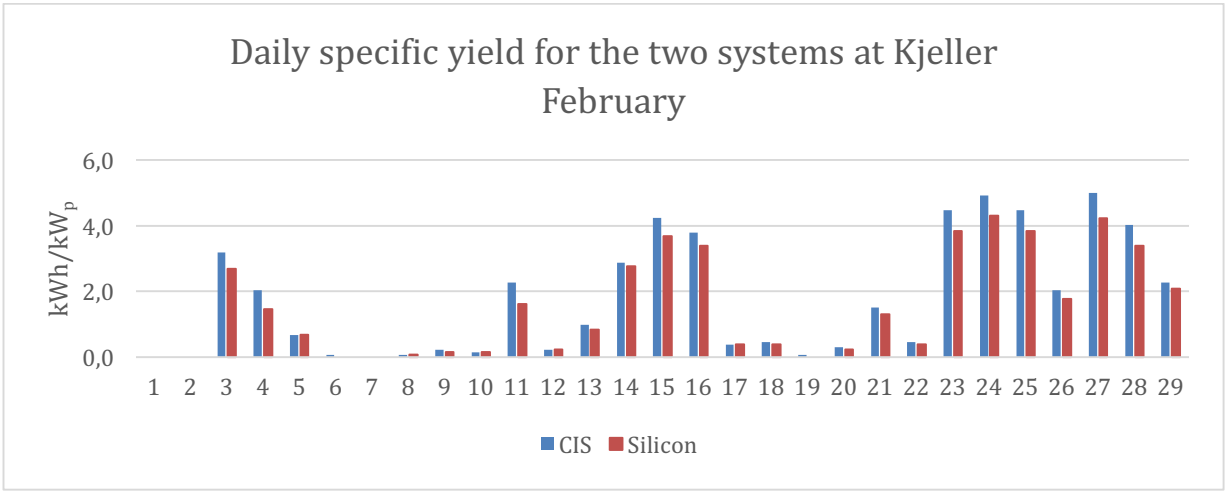

Figure 69: Daily specific yield for the two systems at Kjeller in February.

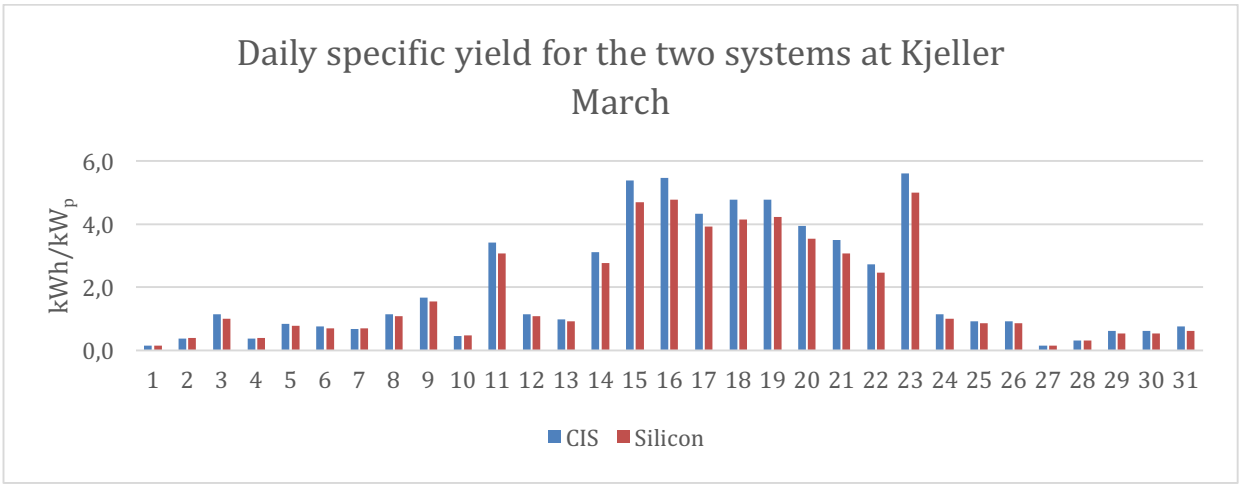

Figure 70: Daily specific yield for the two systems at Kjeller in March.

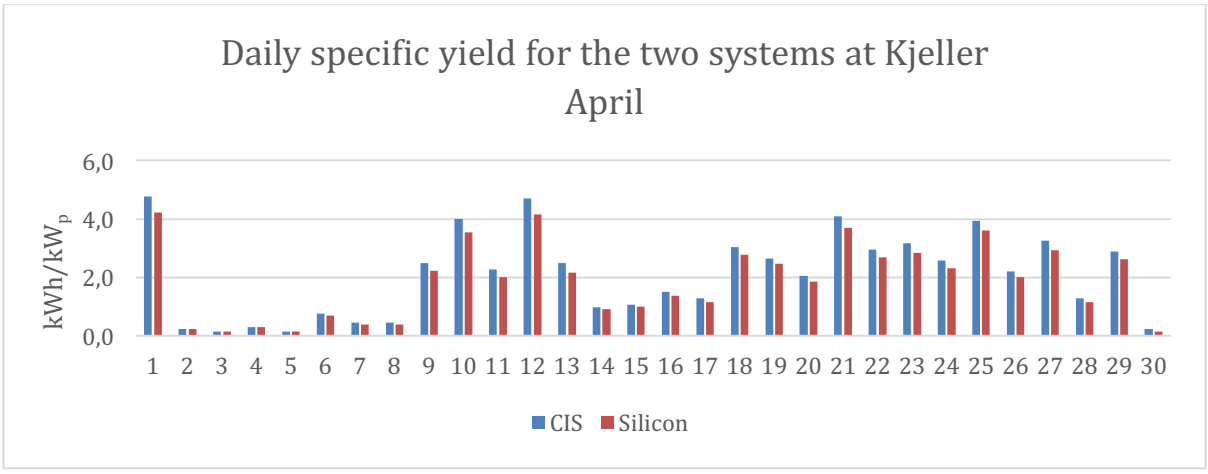

Figure 71: Daily specific yield for the two systems at Kjeller in April.

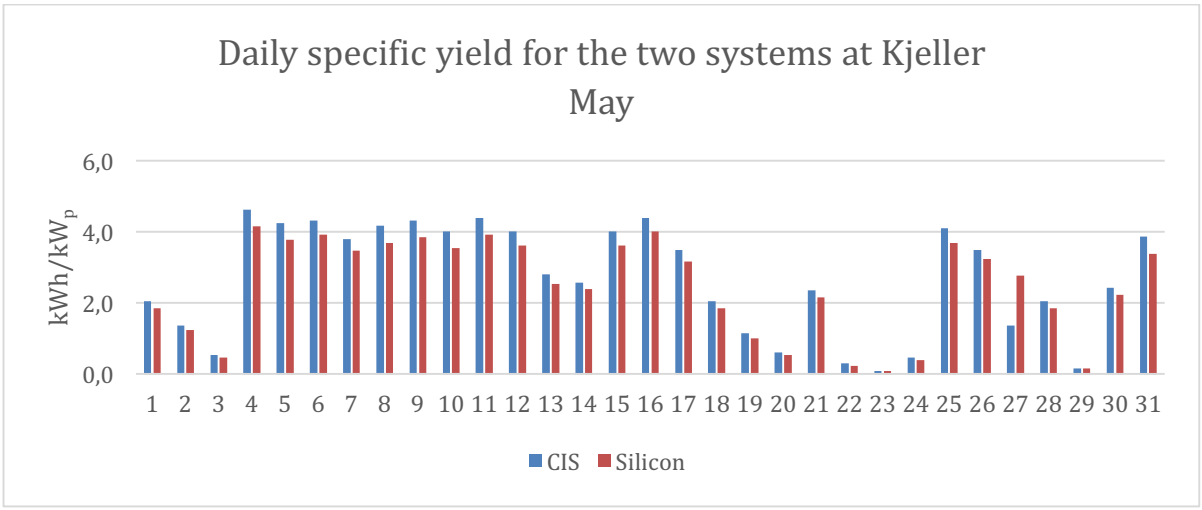

Figure 72: Daily specific yield for the two systems at Kjeller in May.

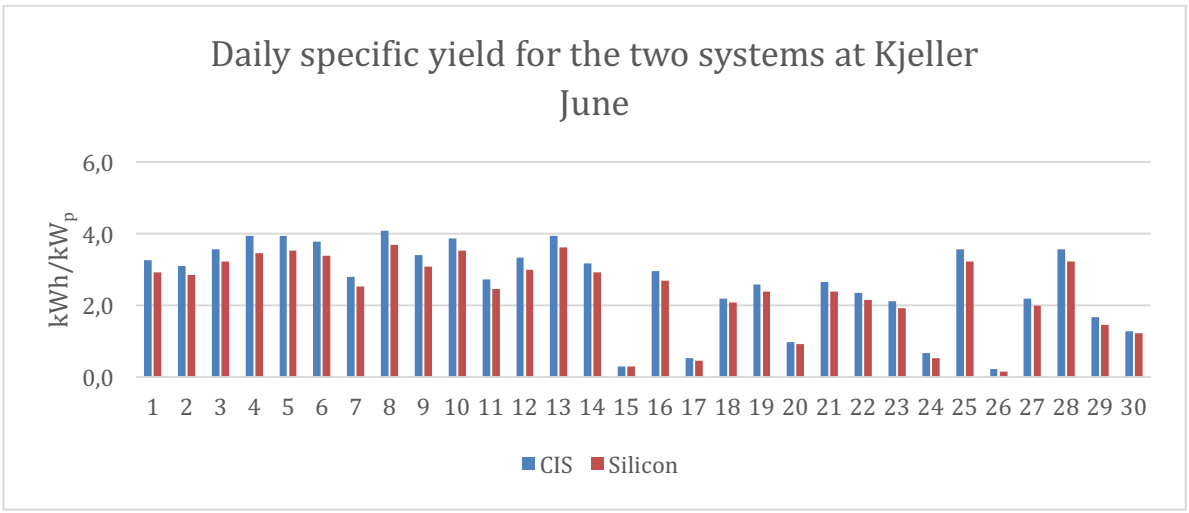

Figure 73: Daily specific yield for the two systems at Kjeller in June.

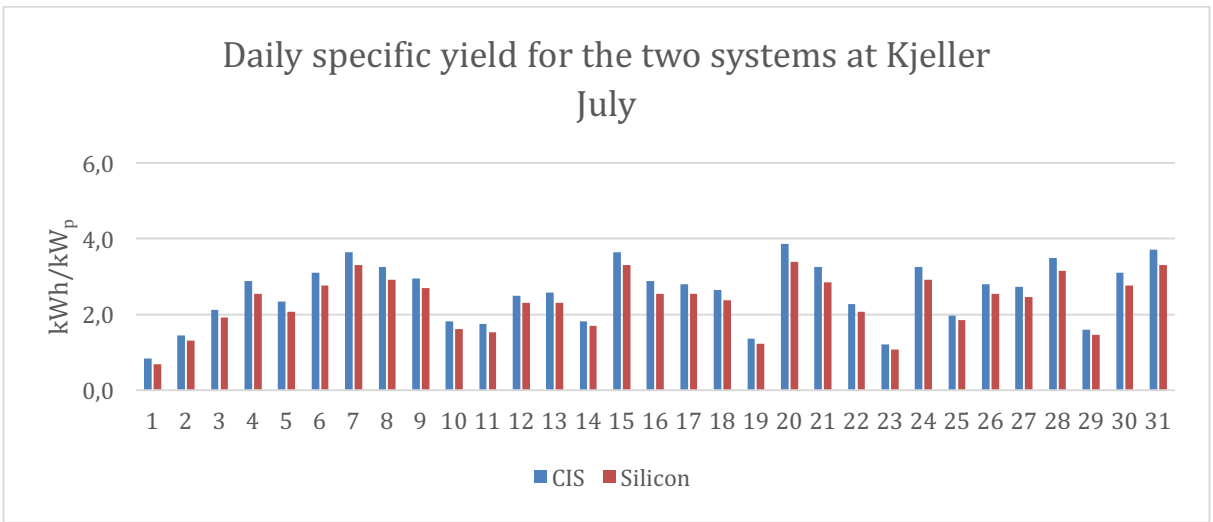

Figure 74: Daily specific yield for the two systems at Kjeller in July.

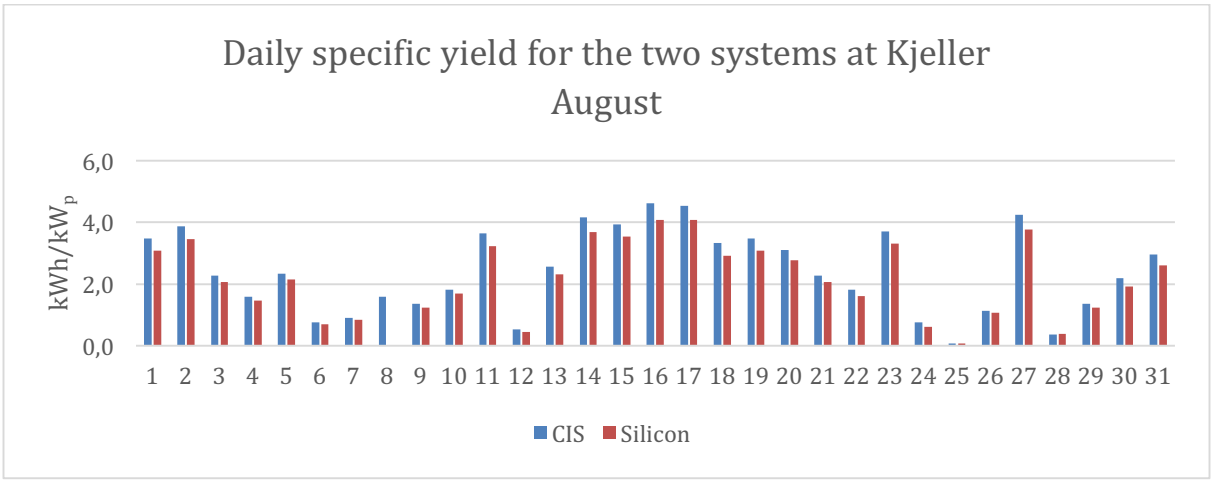

Figure 75: Daily specific yield for the two systems at Kjeller in August.

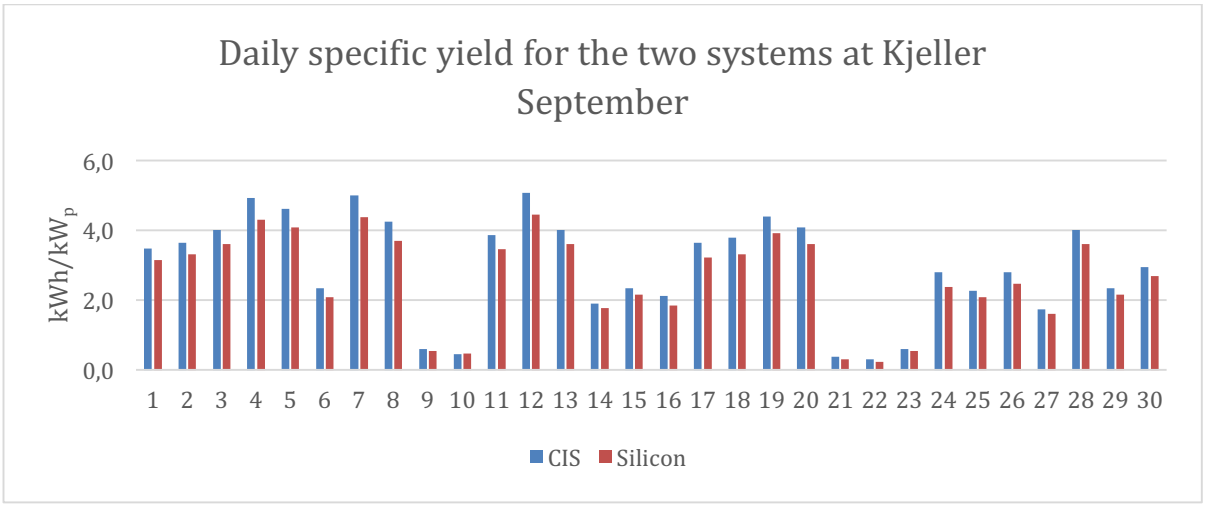

Figure 76: Daily specific yield for the two systems at Kjeller in September.

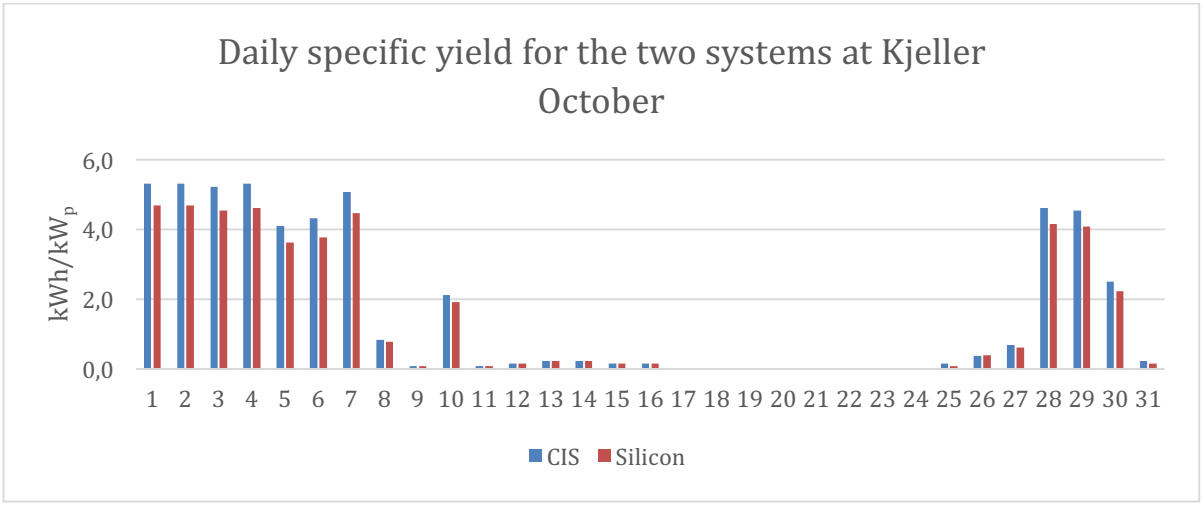

Figure 77: Daily specific yield for the two systems at Kjeller in October.

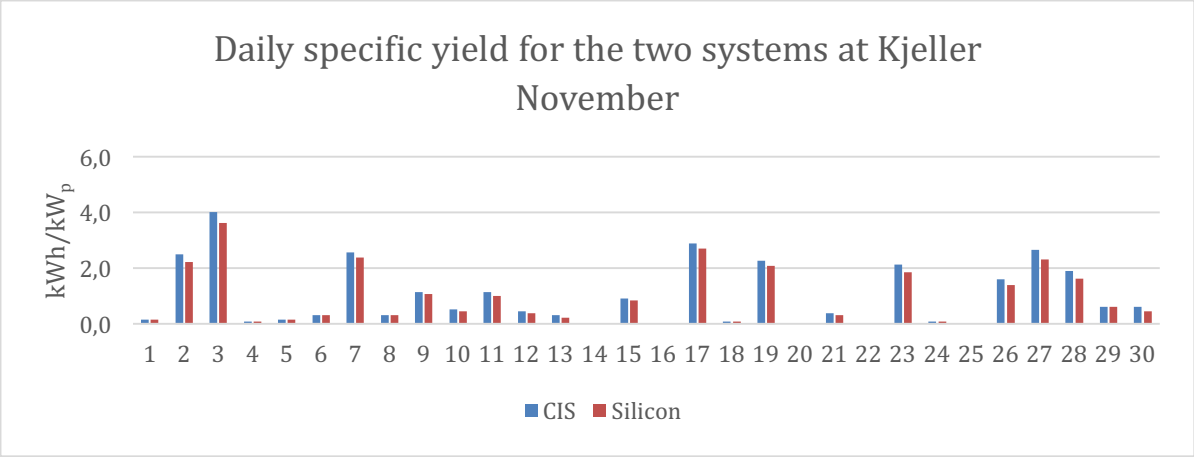

Figure 78: Daily yield for the two systems at Kjeller in November.

The CIS modules has higher specific yield than the silicon modules most of the year from January to November. It is only a few days during this period that the silicon modules have a higher specific yield than, or approximately the same yield as the CIS modules. The days when this occur are days with low yield, and thus low irradiation It seems like the CIS modules are performing better than the silicon modules with higher irradiation. With higher irradiation follows higher module temperature. It could be that the CIS modules are performing better than the silicon modules under higher module temperature. One exception is May 27. The daily specific yield for this day is 2.77 for the silicon modules and 1.36 for the CIS modules. This is the only day during the period January to November, which the silicon modules are performing particularly better than the CIS modules. The AC power for the two systems on May 27 are shown in Figure 79.

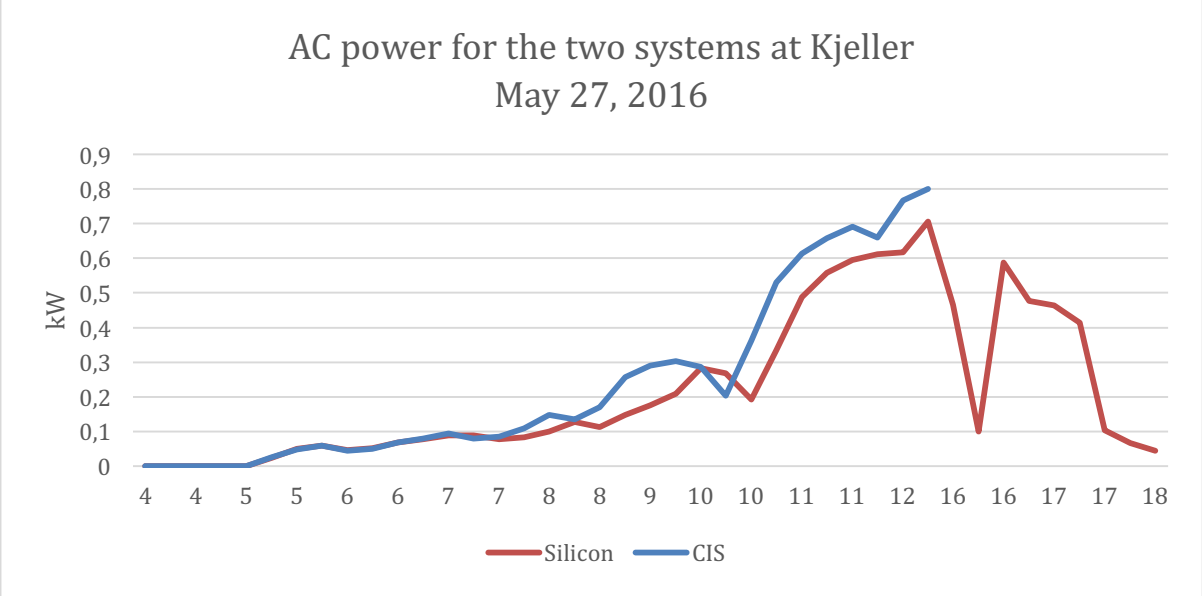

Figure 79: The AC power for the two systems at Kjeller. May 27, 2016.

Figure 79 shows how the AC power from the CIS inverter is cut around 13.00. This can be due to a technical failure and explains the abnormal difference between the daily specific yields for the two systems on this day.

The next section studies the impact of irradiation and air temperature for the January, March, May, July, September and November in Figure 80 to Figure 91. The optimal study is to be able to compare the specific daily yield with module temperature. When this is not available at the site, the temperature and horizontal irradiation at Blinder are used for comparison.

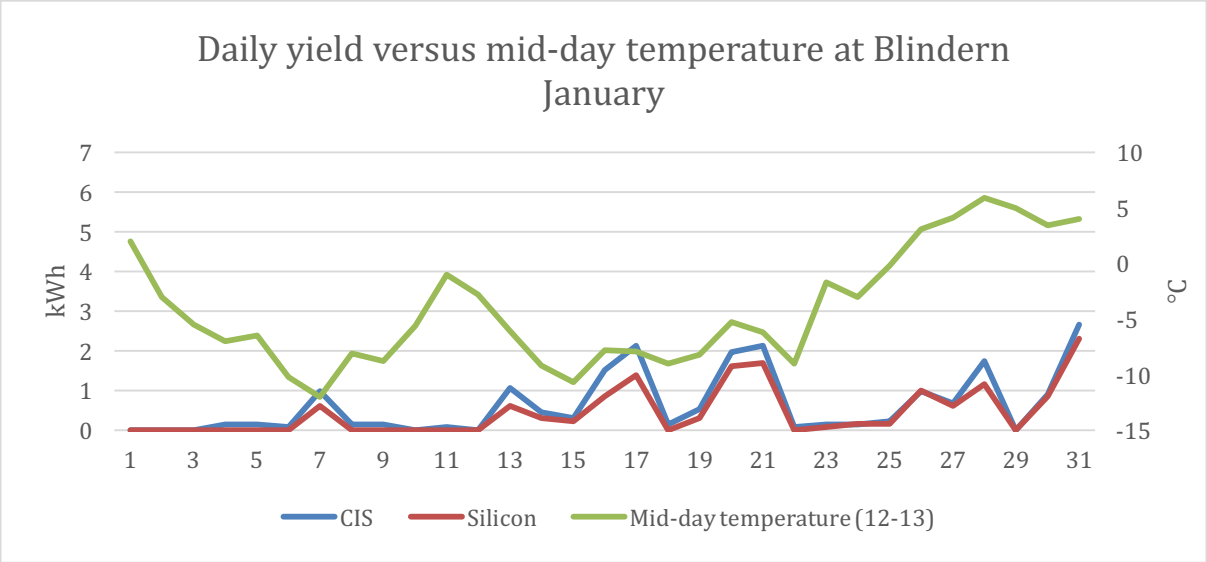

Figure 80: Daily specific yield versus mid-day temperature at Blindern. In January.

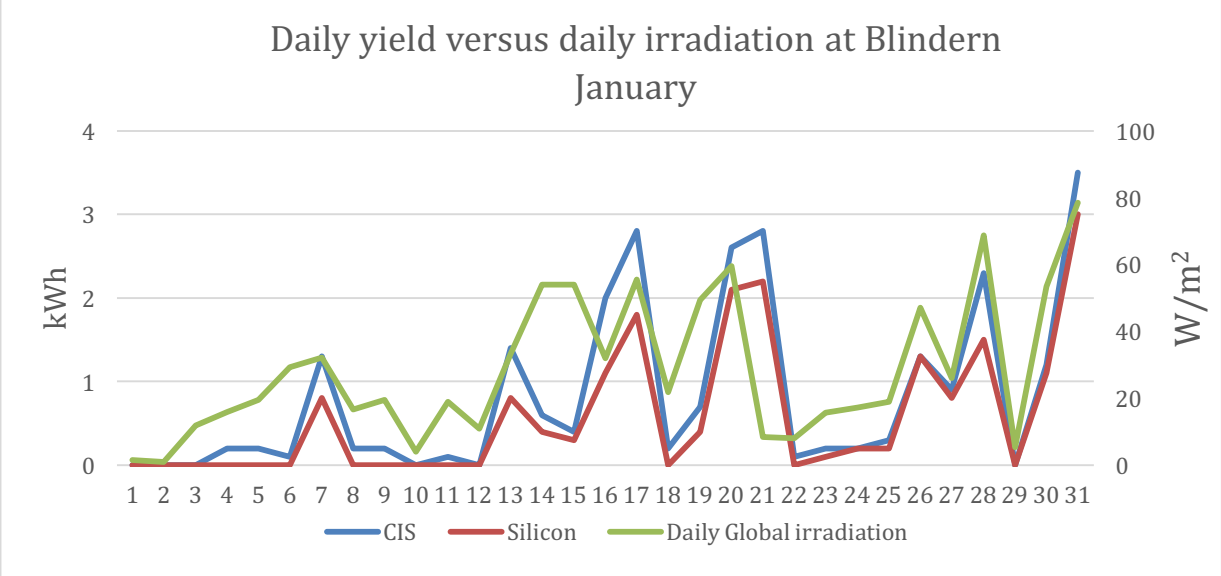

Figure 81: Daily specific yield versus daily irradiation at Blindern. In January.

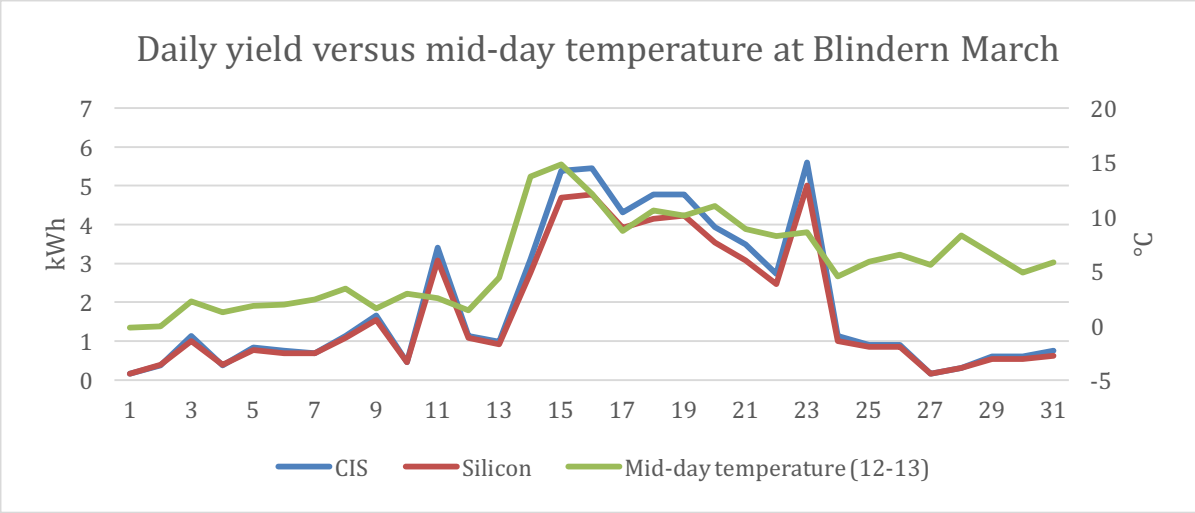

Figure 82: Daily specific yield versus mid-day temperature at Blindern. In March.

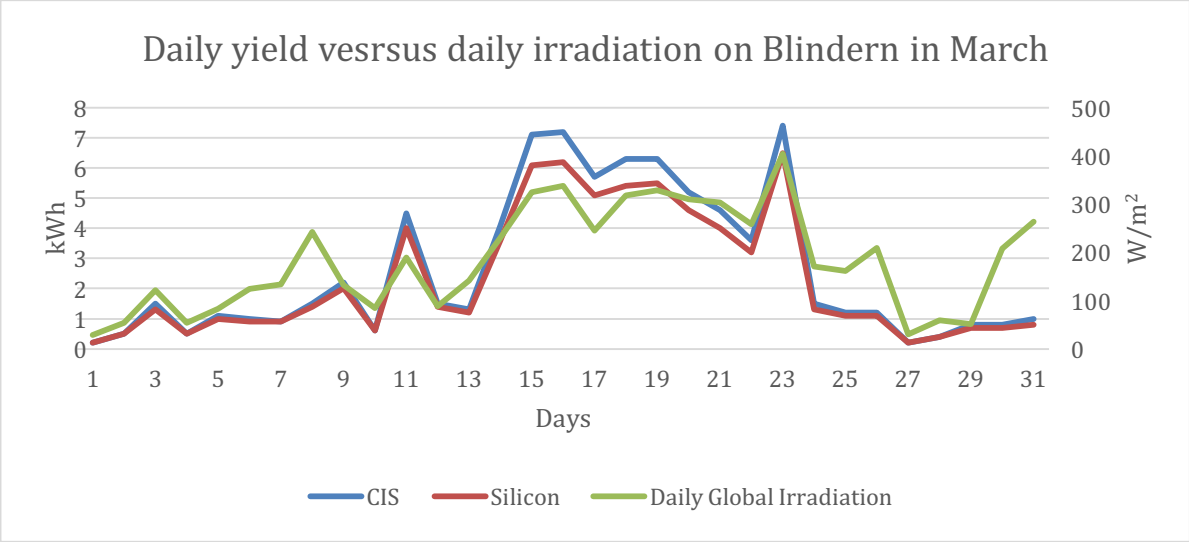

Figure 83: Daily specific yield versus daily irradiation at Blindern. In March.

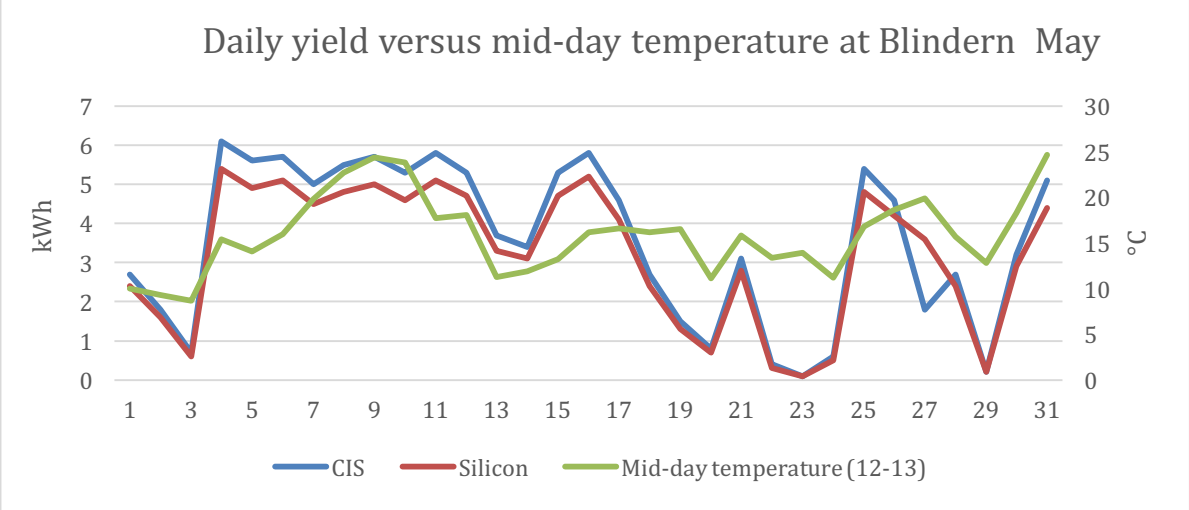

Figure 84: Daily specific yield versus mid-day temperature at Blindern. In May.

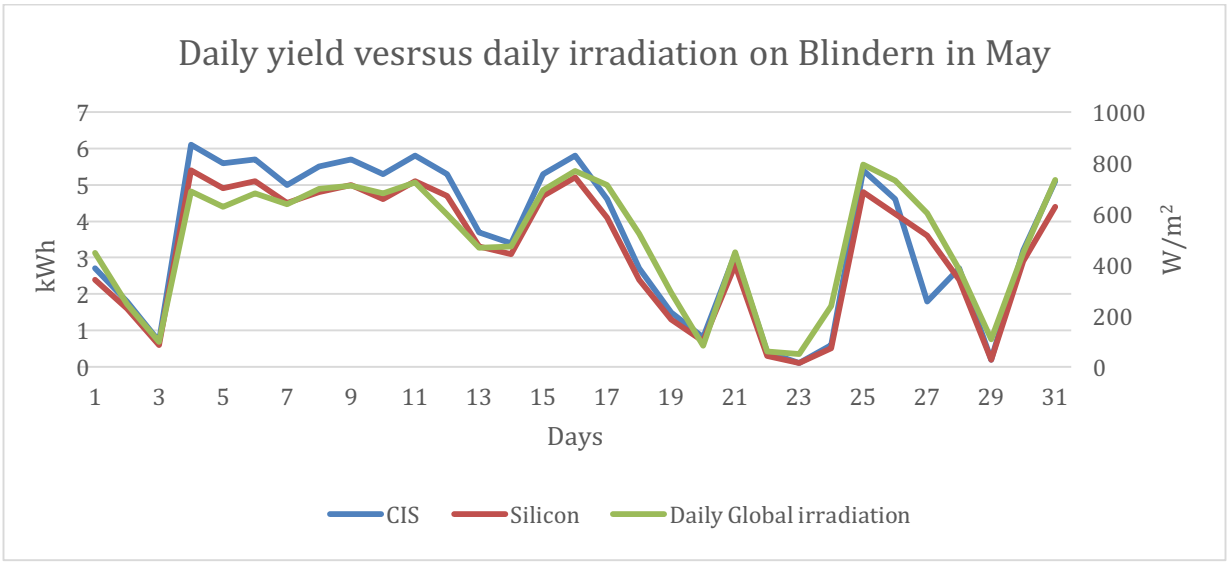

Figure 85: Daily specific yield versus daily irradiation at Blindern. In May.

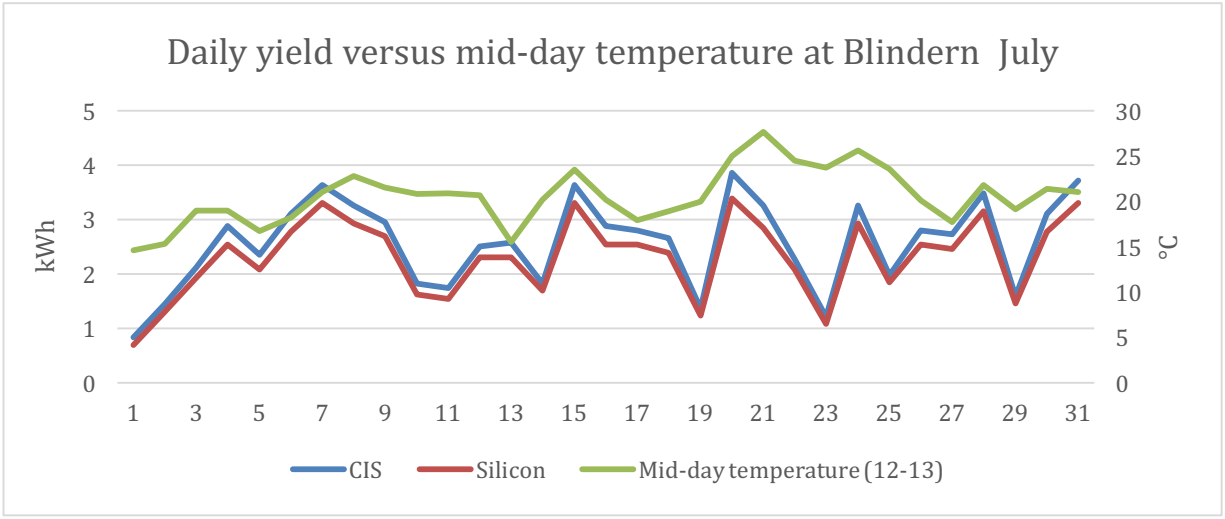

Figure 86: Daily specific yield versus mid-day temperature at Blindern. In July.

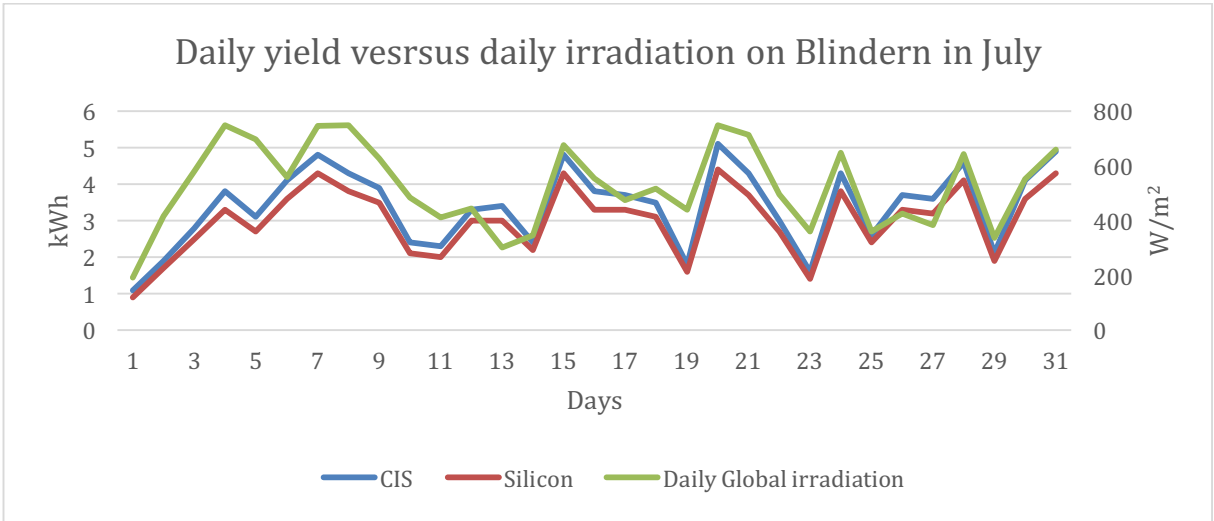

Figure 87: Daily specific yield versus daily irradiation at Blindern. In July.

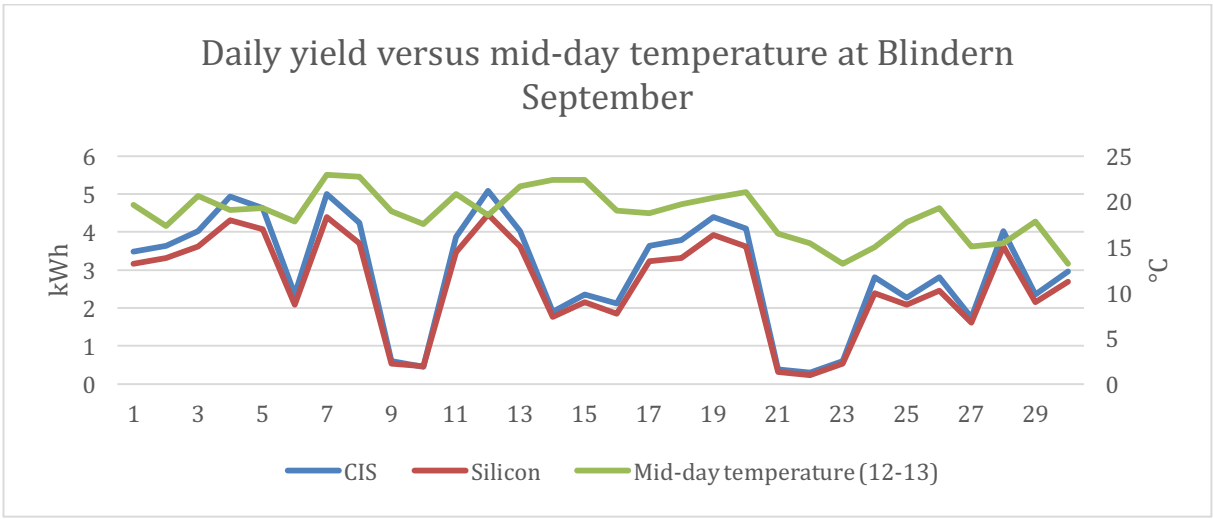

Figure 88: Daily specific yield versus mid-day temperature at Blindern. In September.

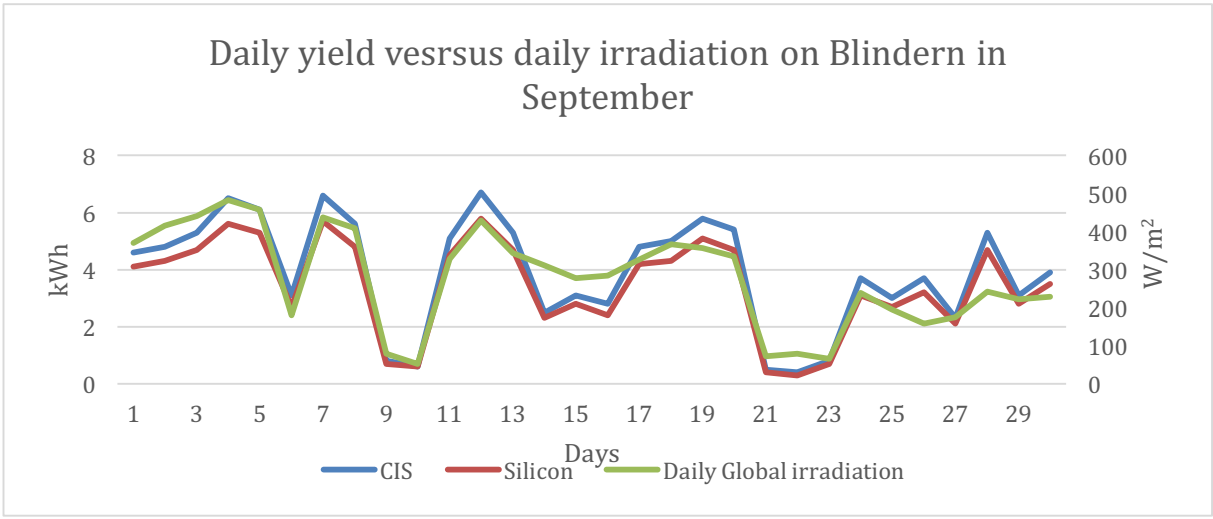

Figure 89: Daily specific yield versus daily irradiation at Blindern. In September.

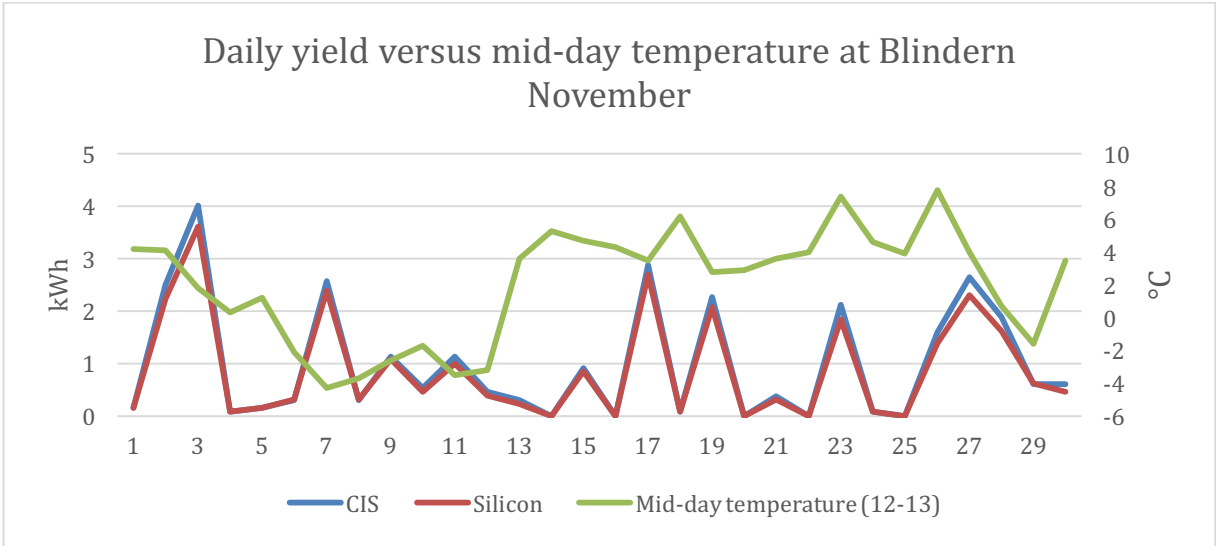

Figure 90: Daily specific yield versus mid-day temperature at Blindern. In November.

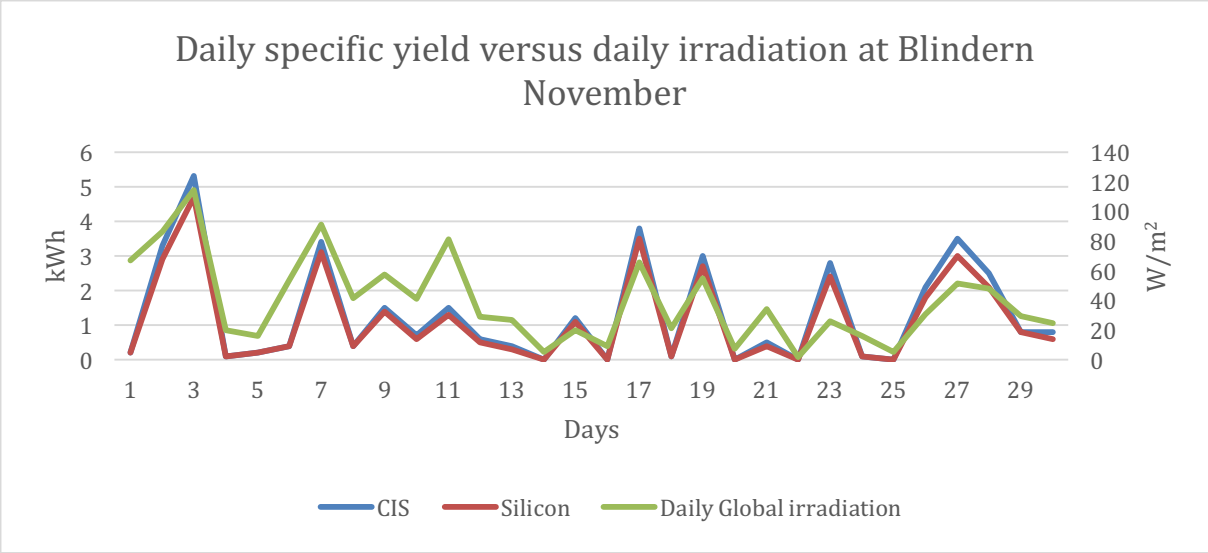

Figure 91: Daily specific yield versus daily irradiation at Blindern. In November.

In Figure 80 to Figure 91 the curves are more similar for days with low specific yield. For days with high specific yield the difference between the curves is bigger. A trend for all the curves is that at the bottom they are more similar than for the peaks of the curves, where the CIS modules are performing better than the silicon modules. Again, it seems like the CIS modules are performing better than the silicon modules at higher irradiation and thus higher module temperature.

The next section studies March 23, 2016 and July 2, 2016, which both have a daily horizontal irradiation of approximately 4000 W/m^2 each. The irradiation measured at Blindern is assumed to have a linear relationship with the irradiation in the module plane at Kjeller. It is assumed that the irradiation in the module plane also will be equal for July 2 and March 23. Figure 92 and Figure 93 shows the global horizontal irradiation at Blindern. Table 26 shows daily irradiation at Blindern and daily specific yield for the two systems at Kjeller at July 2 and March 23. March 23 is a day with clear sky while July 2 is a day with varying cloud coverage. During this thesis, the impact of clouds has been studied. Even though the clouds will make different impact on Blindern and Kjeller, we still considered the total daily irradiation as equal.

Table 26: Daily irradiation at Blindern and daily specific yield for the two systems at Kjeller at July 2 and March 23.

Date	Irradiation (W/m^2) at Blindern	Specific yield (kWh/kW$_p$) CIS	Specific yield (kWh/kW$_p$) Silicon
July 2	4164	1,4	1,3
March 23	4049	5,6	5,0

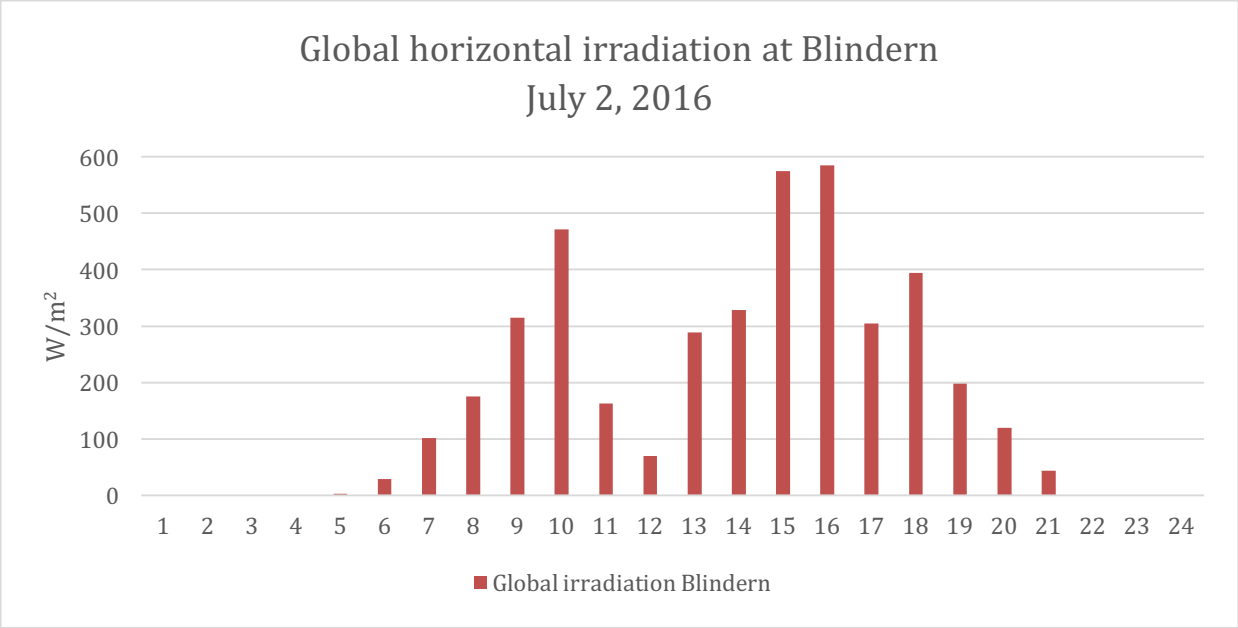

Figure 92: Global horizontal irradiation at Blindern. July 2, 2016.

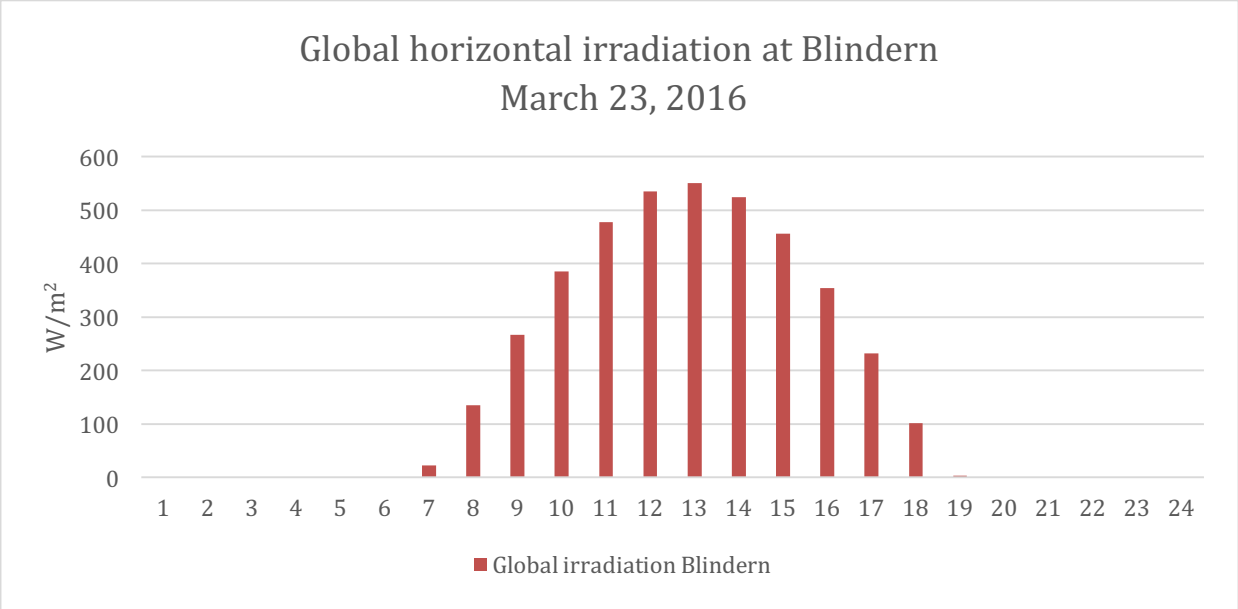

Figure 93: Global horizontal irradiation at Blindern. March 23, 2016.

Figure 94 shows the hourly air temperature measured at Blindern for March 23 and July 2, 2016.

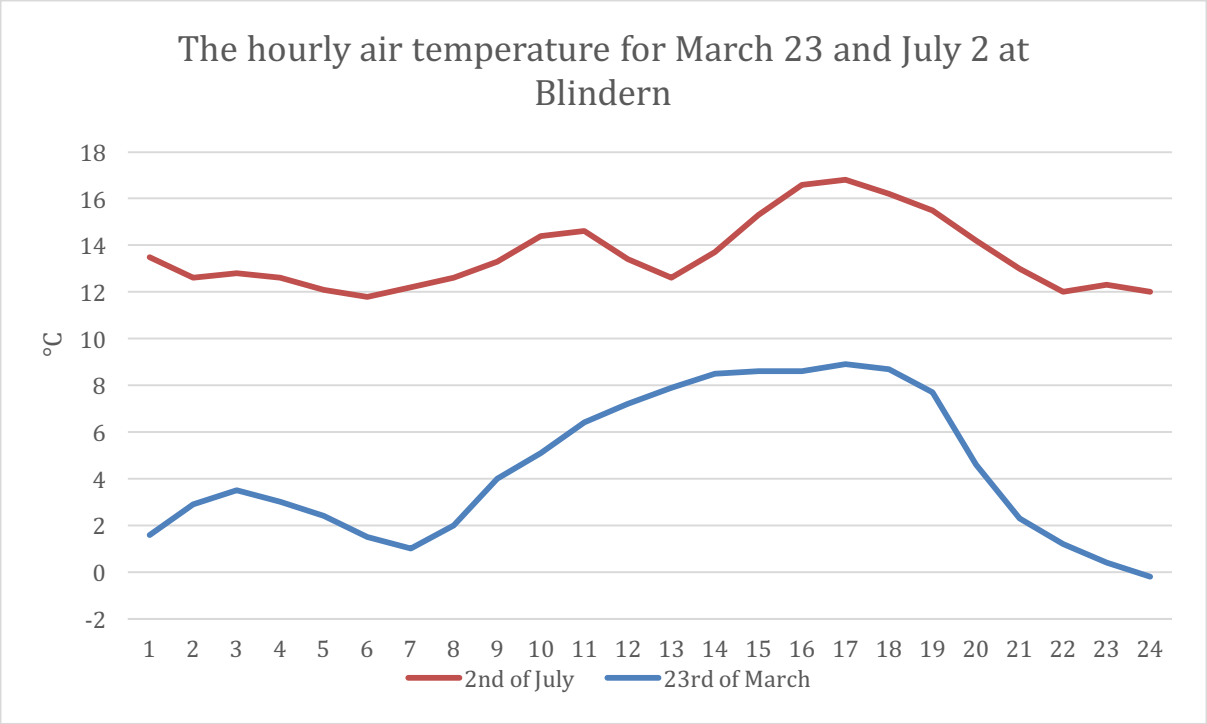

Figure 94: The hourly temperature measured at Blindern for March 23 and July 2, 2016.

The daily air temperature for March 23 is lower than for July 2, as expected. Both the systems are performing better in March, with lower daily temperature. The difference in performance are higher for March 23, where the daily temperature is lower, but the yield is higher. For March the difference is 12 % and for July 2 the difference is 7,7%.

Figure 95 and Figure 96 shows the AC power for the two systems for July 2 and March 23. The figures show how the curves are more similar for days with lower yield than for days with higher yield. For Figure 95, the peaks for the silicon modules are higher than for the CIS modules where the peaks are at their highest during the day. Figure 96 shows that for March the CIS modules are performing better until the end of the day where the silicon modules for a short time has higher yield than the CIS modules. From figure 96 it can seem like the silicon modules are performing better than the CIS modules under low irradiation. For Figure 95, the silicon modules are performing better than the CIS modules when the irradiation is at its maximum that day.

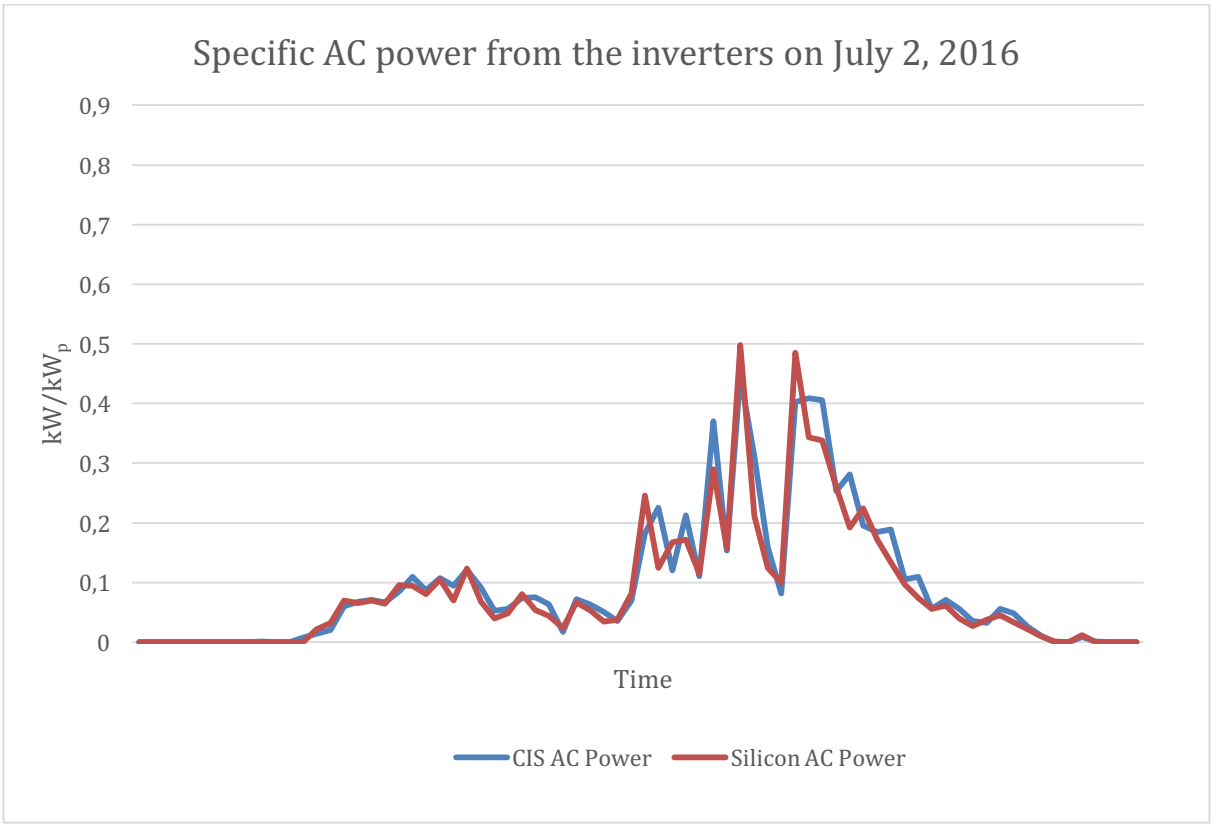

Figure 58: Specific AC power from the inverters on July 2, 2016

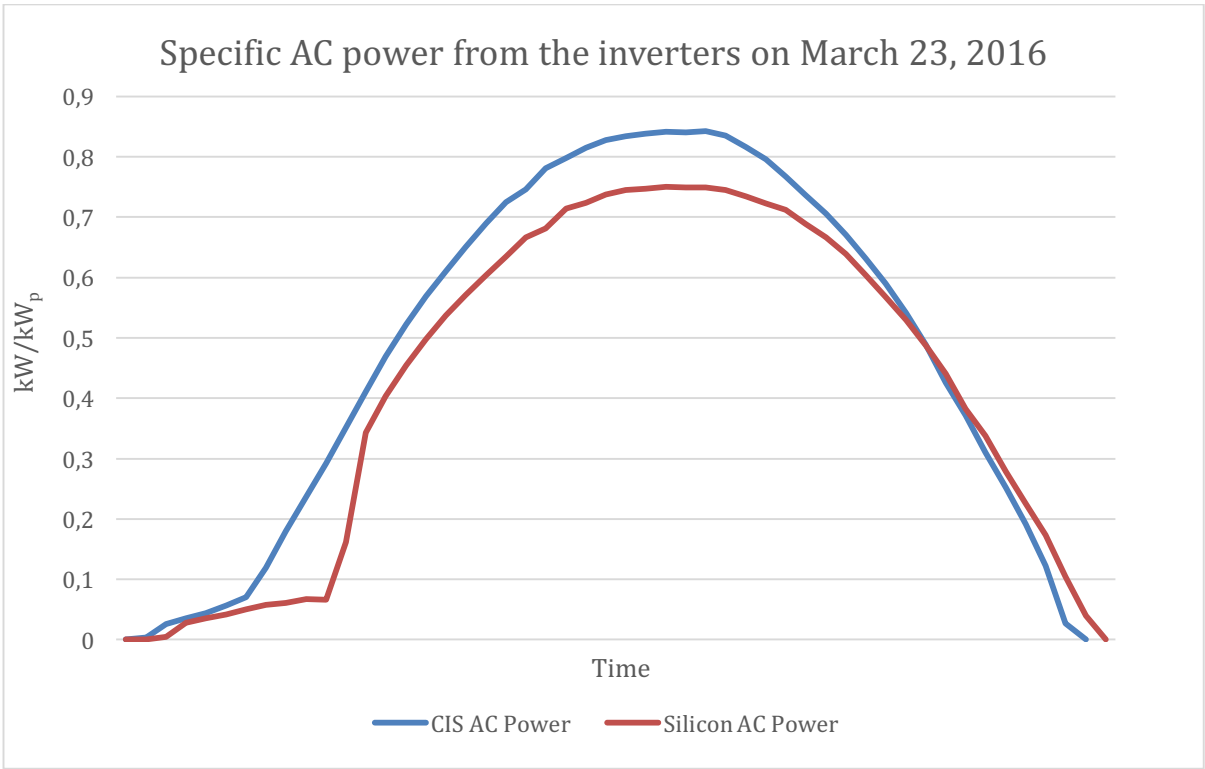

Figure 59: Specific AC power from the inverters on March 23, 2016

5. Conclusion

The following problem statements was investigated in this thesis

- What are the available sources of irradiation data for a PV system in Oslo, Norway?
- How much does this irradiation data differ from each other?
- How is irradiation measured and how do the different methods differ from each other?
- Is it possible to use irradiation data from other sources, when local data are not available at the PV site?
- What is the error of replacing missing data points with existing data points from other sources?
- What is possible to say about a PV systems performance without local meteorological data, only with access to inverter data?
- What is the result of using meteorological data from other locations for a PV site without local meteorological data?

What are the available sources for irradiation data for a PV system in Oslo, Norway?
This thesis has investigated several sources for irradiation data for a PV system in Oslo. Measured values is available from pyranometers or from reference cells, together with data from databases that rely on satellite data from a given period. The sources are suitable for different purposes. The average data from the databases are best suited for design of a PV system and to estimate the average annual yield. The measured values are more accurate and thus more suitable for analytical monitoring. The spatial resolution for the data from the databases has low resolution, especially the data from NASA. Data from NASA will show an equal value for the irradiation for an area of 50 km by 100 km.

How much does the irradiation data from the different sources differ from each other?
The total irradiation for the reference year August 2015 to August 2016 is lower for the measured pyranometer values than for the values from NASA and Blindern. The use of databases in PV design will lead to an overestimate of the reference year. When considering the uncertainty and the minimum and maximum deviation from the average year for the databases, the total irradiation for the reference year at Ås and Blindern will be in range of the of the values of the years used to make the average value for the databases. The difference in the annual irradiation between the two remote sources, Ås, and Blindern was 42 kWh/m^2. The annual irradiation for the local sources at Økern ranged from 800 kWh/m^2 to 870 kWh/m^2. For the two comparable reference cells on Økern were the difference in annual irradiation 38 kWh/m^2.

The difference between the measured horizontal values at Ås and Blindern and the irradiation measured in the module plane at Økern can mainly be explained by the differences between the measurement methods for a reference cell and the pyranometer. Both the diffuse, direct

and reflected share of the total irradiation are influenced by the slope and orientation of the module and this leads to the difference in total irradiation.

This thesis is illustrating the difference between both remote and local sources for irradiation data. Even the two reference cells on Økern mounted in the same orientation, with the same slope an only within a distance of few meters of each other does not receive the same amount of irradiation during the reference year.

How is irradiation measured and how do the different methods differ from each other?
The functioning of the two different types of irradiation measurement equipment, the pyranometer and the reference cell, are compared in this thesis. The dissimilar functioning of the two methods makes it different to compare irradiation from a reference cell and a pyranometer. The pyranometer have a standard for calibration and operation and is more suitable for measuring irradiation when the goal is to calculate the efficiency of a PV system. The use of a pyranometer for measuring the irradiation makes the efficiency suitable for comparison with other PV technology. The reference cell needs to match the PV technology and that makes it less suitable for comparison of the PV efficiencies. The reference cell however can be quite useful when the goal is monitoring of the PV systems. The reference cell gives directly, without any comprehensive calculations, the amount of irradiation available for the PV system to convert into electrical energy.

A program able to convert horizontal irradiation to irradiation in the module plane, and opposite, would have been convenient if a PV system doesn't have local data for the irradiation. However, the value of a program like this will have little or no value if the input irradiation is located far from the PV site.

Irradiation measured horizontally with a pyranometer is easier to compare than irradiation measured in the module plane. Irradiation measured in the module plane can differ both in the slope, the orientation and the material of the reference cell, which make the data hard to compare.

Is it possible to use irradiation data from other sources, when local data are not available at the PV site?
This thesis shows that the irradiation from the databases are to general for use in analytical monitoring. The irradiation data from the database from NASA has an average annual value of 1006 W/m^2. During the 22 years that the annual average is calculated from is the annual irradiation value varying between 19,3% less than the average and 21,2% more than the average. If the year chosen for monitoring of the PV system has an annual irradiation value close to these outer limits, will the use of the annual average year from the database have little value. It is possible to use horizontal irradiation, if this is available in the vicinity of the PV system. This demands a calculation from horizontal irradiation to irradiation in the module plane, if the modules of the PV system are mounted with a slope. The use of irradiation data from other reference cells demands a match of the materials of the modules, and if the slope of the reference cells do not match, then this must be considered.

What is the error of replacing missing data points with existing data points from other sources?

When data sets are missing a certain number of data points, they can be replaced with existing values from a remote or local source. This will off course depend on the number of missing data points. In this thesis were four data points missing in October and six data points missing in January for Blindern and Ås respectively. The replacement of the missing data points at Ås with data points from Blindern was calculated to give a monthly error of -1%. The replacement of the missing data points at Blindern with data points from Ås was calculated to give a monthly error of 0,4%. This error will depend on the meteorological factors of the days when the data points are missing. The error will be greater for days with cloud coverage than days with a clear sky.

What is possible to say about a PV systems performance without local meteorological data, only with access to inverter data?

Analytical monitoring will be difficult without meteorological data. The annual yield for a system can be estimated in simulation programs by using irradiation from databases. However, as this thesis has illustrated, will the data from the databases differ from the actual annual irradiation. If the actual annual yield differs from the estimated yield is it difficult to say anything about what is causing this deviation, without having meteorological data measured parallel with the inverter data. Irradiation data, module and air temperature and wind speed are necessary. Information about the amount of snow coverage and shading of the modules will also be necessary. With only inverter data is it only possible to give a detailed analytical monitoring of the efficiency of the inverter.

What is the result of using meteorological data from other locations for a PV site without local meteorological data?

The irradiation data in the module plane from PVGIS was chosen for analyzing the performance of the PV systems at Kjeller. The use of irradiation data from a database resulted in abnormal values for the PR, which for the CIS modules reached a value of over 1 in February and close to 1 in both September and December. Irradiation and air temperature from Blindern was compared with the specific yield from both systems. The correlation between the horizontal irradiation at Blindern and the specific yield is clear, however, when the curves deviates from each other is it necessary with more information about the meteorological conditions to know the reason for the deviation. The PV system at Kjeller is interesting in that way that it is two different PV technologies influenced by approximately the same meteorological factors. Meteorological factors measured parallel with the inverter data could give valuable information about the performance of each of the systems under changing real conditions. The limited research done for the two systems in this thesis has shown that the CIS modules has a higher specific yield than the silicon modules, even though the silicon modules are specified with a higher module efficiency than the CIS modules. The manufacturer of the CIS modules claims that the CIS modules have better performance than silicon modules under real conditions. The results from this thesis can indicate that this is a fact for the systems located at Kjeller.

6. Further works

For further work it would be interesting with analytical monitoring of a complete PV system, a system with both inverter data and meteorological data. The PV system at Økern has good meteorological data and could have been a good choice of a test system if the inverter data is made available in a good resolution. The inverter data from Økern could be arranged in a system with possibilities to extract desired information by the use of a web user interface as the interface used for the system at Kjeller.

The value and the usefulness of a program for converting horizontal irradiation values to values for irradiation in the module plane and opposite, can be investigated further. The available data for measured irradiation for an area as Oslo could be examined. How many of the PV systems in Oslo are equipped with instruments for measuring meteorological factors?

The usefulness of a common database for the measured values can also be investigated. The economics will probably need to be considered for this question. The pyranometer or a reference cell is expensive, considering purchase, installation, operation and maintenance. The question is if the providers of the data are wanting to share this information for free

During the investigation of the PV system at Kjeller it was clear that the two systems had different performance and different specific yield. These two systems are highly suitable for a more thorough study of the performance of CIS and silicon modules under real conditions. Installation of equipment for measuring meteorological data at the site would have made the two systems an excellent test site.

7. References

[1] Feldman, D., Barbose, G., Margolis, R., Bolinger, M., Chung, D., Fu, R., Seel, J.,Davidson, C., Darghouth, N. & Wiser, R. (2015). *Photovoltaic System Pricing Trend:. Historical, Recent, and Near-Term Projections*. Washington D.C.: U.S Department of Energy.
Available from: http://www.nrel.gov/docs/fy15osti/64898.pdf (read Des. 14, 2016)

[2] Jahn, U & Nasse, W. (2004). *Operational performance of grid-connected PV systems on buildings in Germany*. Canada: John Wiley & Sons, Inc.
Available from: http://138.4.46.62:8080/ies/ficheros/2_52_ref3.pdf. (read Des. 14, 2016)

[3] Wyote, A., Richter, M., Moser, D., Reich, N., Green, M., Mau, S. & Beyer, H. G. (2014). *Analytical Monitoring of Grid-connected Photovoltaic Systems: Good Practices for Monitoring and Performance Analysis*, Paris: IEA International Energy Agency, PVPS T13-03:2014.

[4] Lie, Ø. (2016, February 3). *Solkraft for eneboliger firedoblet i fjor.* Oslo: Teknisk Ukeblad. Available from: http://www.tu.no/artikler/solkraft-for-eneboliger-firedoblet-i-fjor/276723
(read Des. 14, 2016)

[5] Smets, A., Jäger, K, Isabelle. O., Van Swaaij, R. & Zeman, M. (2016). *Solar Energy: The Physics and Engineering of Photovoltaic Conversion Technologies and Systems.* England, UIT Cambridge Ltd. 462 s.

[6] The International Energy Agency. (2016). *Key World Energy Statistics.*Paris: The International Energy Agency. Available from:
https://www.iea.org/publications/freepublications/publication/KeyWorld2016.pdf
(read Des. 14, 2016)

[7] Honsberg, C & Bowden, S. *The Photovoltaic Education Network.* Available from: http://pveducation.org (read Des. 14, 2016)

[8] Duffie, John A., Beckman, W. A. (1980) *Solar Engineering of Thermal Processes.* Canada, John Wiley & Sons, Inc. 910 s.

[9] Pothecary, S. (2016, September 19). *Kaneka achieves new efficiency record for a practical size crystalline silicon PV cell.*
Available from: http://www.pv-magazine.com/news/details/beitrag/kaneka-achieves-new-efficiency-record-for-a-practical-size-crystalline-silicon-pv-cell_100026182/#axzz4Kt4uC3dJ
(read Des. 14, 2016)

[10] Burger, B., Kiefer, K., Kost, C., Nold, S., Philipps, S., Preu, R., Rentsch, J., Schlegl, T., Stryi-Hipp, G., Willeke, G et. al. (2016). *Photovoltaics Report.* Freiburg: Fraunhofer ISE. Available from https://www.ise.fraunhofer.de/de/downloads/pdf-files/aktuelles/photovoltaics-report-in-englischer-sprache.pdf (read Des. 14, 2016)

[11] Derevyanko, V. (2010). *PVsyst 6 Help*. Switzerland: PVsyst SA. Available from: http://files.pvsyst.com/help/ (read Des. 14, 2016)

[12] Chouder, A. & Silvestre, S. (2009). *Analysis Model of Mismatch Power Losses in PV Systems.* Barcelona: UPC. Available from: http://www.academia.edu/29493167/Analysis_Model_of_Mismatch_Power_Losses_in_PV_Systems (read Des. 14, 2016)

[13] Schwingshackl, C., Petitta, M., Wagner, J. E., Belluardo, G., Moser, D., Castelli, M., Zebisch, M., & Tetzlaff, A. (2013). *Wind effect on PV module temperature: Analysis of different techniques for an accurate estimation*. Bolzano: European Geosciences Union. Available from : http://ac.els-cdn.com/S1876610213016044/1-s2.0-S1876610213016044-main.pdf?_tid=33b65f1a-c1ed-11e6-bb33-00000aab0f27&acdnat=1481713700_8b8ac32f8eef5c8c9ebd52a1f553d2be (read Des. 14, 2016)

[14] Nordmann, T & Clavadetscher, L. (2003). *Understanding Temperature Effects on PV System Performance*. Erlenbach: TNC Consulting AG. 4 s.

[15] Pulver, S., Cormode, D., Cronin, A., Jordan, D., Kurtz, S. & Smith, R. *Measuring degradation rates without irradiance data*. Golden: National Renewable Energy Laboratory. *6 s.*

[16] Meydbray, J., Emery, K., and Kurtz, S. (2012). *Pyranometers and Reference Cells, What's the Difference?* Golden: National Renewable Energy Laboratory. Available from: http://www.nrel.gov/docs/fy12osti/54498.pdf (read Des. 14, 2016)

[17] Dunn, L., Gostein, M. & Emery, K. (2012). *Comparison of Pyranometers vs. PV Reference Cells for Evaluation of PV Array Performance.* Golden: National Renewable Energy Laboratory. Available from: http://imtsolar.com/wp-content/uploads/2013/01/Nrel-White-Paper.pdf (read Des. 14, 2016)

[18] *National Renewable Energy Laboratory's Best Research-Cell Efficiencies.* (2016, Feb. 2) Available from: http://www.nrel.gov/pv/assets/images/efficiency_chart.jpg. (read Des. 14, 2016)

[19] *Energy.gov's Copper Induim Gallium Diselenide*. Available from: http://www.energy.gov/eere/sunshot/copper-indium-gallium-diselenide (read Des. 14, 2016)

[20] *ZSW Sets New World Record for Thin-film Solar Cells* (2016, June 25) Available from: https://www.zsw-bw.de/en/newsroom/news/news-detail/news/detail/News/zsw-sets-new-world-record-for-thin-film-solar-cells.html. (read Des. 14, 2016)

[21] *PVGIS Radiation Databases, Help*. Available from: http://re.jrc.ec.europa.eu/pvgis/apps4/databasehelp_en.html (read Des. 14, 2016)

[22] *NASA-SSE Data, Help.* Available from: http://files.pvsyst.com/help/nasa_data.htm (read Des. 14, 2016)

[23] *FAQ for Kipp & Zonen's Pyranometers.*
Available from: http://www.kippzonen.com/FaqCategory/3/Pyranometers
(read Des. 14, 2016)

[24] *NASA Surface meteorology and Solar Energy: Daily Averaged Data*
Available from: https://eosweb.larc.nasa.gov/cgi-bin/sse/daily.cgi?email=skip@larc.nasa.gov
(read Des. 14, 2016)

[25] *Photovoltaic Geographical Information System - Interactive Maps from The European Commission.*
Available from: http://re.jrc.ec.europa.eu/pvgis/apps4/pvest.php (read Des. 14, 2016)

[26] *Timeanddate.no*. Available from:
https://www.timeanddate.no/astronomi/sol/norge/oslo?maaned=8&year=2016
(read Des. 14, 2016)

[27] *Solar Frontier – Performance of the CIS-technology*. Available from: http://www.solar-frontier.com/eng/technology/Performance/index.html (read Des. 14, 2016)

The data extracted from the LMT-database for meteorological data at Ås is provided by:
Agrometeorology Norway, lmt.nibio.no, Ås, August 20, 2015 – August 21, 2016.

The data extracted from the eKilma-database for meteorological data at Blindern is provided by:
The Norwegian Meteorological Institute, eklima.met.no/, Oslo, August 20, 2015 – August 21, 2016.

8. Appendices

8.1 Økern

Campbell Scientific CR1000 datalogger:

CR1000 Specifications

Electrical specifications are valid over a -25° to +50°C, non-condensing environment, unless otherwise specified. Recalibration recommended every three years. Critical specifications and system configuration should be confirmed with Campbell Scientific before purchase.

PROGRAM EXECUTION RATE
10 ms to one day @ 10 ms increments

ANALOG INPUTS (SE1-SE16 or DIFF1-DIFF8)
8 differential (DF) or 16 single-ended (SE) individually configuredinput channels. Channel expansion provided by optional analog multiplexers.

RANGES and RESOLUTION: Basic resolution (Basic Res) is the A/D resolution of a single A/D conversion. A DIFF measurement with input reversal has better (finer) resolution by twice than Basic Res.

Range (mV)[1]	DF Res (µV)[2]	Basic Res (µV)
±5000	667	1333
±2500	333	667
±250	33.3	66.7
±25	3.33	6.7
±7.5	1.0	2.0
±2.5	0.33	0.67

[1]Range overhead of ~9% on all ranges guarantees that full-scale values will not cause over range.
[2]Resolution of DF measurements with input reversal.

ACCURACY[3]:
±(0.06% of reading + offset), 0° to 40°C
±(0.12% of reading + offset), -25° to 50°C
±(0.18% of reading + offset), -55° to 85°C (-XT only)
[3]Accuracy does not include the sensor and measurement noise. Offsets are defined as:
Offset for DF w/input reversal = 1.5·Basic Res + 1.0 µV
Offset for DF w/o input reversal = 3·Basic Res + 2.0 µV
Offset for SE = 3·Basic Res + 3.0 µV

ANALOG MEASUREMENT SPEED:

Integration Type/Code	Integration Time	Settling Time	Total Time[4] SE w/ No Rev	Total Time[4] DF w/ Input Rev
250	250 µs	450 µs	~1 ms	~12 ms
60 Hz[5]	16.67 ms	3 ms	~20 ms	~40 ms
50 Hz[5]	20.00 ms	3 ms	~25 ms	~50 ms

[4]Includes 250 µs for conversion to engineering units.
[5]AC line noise filter.

INPUT NOISE VOLTAGE: For DF measurements with input reversal on ±2.5 mV input range (digital resolution dominates for higher ranges).
250 µs Integration: 0.34 µV RMS
50/60 Hz Integration: 0.19 µV RMS

INPUT LIMITS: ±5 Vdc

DC COMMON MODE REJECTION: >100 dB

NORMAL MODE REJECTION: 70 dB @ 60 Hz when using 60 Hz rejection

INPUT VOLTAGE RANGE W/O MEASUREMENT CORRUPTION: ±8.6 Vdc max.

SUSTAINED INPUT VOLTAGE W/O DAMAGE: ±16 Vdc max.

INPUT CURRENT: ±1 nA typical, ±6 nA max. @ 50°C; ±90 nA @ 85°C

INPUT RESISTANCE: 20 GΩ typical

ACCURACY OF BUILT-IN REFERENCE JUNCTION THERMISTOR (for thermocouple measurements):
±0.3°C, -25° to 50°C
±0.8°C, -55° to 85°C (-XT only)

ANALOG OUTPUTS (VX1-VX3)
3 switched voltage, sequentially active only during measurement.

RANGE AND RESOLUTION:

Channel	Range	Resolution	Current Source/Sink
(VX 1–3)	±2.5 Vdc	0.67 mV	±25 mA

ANALOG OUTPUT ACCURACY (VX):
±(0.06% of setting + 0.8 mV), 0° to 40°C
±(0.12% of setting + 0.8 mV), -25° to 50°C
±(0.18% of setting + 0.8 mV), -55° to 85°C (-XT only)

VX FREQUENCY SWEEP FUNCTION: Switched outputs provide a programmable swept frequency, 0 to 2500 mv square waves for exciting vibrating wire transducers.

PERIOD AVERAGE
Any of the 16 SE analog inputs can be used for period averaging. Accuracy is ±(0.01% of reading + resolution), where resolution is 136 ns divided by the specified number of cycles to be measured.

INPUT AMPLITUDE AND FREQUENCY:

Voltage Gain	Input Range (±mV)	Signal (peak to peak) Min. (mV)[6]	Signal (peak to peak) Max (V)[7]	Min Pulse Width (µV)	Max[8] Freq (kHz)
1	250	500	10	2.5	200
10	25	10	2	10	50
33	7.5	5	2	62	8
100	2.5	2	2	100	5

[6]Signal centered around Threshold (see PeriodAvg() instruction).
[7]With signal centered at the datalogger ground.
[8]The maximum frequency = 1/(twice minimum pulse width) for 50% of duty cycle signals.

RATIOMETRIC MEASUREMENTS
MEASUREMENT TYPES: Provides ratiometric resistance measurements using voltage excitation. 3 switched voltage excitation outputs are available for measurement of 4- and 6-wire full bridges, and 2-, 3-, and 4-wire half bridges. Optional excitation polarity reversal minimizes dc errors.

RATIOMETRIC MEASUREMENT ACCURACY:[9,10, 11]
±(0.04% of Voltage Measurement + Offset)
[9]Accuracy specification assumes excitation reversal for excitation voltages < 1000 mV. Assumption does not include bridge resistor errors and sensor and measurement noise.
[10]Estimated accuracy. ΔX (where X is value returned from the measurement with Multiplier = 1, Offset = 0):
BrHalf() instruction: $\Delta X = \Delta V_x/V_x$
BrFull() instruction $\Delta X = 1000 \cdot \Delta V_x/V_x$, expressed as mV·V^{-1}.
ΔV^{-1} is calculated from the ratiometric measurement accuracy. See Resistance Measurements Section in the manual for more information.
[11]Offsets are defined as:
Offset for DIFF w/input reversal = 1.5·Basic Res + 1.0 µV
Offset for DIFF w/o input reversal = 3·Basic Res + 2.0 µV
Offset for SE = 3·Basic Res + 3.0 µV
Excitation reversal reduces offsets by a factor of two.

PULSE COUNTERS (P1-P2)
2 inputs individually selectable for switch closure, high frequency pulse, or low-level ac. Independent 24-bit counters for each input.

MAXIMUM COUNTS PER SCAN: 16.7×10^6

SWITCH CLOSURE MODE:
Minimum Switch Closed Time: 5 ms
Minimum Switch Open Time: 6 ms
Max. Bounce Time: 1 ms open w/o being counted

HIGH-FREQUENCY PULSE MODE:
Maximum Input Frequency: 250 kHz
Maximum Input Voltage: ±20 V
Voltage Thresholds: Count upon transition from below 0.9 V to above 2.2 V after input filter with 1.2 µs time constant.

LOW-LEVEL AC MODE: Internal ac coupling removes ac offsets up to ±0.5 Vdc.
Input Hysteresis: 12 mV RMS @ 1 Hz
Maximum ac Input Voltage: ±20 V
Minimum ac Input Voltage:

Sine Wave (mV RMS)	Range(Hz)
20	1.0 to 20
200	0.5 to 200
2000	0.3 to 10,000
5000	0.3 to 20,000

DIGITAL I/O PORTS (C1-C8)
8 ports software selectable, as binary inputs or control outputs. Provide on/off, pulse width modulation, edge timing, subroutine interrupts / wake up, switch closure pulse counting, high frequency pulse counting, asynchronous communications (UARTs), and SDI-12 communications. SDM communications are also supported.

LOW FREQUENCY MODE MAX: <1 kHz
HIGH-FREQUENCY MODE MAX: 400 kHz
SWITCH-CLOSURE FREQUENCY MAX: 150 Hz
EDGE TIMING RESOLUTION: 540 ns
OUTPUT VOLTAGES (no load): high 5.0 V ±0.1 V; low <0.1
OUTPUT RESISTANCE: 330 Ω
INPUT STATE: high 3.8 to 16 V; low -8.0 to 1.2 V
INPUT HYSTERESIS: 1.4 V
INPUT RESISTANCE: 100 kΩ with inputs <6.2 Vdc
220 Ω with inputs ≥6.2 Vdc
SERIAL DEVICE/RS-232 SUPPORT: 0 TO 5 Vdc UART

SWITCHED 12 VDC (SW-12)
1 independent 12 Vdc unregulated source is switched on and off under program control. Thermal fuse hold current = 900 mA at 20°C, 650 mA at 50°C, 360 mA at 85°C.

EU DECLARATION OF COMPLIANCE
https://s.campbellsci.com/documents/us/compliance/eudoc_cr1000-series.pdf
https://s.campbellsci.com/documents/us/compliance/eudoc_cr1000kd.pdf

COMMUNICATIONS
RS-232 PORTS:
DCE 9-pin: (not electrically isolated) for computer connection or connection of modems not manufactured by Campbell Scientific.
COM1 to COM4: 4 independent Tx/Rx pairs on control ports (non-isolated); 0 to 5 Vdc UART
Baud Rates: selectable from 300 bps to 115.2 kbps.
Default Format: 8 data bits; 1 stop bits; no parity
Optional Formats: 7 data bits; 2 stop bits; odd, even parity

CS I/O PORT: Interface with telecommunications peripherals manufactured by Campbell Scientific.

SDI-12: Digital control ports C1, C3, C5, and C7 are individually configured and meet SDI-12 Standard v 1.3 for datalogger mode. Up to 10 SDI-12 sensors are supported per port.

PERIPHERAL PORT: 40-pin interface for attaching CompactFlash or Ethernet peripherals

PROTOCOLS SUPPORTED: PakBus, AES-128 Encrypted PakBus, Modbus, DNP3, FTP, HTTP, XML, HTML, POP3, SMTP, Telnet, NTCIP, NTP, Web API, SDI-12, SDM.

SYSTEM
PROCESSOR: Renesas H8S 2322 (16-bit CPU with 32-bit internal core running at 7.3 MHz)
MEMORY: 2 MB of flash for operating system; 4 MB of battery-backed SRAM for CPU usage and final data storage; 512 kB flash disk (CPU) for program files.
REAL-TIME CLOCK ACCURACY: ±3 min. per year. Correction via GPS optional.
REAL-TIME CLOCK RESOLUTION: 10 ms

SYSTEM POWER REQUIREMENTS
VOLTAGE: 9.6 to 16 Vdc
INTERNAL BATTERIES: 1200 mAh lithium battery for clock and SRAM backup that typically provides three years of backup
EXTERNAL BATTERIES: Optional 12 Vdc nominal alkaline and rechargeable available. Power connection is reverse polarity protected.
TYPICAL CURRENT DRAIN at 12 Vdc:
Sleep Mode: < 1 mA
1 Hz Sample Rate (1 fast SE meas.): 1 mA
100 Hz Sample Rate (1 fast SE meas.): 6 mA
100 Hz Sample Rate (1 fast SE meas. w/RS-232 communication): 20 mA
Active external keyboard display adds 7 mA (100 mA with backlight on).

PHYSICAL
DIMENSIONS: 23.9 x 10.2 x 6.1 cm (9.4 x 4 x 2.4 in); additional clearance required for cables and leads.
MASS/WEIGHT: 1 kg / 2.1 lb

WARRANTY
3 years against defects in materials and workmanship.

Campbell Scientific 109 temperature sensor:

6. Specifications

Features:

- Measures air, soil, or water temperature
- Compatible with AM16/32-series multiplexers
- Easy to install or remove
- Durable
- Compatible with the following CRBasic dataloggers: CR6, CR200(X), and CR800 series, CR1000, CR3000, and CR5000

Sensor Element:	Measurement Specialties™ 10K3A1iA thermistor
Survival Range:	–50 to 100 °C
Measurement Range:	–50 to 70 °C
Time Constant in Air:	30 to 60 s in a wind speed of 5 m/s
Maximum Cable Length:	1000 ft
Accuracy[1]	
Worst case:	±0.60 °C (–50 to 70 °C) ±0.25 °C (–10 to 70 °C)
Interchangeability Error:	±0.10 °C (0 to 70 °C) ±0.13 °C at –10 °C ±0.15 °C at –20 °C ±0.18 °C at –30 °C ±0.20 °C at –40 °C ±0.50 °C at –50 °C
Steinhart-Hart Linearization Error:	≤ 0.03 °C (–50 to 70 °C)
Probe Weight and Dimensions	
Weight with 10 ft cable:	136 g (5 oz)
Length:	10.4 cm (4.1 in)
Diameter:	0.762 cm (0.3 in)

[1]See FIGURE 6-1, *Worst-case probe and measurement errors*, and FIGURE 6-2, *Steinhart-Hart linearization error*. Overall probe accuracy is a combination of thermistor interchangeability, bridge-resistor accuracy, and error of the Steinhart-Hart equation. Interchangeability is the principle component error and is predominantly offset. Offset can be determined with a single-point calibration. Offset can be entered in the **Therm109()** instruction ***Offset*** parameter. The bridge resistor has a 0.1% tolerance with a 10 ppm temperature coefficient. At temperature extremes, the possible error in the CR200(X) series datalogger measurement may be greater than the error that exists in the probe.

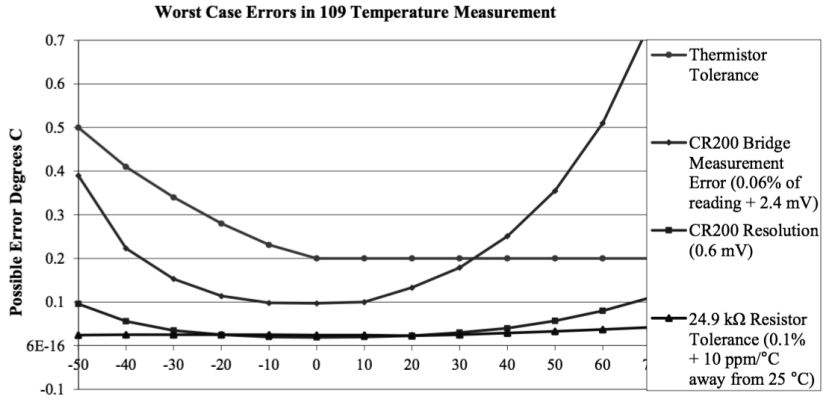

FIGURE 6-1. Worst case probe and measurement errors

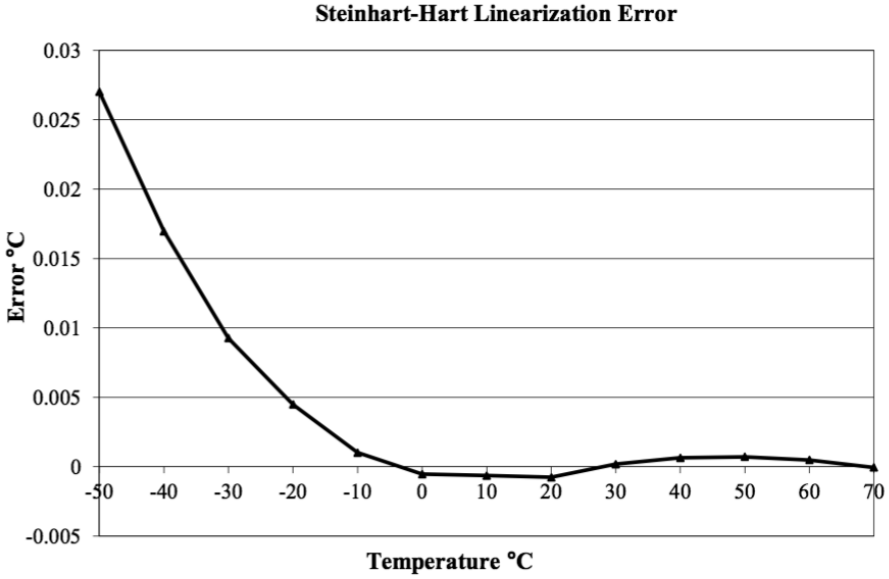

FIGURE 6-2. Steinhart-Hart linearization error

Lambrecht 14577 wind speed sensor:

WIND SPEED SENSOR

WIND WARNING DEVICE "WWS"

Wind Warning Device
WWS (14787)

Wind Speed Sensor
INDUSTRY (14577)

Indicator (8537)

Alarming...

in many and various applications - with a particularly attractive price-performance ratio!
Our wind warning system comprises the wind warning device, the INDUSTRY wind speed sensor, which has been tried and tested worldwide and the indicator type 8537.
It ensures continuous monitoring of the wind velocity with advance and primary warnings. Two freely configurable relays provide a high degree of flexibility; on-delay and drop-out delay can be adjusted separately.

- safety due to immediate detection of malfunctions
- individual, application-oriented setting of the functional parameters
- simple and rapid top hat rail mounting
- clear and lucid display of the measured values and the switching states

cranes • solar tracking systems • cable railways • harbour loading facilities • traffic meteorology • building maintenance units • fire services • excavators • amusement parks • locks

Professional Line	**(14787)**	**Wind Warning Device WWS**	**Id-No. 00.14787.000 000**
Relay outputs:		max. switching voltage AC	250 V AC
		max. switching current AC	2 A AC
		max. switching voltage DC	50 V DC
		max. switching current DC	2 A DC
Supply voltage:		supply voltage	50...253 V AC 20...350 V DC
		max. power consumption at 24 V DC	2.6 W
		max. power consumption at 230 V AC	5 VA
Environmental conditions:		permissible ambient temperature	-10...+60 °C
		storage and transport	-10...+70 °C
LCD display:		background lighting	three-coloured red, green, blue
Housing:		dimensions	33 x 110 x 128 mm
	(14577)	**Wind Speed Sensor INDUSTRY**	**Id-No. 00.14577.100 040**
Measuring range:		0.7...50 m/s	
Accuracy:		± 2 % FS	
Supply voltage:		24 (20...28) V DC · max. 800 mA · heating · electr. controlled · 18 W	
Accessories:			
00.08537.000 000		**Indicator** for WWS	
32.14567.006 000		**(14567 U6) Mast adapter**	
64.59020.960 000		**Power supply unit** for DIN-Rail top hat rail mounting	

LAMBRECHT meteo

Tel +49 (0) 551-4958-0 E-mail info@lambrecht.net www.lambrecht.net 03.15

Campbell Scientific 110PV surface temperature sensor:

Specifications

- Measurement Range: -40° to +135°C
- Survival Range: -50° to +140°C
- Temperature Uncertainty

Temperature	Tolerance
-40°C to 70°C	±0.2°C
71° to 105°C	±0.5°C
106° to 135°C	±1°C

- Time Constant In Air

Test	T
Still Air	252 seconds
Surface	25 seconds

- Steinhart-Hart Linearization Equation Error (maximum): 0.0024°C at -40°C
- Maximum Water Submersion Depth*

Meters	Feet	PSI
15.24	50	21

- Maximum Lead Length: 304.8 m (1000 ft)
- Disk Diameter: 2.54 cm (1.0 in)
- Overall Probe Length: 6.35 cm (2.5 in)
- Overmolded Joint Dimensions

Width	Height	Length
1.12 cm (0.44 in)	1.47 cm (0.58 in)	5.72 cm (2.25 in)

- Disk Material: Anodized Aluminum
- Cable Jacket Material: Santoprene
- Cable/Probe Connection Material: Santoprene
- Weight: 90.7 g with 3.2 m cable (0.2 lb with 10.5 ft cable)

**The 110PV's adhesive tab and the Kapton tape are not intended for submersion. Therefore, if the 110PV will be submerged, mount the sensor to the measurement surface using a user-supplied method that is compatible with submersion.*

CAMPBELL SCIENTIFIC Campbell Scientific, Inc. | 815 W 1800 N | Logan, UT 84321-1784 | (435) 227-9120 | www.campbellsci.com
USA | AUSTRALIA | BRAZIL | CANADA | CHINA | COSTA RICA | FRANCE | GERMANY | SE ASIA | SOUTH AFRICA | SPAIN | UK

Ingenieurbüro Mencke & Tegtmeyer GmbH Si-01 TC-T irradiance sensor:

SILICON IRRADIANCE SENSOR

Technical Data

SI-SENSOR
General Information

- Solar cell: Monocrystalline silicon (50 mm x 33 mm)
- Operating temperature: -35°C to 80°C
- Electrical connection: 3 m shielded cable
- Load impedance for Si-01TC-batt: minimal 1 MΩ
- Load impedance for Si-01TC and -TC-T and Si-13TC and -TC-T: min. 10 kΩ
- Load impedance for Si-420TC and -TC-T: minimal 20 Ω and maximal 400 Ω
- Case, protection mode: Powder-coated aluminium, IP 65
- Dimension, weight: 155 mm x 85 mm x 39 mm, approx. 350 to 470 g
- Customs number for all sensors: 85 41 40 90

Digital

- Protocol: M&T (type -MT), MODBUS RTU (type -MB), CANopen CiA 487
- Interface: RS485 up to 38.4 kBaud, CAN up to 250 kBaud
- Galvanic isolation: 1.000 V between power supply and bus

DIMENSIONS

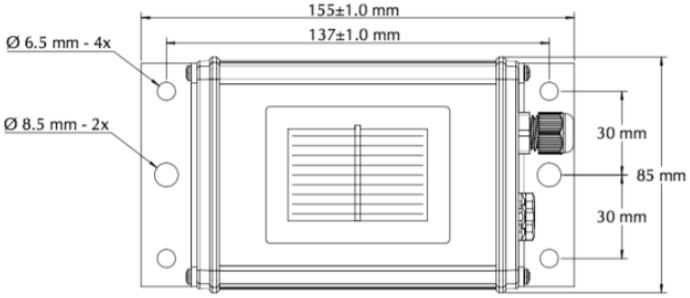

INCIDENT ANGLE MODIFIER

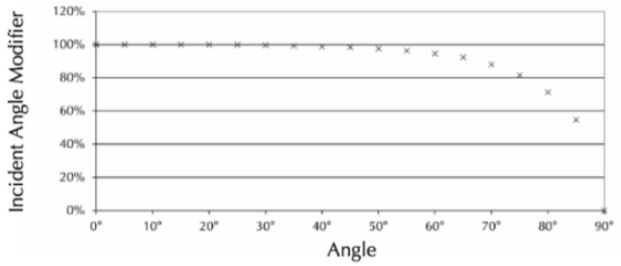

SPECTRAL RESPONSE

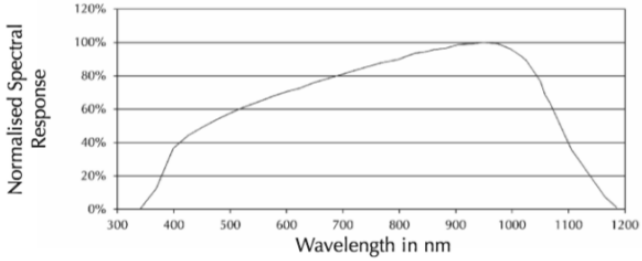

SILICON IRRADIANCE SENSOR

Technical Data

Sensor Types:

Type Measured Variable	Irradiance Power Supply Current Consumption	Irradiance Temperature compensation	Irradiance Output Signal	Cell Temperature Output Signal
Si-01TC-batt Irradiance	Internal Lithium Battery typic 15 µA	Yes	0 to 1.4 V for 0 to 1,400 W/m²	./.
Si-01TC Irradiance	24 V_{DC} (5 to 28 V_{DC}) typic < 1 mA	Yes	0 to 1.4 V for 0 to 1,400 W/m²	./.
Si-01TC-T Irradiance, Cell Temperature	24 V_{DC} (5 to 28 V_{DC}) typic < 1 mA	Yes	0 to 1.4 V for 0 to 1,400 W/m²	0 to 2 V for -123.5 to +76.5°C
Si-02 Irradiance	./. ./.	No	approx. 80 mV for 1,400 W/m²	./.
Si-02-Pt100 Irradiance, Cell Temperature	./. ./.	No	approx. 80 mV for 1,400 W/m²	Pt100, class A
Si-02-Pt1000 Irradiance, Cell Temperature	./. ./.	No	ca. 80 mV for 1,400 W/m²	Pt1000, class A
Si-13TC Irradiance	24 V_{DC} (12 to 28 V_{DC}) typic < 1 mA	Yes	0 to 10 V for 0 to 1,300 W/m²	./.
Si-13TC-T Irradiance, Cell Temperature	24 V_{DC} (12 to 28 V_{DC}) typic 4 mA	Yes	0 to 10 V for 0 to 1,300 W/m²	0 to 10 V for -26.1 to 89.0°C
Si-420TC Irradiance	24 V_{DC} (12 to 25 V_{DC}) typic 5 to 23 mA	Yes	4 to 20 mA for 0 to 1,200 W/m²	./.
Si-420TC-T Irradiance, Cell Temperature	24 V_{DC} (12 to 25 V_{DC}) typic 18 to 46 mA	Yes	4 to 20 mA for 0 to 1,200 W/m²	4 to 20 mA for -123.5 to 76.5°C
Si-CANopenTC-T Irradiance, Cell Temperature	24 V_{DC} (12 to 28 V_{DC}) typic 35 mA	Yes	CANopen CiA 487 0 to 1,400 W/m²	CANopen CiA 487 -25 to +75°C
Si-RS485TC-T Irradiance, Cell Temperature	24 V_{DC} (12 to 28 V_{DC}) typical 35 mA	Yes	M&T, MODBUS 0 to 1,400 W/m²	M&T, MODBUS -40 to +90°C
Si-RS485TC-2T Irradiance, Cell Temperature, Ambient Temperature (firmly connected with 3 m cable)	24 V_{DC} (12 to 28 V_{DC}) typic 35 mA	Yes	M&T, MODBUS 0 to 1,400 W/m²	M&T, MODBUS -40 to +90°C
Si-RS485TC-T-Tm Irradiance, Cell Temperature, Module Temperature (firmly connected with 3 m cable)	24 V_{DC} (12 to 28 V_{DC}) typic 35 mA	Yes	M&T, MODBUS 0 to 1,400 W/m²	M&T, MODBUS -40 to +90°C
Si-RS485TC-2T-v Irradiance, Cell Temperature Accessories: External Temperature, Wind Speed	24 V_{DC} (12 bis 28 V_{DC}) typic 35 mA	Yes	M&T, MODBUS 0 to 1,400 W/m²	M&T, MODBUS -40 to +90°C

ACCESSORIES FOR Si-RS485TC-2T-v

- Tamb-Si, Ambient temperature sensor in stainless steel sleeve with 3 m cable and connector (IP67), measuring range: -40 to +85°C
- Tmodul-Si, Module temperature sensor in aluminium block with 3 m cable and connector (IP67), measuring range: -40 to +85°C
- Vwind-Si, Wind speed sensor with 5 m cable and connector (IP67), measuring range: 0.9 to 40 m/s

SILICON IRRADIANCE SENSOR

Measurement Uncertainty of Irradiance
(does not apply for sensors with filter glass or polycrystalline cells)

Parameter	Sensor Type	Typical Measurement Uncertainty
Response time (99 %)	Si-02(-Pt100/-Pt1000)	0.001 s
for G > 50 W/m²	Si-01TC(-T), Si-13TC(-T), Si-420TC(-T)	0.15 s
	Si-RS485TC(-2T-v), Si-CANopenTC-T	1 s
Offset	Si-02(-Pt100/-Pt1000)	0 W/m²
	Si-01TC(-T), Si-13TC(-T)	2 W/m²
	Si-420TC(-T)	2.2 W/m²
	Si-RS485TC(-2T-v), Si-CANopenTC-T	1 W/m²
Stability per anno [1]	all	0.50 %
Non-Linearity [1]	all	0.10 %
Temperature Dependancy [2]	Si-02(-Pt100/-Pt1000) (with external temperature comp.) [3]	0.20 %
for -35 to +80°C	Si-02(-Pt100/-Pt1000) (without external temperature comp.)	3.00 %
	Si-01TC(-T), Si-13TC(-T), Si-420TC(-T)	0.40 %
	Si-RS485TC(-2T-v), Si-CANopenTC-T	0.40 %
Factory-Calibration	all (repeatability against reference)	0.75 %
	all (measurement uncertainty of reference at STC and vertical light beam)	0.50 %
Measurement Uncertainty over all [4]	**±5 W/m² ± 2.5 % of measurement value** valid for temperature compensation, spectrum AM 1.5 and vertical light beam	

Sensor Type	Measurement Uncertainty of the internal Temperature Measurement	
	Condition	Measurement Uncertainty [4]
Si-02-Pt100, Si-02-Pt1000	-35 to +80°C	IEC 60751, class A
Si-01TC-T	-20 to +70°C / -35 to +80°C	2.0 K / 2.5 K
Si-13TC-T	-20 to +70°C / -25 to +80°C	2.0 K / 2.5 K
Si-420TC-T	-20 to +70°C / -35 to +75°C	2.0 K / 2.5 K
Si-RS485TC-XX	-35 to +80°C	1.0 K

[1] Percentage rate referred to the measurement range
[2] Percentage rate referred to the measurement value
[3] External temperature compensation must be calculated on data acquisition side (temperature coefficient at AM 1.5: 0.0005 1/K)
[4] Based on GUM (Guide to the Expression of Uncertainty in Measurement) with k=2, not valid for Si-02 or Si-02(-Pt100/-Pt1000) without external temperature compensation

EXTEND OF Supply

Options

- Silicon sensor with shielded cable, 0.14 mm², UV- and temperature resistant, 3m length and ferrules (except Si-01TC-batt)
- Calibration protocol and quick reference guide
- DaKKS calibration certificate
- Customized cable lengths
- Version with waterproof connector (Si-01TC-batt always with connector)
- Adaptation of spectral response to different PV materials
- Customised scaling or measuring range

8.2 Ås

Kippp and Zonen CM3 pyranometer:

2. Specifications

The CM3 is an ISO Second Class pyranometer. While the worst case accuracy for daily sums given by Kipp & Zonen is ±10%, the typical accuracy is ±5%. Tests at Campbell Scientific on one CM3 indicated an accuracy of ±2% when compared to a recently calibrated Eppley PSP.

ISO SPECIFICATIONS:

Response Time 95%:	18 seconds
Zero offset due to 200 W/m^2 thermal radiation:	< 15 Wm^{-2}
Zero offset due to temperature change of 5°K / hr:	< ±4 Wm^{-2}
Non stability (% change/year):	< ± 1%
Non linearity (at 1000 W/m^2):	< ± 2.5%
Directional error (at 1000 W/m^2):	< ± 25 Wm^{-2}
Temperature Dependence of sensitivity:	± 6% (-10 to + 40°C)
Tilt response (±80°) (at 1000 W/m^2):	< ± 2%

OTHER SPECIFICATIONS

Expected accuracy for daily sums:	± 10%
Spectral range (50% points, nm):	305-2800 nm
Sensitivity:	10 - 35 µV/Wm^{-2}
Expected signal output in atmospheric application:	0 - 50 mV
Impedance:	79 - 200 (Ω)
Operating Temperature:	-40 to +80°C
Max. irradiance:	2000 Wm^{-2}
Detector:	Copper-constantin multi junction thermopile
Cable length:	15 feet (5 m)
Level accuracy:	1 degree

DIMENSIONS / SHIPPING DIMENSIONS

CM3:	3x3x3 in / 6x6x6 in
CM3MT:	1x5x5 in / 6x6x6 in

WEIGHT/SHIPPING WEIGHT

CM3:	0.8 lbs / 3 lbs
CM3MT:	0.6 lbs / 3 lbs

Reissmann Pt100 temperature sensor:

Product Information

REISSMANN

Measuring resistor with the Pt100-sensor referring to DIN EN 60751

Winding temperature monitoring and surface temperature measuring with the Pt100-Sensor

Pt100, Pt500, Pt1000

- Technical Data

Electrical Data:

Nominal resistance:	100 Ω at 0°C (Pt 100)
Basic thermistor values:	for platinum measuring resistors as in chart
Measuring range:	-50°C to +230°C, other ranges on request
Measuring current:	max. 1mA (no self-heating!)
Circuit:	standard: 2-wire, on request: 3-wire or 4-wire circuit
Insulation strength:	2.5 kV, on request up to 8 kV

Mechanical Data

Type:	Pt-sensor for surface measuring	Pt-sensor for winding monitoring
	Alu-housing screw-in sensor SW 10/M4 ring shaped cable eye for self-tapping sheet metal screw	e.g.: electric motors, transformers: in stabilised shrink tube design
Lead-in:	AWG 24, Cu-strand silvered, Teflon insulation, (optional: AWG 26, Cu-strand silvered, Teflon insulation, shielded cable) Standard colour: red/white, Standard length: 500mm ± 1%	
Insulation Class:	H	
Remarks:	Special designs for liquid or gaseous media, in V2A or other materials are manufactured on request for customers specific applications and specification, also for Pt500-, Pt1000-thermistors	
Order specification:	resistor thermometer as: 2-wire-, 3-wire-, 4-wire-circuits	

Product Information

REISSMANN

Measuring resistor with the Pt100-sensor referring to DIN EN 60751

Winding temperature monitoring and surface temperature measuring with the Pt100-Sensor

Pt100, Pt500, Pt1000

Characteristic temperature curves:	All sensors conform to DIN EN 60751: -50 ... 0°C: $R(t)= R(0) * (1 + A * t + B * t^2 + C * [t - 100] * t^3)$ 0 ... 600°C: $R(t)= R(0) * (1 + A * t + B * t^2)$ $A = 3.90802 * 10^{-3}$; $B = -5.802 * 10^{-7}$; $C = -4.2735 * 10^{-12}$ R(0) = thermistor value in Ohms at 0°C
Classes:	The temperature sensors are available in the following classes:

1/3 DIN class B+	± (0,10 + 0,0017 * t)	
1/3 DIN class B-	± (0,10 + 0,0050 * t)	
DIN class A	± (0,15 + 0,0020 * t)	
DIN class B	± (0,30 + 0,0050 * t)	
2 DIN class B	± (0,60 + 0,0050 * t)	t = absolute value of temperature in °C

Special versions are available on request.

Permissible deviation according to DIN EN 60751:

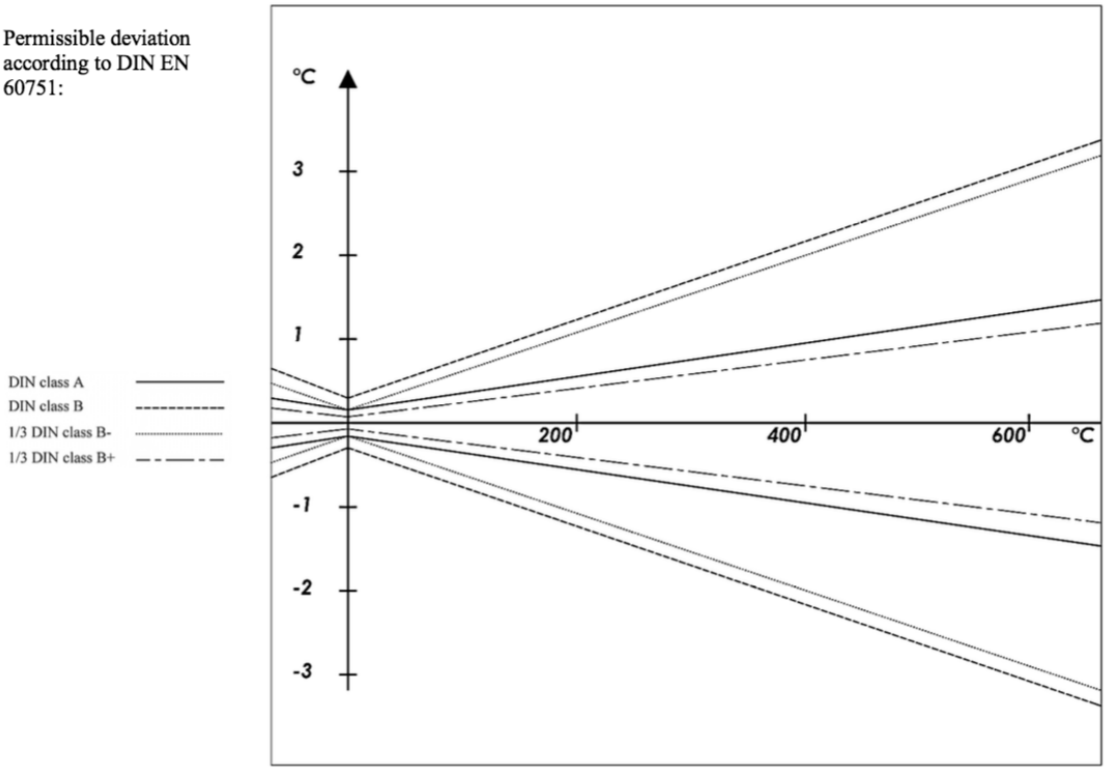

REISSMANN

Measuring resistor with the Pt100-sensor referring to DIN EN 60751

Winding temperature monitoring and surface temperature measuring with the Pt100-Sensor

Pt100, Pt500, Pt1000

Resistance data sheet: Resistance values for the thermistors from -50°C to 600°C in 1°C steps. Resistance values in the chart have to be multiplied by factor 100 for Pt100, by factor 500 for Pt500, by factor 1000 for Pt1000.

°C	0	1	2	3	4	5	6	7	8	9
-50	0.803									
-40	0.843	0.839	0.835	0.831	0.827	0.823	0.819	0.815	0.811	0.807
-30	0.882	0.878	0.874	0.870	0.866	0.862	0.859	0.855	0.851	0.847
-20	0.922	0.918	91,37	0.910	0.906	0.902	0.898	0.894	0.890	0.886
-10	0.961	0.957	0.953	0.949	0.945	0.941	0.937	0.933	0.929	0.926
0	1.000	0.996	0.992	0.988	0.984	0.980	0.977	0.973	0.969	0.965
0	1.000	1.004	1.008	1.012	1.016	1.020	1.023	1.027	1.031	1.035
10	1.039	1.043	1.047	1.051	1.055	1.058	1.062	1.066	1.070	1.074
20	1.078	1.082	1.086	1.090	1.093	1.097	1.101	1.105	1.109	1.113
30	1.117	1.121	1.124	1.128	1.132	1.136	1.140	1.144	1.148	1.152
40	1.155	1.159	1.163	1.167	1.171	1.175	1.179	1.182	1.186	1.190
50	1.194	1.198	1.202	1.205	1.209	1.213	1.217	1.121	1.125	1.129
60	1.232	1.236	1.240	1.244	1.248	1.252	1.255	1.259	1.263	1.267
70	1.271	1.275	1.278	1.282	1.286	1.290	1.294	1.297	1.301	1.305
80	1.309	1.313	1.317	1.320	1.324	1.328	1.332	1.336	1.339	1.343
90	1.347	1.351	1.355	1.358	1.362	1.366	1.370	1.374	1.377	1.381
100	1.385	1.389	1.393	1.396	1.400	1.404	1.408	1.412	1.415	1.419
110	1.423	1.427	1.430	1.434	1.438	1.442	1.446	1.449	1.453	1.457
120	1.461	1.464	1.468	1.472	1.476	1.479	1.483	1.487	1.491	1.494
130	1.498	1.502	1.506	1.501	1.513	1.517	1.521	1.525	1.528	1.532
140	1.536	1.539	1.543	1.547	1.551	1.554	1.558	1.562	1.566	1.569
150	1.573	1.577	1.581	1.584	1.588	1.592	1.596	1.599	1.603	1.607
160	1.610	1.614	1.618	1.622	1.625	1.629	1.633	1.636	1.640	1.644
170	1.648	1.651	1.655	1.659	1.662	1.666	1.670	1.674	1.677	1.681
180	1.685	1.688	1.692	1.696	1.699	1.703	1.707	1.711	1.714	1.718
190	1.722	1.725	1.729	1.733	1.736	1.740	1.744	1.747	1.751	1.755
200	1.758	1.762	1.766	1.769	1.773	1.777	1.780	1.784	1.788	1.791
210	1.795	1.799	1.802	1.806	1.810	1.813	1.817	1.821	1.824	1.828
220	1832	1.835	1.839	1.843	1.846	1.850	1.854	1.857	1.861	1.865
230	1.868	1.872	1.875	1.879	1.883	1.886	1.890	1.894	1.897	1.901
240	1.905	1.908	1.912	1.915	1.919	1.923	1.926	1.930	1.934	1.937
250	1.941	1.944	1.948	1.952	1.955	1.959	1.962	1.966	1.970	1.973
260	1.977	1.980	1.984	1.988	1.991	1.995	1.998	2.002	2.006	2.009
270	2.013	2.016	2.020	2.024	2.027	2.031	2.034	2.038	2.042	2.045
280	2.049	2.052	2.056	2.060	2.063	2.067	2.070	2.074	2.077	2.081
290	2.085	2.088	2.092	2.095	2.099	2.102	2.106	2.110	2.113	2.117
300	2120	2.124	2.127	2.131	2.134	2.138	2.142	2.145	2.149	2.152
310	2.156	2.159	2.163	2.166	2.170	2.173	2.177	2.181	2.184	2.188
320	2.191	2.195	2.198	2.202	2.205	2.209	2.212	2.216	2.219	2.223
330	2.226	2.230	2.234	2.237	2.241	2.244	2.248	2.251	2.255	2.258
340	2.262	2.265	2.269	2.272	2.276	2.279	2.283	2.286	2.290	2.293
350	2.297	2.300	2.304	2.307	2.311	2.314	2.318	2.321	2.325	2.328
360	2.332	2.335	2.339	2.342	2.346	2.349	2.353	2.356	2.360	2.363
370	2.367	2.370	2.373	2.377	2.380	2.384	2.387	2.391	2.394	2.398
380	2.401	2.405	2.408	2.412	2.415	2.419	2.422	2.426	2.429	2.432
390	2.436	2.439	2.443	2.446	2.445	2.453	2.457	2.460	2.463	2.467
400	2.470	2.474	2.477	2.481	2.484	2.488	2.491	2.494	2.498	2.501
410	2.505	2.508	2.512	2.515	2.518	2.522	2.525	2.529	2.532	2.536
420	2.539	2.542	2.546	2.549	2.553	2.556	2.560	2.563	2.566	2.570
430	2.573	2.577	2.580	2.583	2.587	2.590	2.594	2.597	2.600	2.604
440	2.607	2.611	2.614	2.617	2.621	2.624	2.628	2.631	2.634	2.638
450	2.641	2.645	2.648	2.651	2.655	2.658	2.661	2.665	2.668	2.672
460	2.675	2.678	2.682	2.685	2.688	2.692	2.695	2.699	2.702	2.705
470	2.709	2.712	2.715	2.719	2.722	2.725	2.729	2.732	2.735	2.739
480	2.742	2.746	2.749	2.752	2.756	2.759	2.762	2.766	2.769	2.772
490	2.776	2.779	2.782	2.786	2.789	2.792	2.796	2.799	2.802	2.806
500	2.809	2.812	2.816	2.819	2.822	2.826	2.829	2.832	2.836	2.839
510	2.842	2.845	2.849	2.852	2.855	2.859	2.862	2.865	2.869	2.872
520	2.875	2.879	2.882	2.885	2.888	2.892	2.895	2.898	2.902	2.905
530	2.908	2.912	2.915	2.918	2.921	2.925	2.928	2.931	2.935	2.938
540	2.941	2.944	2.948	2.951	2.954	2.958	2.961	2.964	2.967	2.971
550	2.974	2.977	2.980	2.984	2.987	2.990	2.993	2.997	3.000	3.003
560	3.007	3.010	3.013	3.016	3.020	3.023	3.026	3.029	3.033	3.036
570	3.039	3.042	3.046	3.049	3.052	3.055	3.059	3.062	3.065	3.068
580	3.071	3.075	3.078	3.081	3.084	3.088	3.091	3.094	3.097	3.101
590	3.104	3.107	3.110	3.113	3.117	3.120	3.123	3.126	3.130	3.133
600	3.136									

8.3 Blindern

Kipp and Zonen CMP21 pyranometer:

6. Specifications

Kipp & Zonen reserves the right to make changes to specifications and other product documentation without prior notice.

6.1 Optical and electrical

Specifications	CMP 3	CMP 6	CMP10 & CMP 11	CMP 21	CMP 22
Classification to ISO 9060:1990	Second Class	First Class	Secondary Standard	Secondary Standard	Secondary Standard
Spectral range (50 % points)	300 to 2800 nm	285 to 2800 nm	285 to 2800 nm	285 to 2800 nm	200 to 3600 nm
Sensitivity	5 to 20 µV/W/m²	5 to 20 µV/W/m²	7 to 14 µV/W/m²	7 to 14 µV/W/m²	7 to 14 µV/W/m²
Impedance	20 to 200 Ω	20 to 200 Ω	10 to 100 Ω	10 to 100 Ω	10 to 100 Ω
Expected output range (0 to 1500 W/m²)	0 to 30 mV	0 to 30 mV	0 to 20 mV	0 to 20 mV	0 to 20 mV
Maximum operational irradiance	2000 W/m²	2000 W/m²	4000 W/m²	4000 W/m²	4000 W/m²
Response time (63 %) Response time (95 %)	< 6 s < 18 s	< 6 s < 18 s	< 1.7 s < 5 s	< 1.7 s < 5 s	< 1.7 s < 5 s
Zero offsets (a) thermal radiation (at 200 W/m²) (b) temperature change (5 K/h)	 < 15 W/m² < 5 W/m²	 < 12 W/m² < 4 W/m²	 < 7 W/m² < 2 W/m²	 < 7 W/m² < 2 W/m²	 < 3 W/m² < 1 W/m²
Non-stability (change/year)	< 1 %	< 1 %	< 0.5 %	< 0.5 %	< 0.5 %
Non-linearity (100 to 1000 W/m²)	< 1.5 %	< 1 %	< 0.2 %	< 0.2 %	< 0.2 %
Directional response (up to 80° with 1000 W/m² beam)	< 20 W/m²	< 20 W/m²	< 10 W/m²	< 10 W/m²	< 5 W/m²
Spectral selectivity (350 to 1500 nm)	< 3 %	< 3 %	< 3 %	< 3 %	< 3 %
Temperature response	< 5 % (-10 °C to +40 °C)	< 4 % (-10 °C to +40 °C)	< 1 % (-10 °C to +40 °C)	< 1 % (-20 °C to +50 °C)	< 0.5 % (-20 °C to +50 °C)
Tilt response (0° to 90° at 1000 W/m²)	< 1 %	< 1 %	< 0.2 %	< 0.2 %	< 0.2 %
Field of view	180°	180°	180°	180°	180°
Accuracy of bubble level	< 0.2°	< 0.1°	< 0.1°	< 0.1°	< 0.1°
Temperature sensor output				10 K Thermistor (optional Pt-100)	10 K Thermistor (optional Pt-100)
Detector type	Thermopile	Thermopile	Thermopile	Thermopile	Thermopile
Operational temperature range	-40 °C to +80 °C	-40 °C to +80 °C	-40 °C to +80 °C	-40 °C to +80 °C	-40 °C to +80 °C
Storage temperature range	-40 °C to +80 °C	-40 °C to +80 °C	-40 °C to +80 °C	-40 °C to +80 °C	-40 °C to +80 °C
Humidity range	0 to 100 % non-condensing	0 to 100 % non-condensing	0 to 100 % non-condensing	0 to 100 % non-condensing	0 to 100 % non-condensing
Ingress Protection (IP) rating	67	67	67	67	67
Recommended applications	Economical solution for routine measurements in weather stations, field testing	Good quality measurements for hydrology networks, greenhouse climate control	Meteorological networks, PV panel and thermal collector testing, materials testing	Meteorological networks, reference measurements in extreme climates, polar or arid	Scientific research requiring the highest level of measurement accuracy and reliability

Note: The performance specifications quoted are worst-case and/or maximum values

Standard 10 k Thermistor or optional Pt-100 temperature sensor with CMP 21 and CMP 22

Individual directional response and temperature dependence test data with CMP 21 and CMP 22

6.2 Dimensions and weight

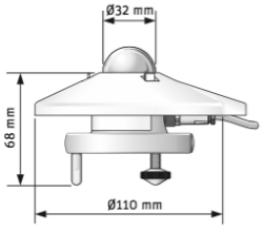

CMP 3
Weight without cable: 0.3 kg

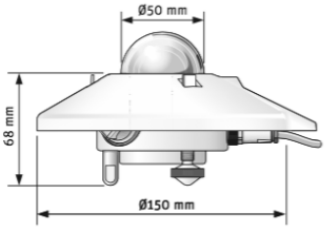

CMP 6, CMP10, CMP 11, CMP 21 and CMP 22
Weight without cable: 0.6 kg

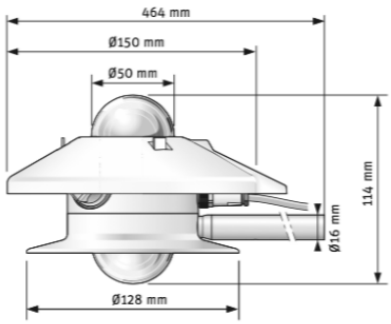

CMA 6 and CMA 11
Weight without cable: 1.2 kg

8.4 Kjeller

Solar Frontier SF165-S CIS modules:

STC* Characteristics

		SF150-S	SF155-S	SF160-S	SF165-S	SF170-S
Maximum power	Pmax	150 W	155 W	160 W	165 W	170 W
Module efficiency		12.2%	12.6%	13.0%	13.4%	13.8%
Factory binning		0/+5W				
Open circuit voltage	Voc	108.0 V	109.0 V	110.0 V	110.0 V	112.0 V
Short circuit current	Isc	2.20 A	2.20 A	2.20 A	2.20 A	2.20 A
Voltage at maximum power	Vmpp	81.5 V	82.5 V	84.0 V	85.5 V	87.5 V
Current at maximum power	Impp	1.85 A	1.88 A	1.91 A	1.93 A	1.95 A

* Standard Test Conditions (STC):
1,000 W/m2 irradiance, module temperature 25 °C, air mass 1.5. Isc and Voc are ±10% tolerance of STC rated values.

NOCT Characteristics**

		SF150-S	SF155-S	SF160-S	SF165-S	SF170-S
Maximum power	Pmax	111 W	115 W	119 W	123 W	126 W
Open circuit voltage	Voc	98.3 V	99.2 V	100.0 V	100.0 V	102.0 V
Short circuit current	Isc	1.76 A	1.76 A	1.76 A	1.76 A	1.76 A
Voltage at maximum power	Vmpp	76.4 V	77.4 V	78.8 V	80.2 V	82.1 V
Current at maximum power	Impp	1.47 A	1.49 A	1.51 A	1.53 A	1.55 A

**Nominal Operating Cell Temperature Conditions (NOCT):
Module operating temperature at 800 W/m2 irradiance, air temperature 20 °C, wind speed 1 m/s and open circuit condition.

Performance at Low Irradiance

Efficiency reduction of maximum power from an irradiance of 1,000 W/m2 to 200 W/m2 at 25 °C (77°F) is typically 2.0%. The standard deviation for the reduction of efficiency is 1.9%.

Temperature Characteristics

NOCT	47 ℃ (116°F)	
Temperature coefficient of Isc	α	+0.01%/K
Temperature coefficient of Voc	β	-0.30%/K
Temperature coefficient of Pmax	δ	-0.31%/K

Mechanical	
Dimensions (L x W x H)	1,257 x 977 x 35 mm (49.5 x 38.5 x 1.4 in.)
Weight	20 kg (44.1 lbs)
Application class (IEC 61730)	A
Fire rating (IEC 61730)	Class C
Safety class (IEC 61140)	II
Snow/wind load*	2,400 Pa (IEC 61646) / 1,600 Pa design load (UL 1703)
Cell type	CIS glass substrate (cadmium free)
Front cover	Clear tempered glass, 3.2 mm
Encapsulant	EVA
Back sheet	Weatherproof plastic film (color: black & silver)
Frame	Anodized aluminum alloy (color: black)
Edge sealant	Butyl rubber
Junction box	Protection rating: IP 67 (with bypass diode)
Adhesive	Silicone
Output cables (conductor)	2.5 mm2 /14 AWG (halogen free)
Cable lengths (symmetrical)	1,200 mm (47.2 in.)
Packing information	25 panels/pallet • 36 pallets/40′ container (900 panels)

*UL: 1.5 x design load is applied to the module, i.e., 2,400 Pa (50.1 lbs/ft2) is applied to meet the 1,600 a UL design load standard

I-V Curve

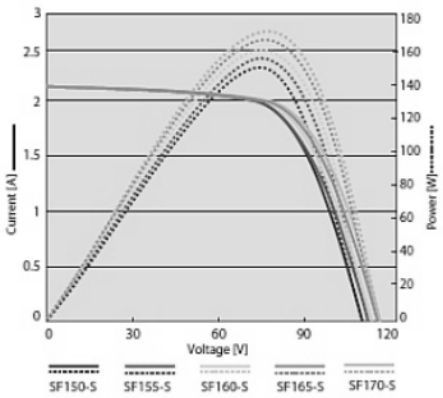

Module Drawing

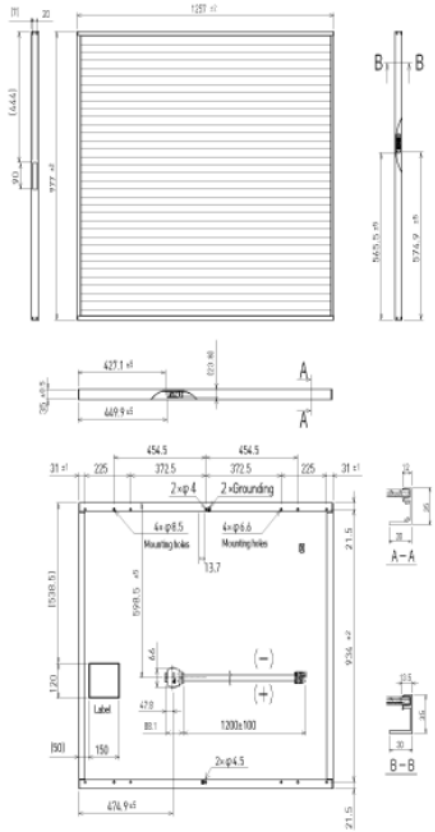

IBC PolySol 260 CS silicon modules:

Smart Systems
for Solar Power

IBC SOLAR

IBC EcoLine – For particulary stable output

IBC PolySol 250 CS, 255 CS, 260 CS

Solar modules made by polycrystalline silicon

Whether for single family homes, industrial roofs or open spaces – the trusted solar modules IBC PolySol CS are perfectly suited for anyone placing high demands on quality and cost efficiency. IBC SOLAR defines the most stringent specifications for components, ensuring you the best results. Thanks to the modules' positive power tolerance and linear performance guarantee, you'll benefit from high output and returns.

Thanks to the anti-reflective coating on the front glass panels, these modules capture even more light to be more efficient and produce optimum yields.

Highlights:

- 10-year product warranty*
- 25 years power warranty*
- Positive power tolerance: –0/+5 Wp
- Highly effective with low-iron photovoltaic glass and anti-reflective coating (3.2 mm)
- Tested according IEC 61215 for snow loads up to 5400 Pa (ca. 550 kg/m^2)
- IEC 61730, application class A for system voltages up to 1000 V, protection class II
- Produced in ISO 9001 and ISO 14001 certified factories
- 100% end control with individual registration of the electrical characteristics
- Quality tested by IBC SOLAR in own laboratory with climate chambers and flasher with integrated electroluminescence measurement

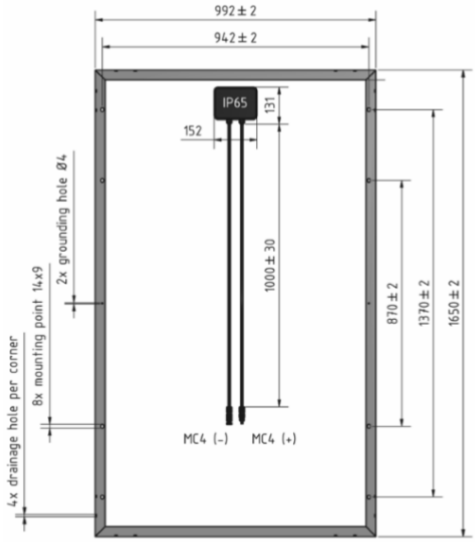

Progression of the power warranty

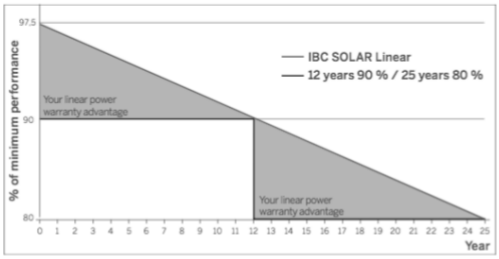

TECHNICAL DATA

IBC PolySol	250 CS	255 CS	260 CS
STC Power Pmax (Wp)	250	255	260
STC Nominal Voltage Umpp (V)	30.4	30.9	31.1
STC Nominal Current Impp (A)	8.23	8.25	8.37
STC Open circuit voltage Uoc (V)	37.6	37.8	38.1
STC Short circuit current Isc (A)	8.81	8.83	8.98
800 W/m² NOCT AM 1.5 Power Pmax (Wp)	183.07	186.77	190.64
800 W/m² NOCT AM 1.5 Nominal Voltage Umpp (V)	27.78	27.96	28.16
800 W/m² NOCT AM 1.5 Open Circuit Voltage Uoc (V)	35.05	35.57	36.04
800 W/m² NOCT AM 1.5 Short Circuit Current Isc (A)	6.92	6.96	7.00
Rel. efficiency reduction @ 200 W/m² (%)	3.9	4.23	4.29
Tempcoeff Isc (%/°C)	+0.064	+0.064	+0.064
Tempcoeff Uoc (mV/°C)	–117.7	–120.7	–121.7
Tempcoeff Pmpp (%/°C)	–0.43	–0.43	–0.43
Module Efficiency (%)	15.3	15.6	15.9
NOCT (°C)	48	48	48
Max. System Voltage (V)	1000	1000	1000
Max. Reverse Current Ir (A)	20	20	20
Current value String fuse (A)	15	15	15
Fuse protection from parallel strings	4	4	4
Height (mm)	45	45	45
Weight (kg)	20.5	20.5	20.5
Article number	**2203800007**	**2203800005**	**2203800006** **2203800008**

2014-08-01

Presented by:

* The linear power warranty is only valid for installations within Europe and Japan. For further information, please refer to the corresponding product and power warranty in accordance with the version of the full warranty conditions received from your specialized IBC SOLAR partner at the time of installation. This warranty is valid only when the product is installed in accordance with the applicable installation instructions. Electrical values under standard test conditions: 1000 W/m²; 25°C, AM 1.5. 800 W/m², NOCT. Specifications according EN 60904-3 (STC). All datas according DIN EN 50380. Subject to modifications that represent progress.

RPI H3 Delta inverter:

RPI H3

High efficiency single phase transformerless inverters for the European market - Perfect choice for residential PV systems

Versatile applications

- Aluminium housing ensures long lasting protection against moisture and corrosion
- Wide input voltage range
- Suitable for indoor and outdoor applications (IP65)
- Compact design for simplified installation

Maximum profitability

- Peak efficiency of 97 %
- Fanless design for reduced maintenance costs
- Affordable residential inverter with all essential functions and reliable performance

www.solar-inverter.com

DELTA

3.0 kVA transformerless solar inverters

Technical data RPI H3

INPUT (DC)	RPI H3
Max. recommended PV power	3.78 kW_p
Max. power	3.2 kW
Nominal power	3.15 kW
Voltage range	125 ... 600 V [1]
MPP operating voltage range	125 ... 550 V
Startup voltage	150 V
Voltage range for maximum power	320 ... 500 V
Max. current	10 A
Number of MPP trackers	1

OUTPUT (AC)	
Maximum apparent power	3 kVA [2]
Nominal apparent power	3 kVA [2]
Voltage range	230 -20%/+22%, 1 Phase (L, N, PE or L, L, PE) [3]
Nominal current	13 A
Nominal frequency	50 / 60 Hz
Frequency range	50 / 60 Hz ± 5 Hz [3]
Power factor adjustable	0.8 cap ... 0.8 ind
Total harmonic distortion (THD)	< 3 % @ nominal apparent power

GENERAL SPECIFICATION	
Model name	RPI H3_110
Part number Delta	RPI302N63E0000
Max. efficiency	97.0 %
Efficiency EU	96.2 %
Operating temperature	-25 ... +60 °C
Full power without derating	-25 ... +40 °C
Storage temperature	-25 ... +60 °C
Humidity	0 ... 95 % non-condensing
Max. operating altitude	2000 m (above sea level)
Standard guarantee	5 years (guarantee extension available upon request)

MECHANICAL DESIGN	
Size (H x W x D)	367 × 420 × 157 mm
Weight	15 kg
Cooling	Natural convection
AC connector	Wieland RST25i3S B1G M01
DC connector	2 pairs of Multi-Contact MC4
Communication interfaces	2 x RS485, 1 x dry contact, 4 x digital inputs
DC disconnector	Integrated
Display	2 LEDs, 2-line LCD

SAFETY / STANDARDS	RPI H3
Protection degree	IP65
Safety class	I
Configurable trip parameters	Yes
Insulation monitoring	Yes
Overload behavior	Current limitation; power limitation
Anti-islanding protection / Grid regulation	VDE 0126-1-1; VDE-AR-N 4105; Synergrid C10/C11 06/2012 / VDE 126 A1; VFR 2013 / 2014; VDE 16 1-1 A1; UTE 15-712; French Islands 50 Hz/60 Hz; EN 50438 2013:Netherlands; UK G83-2
EMC	EN61000-6-2; EN61000-6-3
Safety	IEC62109-1 / -2; CE compliance

1) No risk of electrical damage till 630 V
2) Cos Phi = 1 (VA = W)
3) AC voltage and frequency range will be programmed according to the individual country requirements.

United Kingdom
Email: sales.uk@solar-inverter.com
Tel: 0800 051 4280 (Free Call)

International
Email: sales.europe@solar-inverter.com
Tel: +49 7641 455 547

www.solar-inverter.com

Norges miljø- og biovitenskapelig universitet
Noregs miljø- og biovitskapelege universitet
Norwegian University of Life Sciences

Postboks 5003
NO-1432 Ås
Norway